An Analysis of the Influence of Waterlevel Fluctuations on the Dispersion Process at the Borden Aquifer.

by

David Anthony Farrell

A Thesis
Submitted to the Faculty of Graduate Studies
in Partial Fulfillment of the Requirements of the Degree of

Master of Science in Geophysics

Earth Science Department
University of Manitoba
Winnipeg, Manitoba.

ISBN 0-315-81823-9

AN ANALYSIS OF THE INFLUENCE OF WATERLEVEL FLUCTUATIONS ON THE DISPERSION PROCESS AT THE BORDEN AQUIFER

BY

DAVID ANTHONY FARRELL

A Thesis submitted to the Faculty of Graduate Studies of the University of Manitoba in partial fulfillment of the requirements for the degree of

MASTER OF SCIENCE

Abstract

Waterlevel data collected at the site of an emplaced source experiment at the Borden Tracer-Test site over a period of one and a half years have been analyzed using the least squares method. The analysis shows that the data is comprised of a trend and an uncorrelated residual in space. From the trend, time series for the hydraulic head gradient magnitude and the flow direction are computed. Geostatistical and Fast Fourier Transform methods are then applied to these time series to determine the variances and the integral scales present in the data. Assuming that the data are stationary in both space and time, the variance and integral scale data are combined with the Stanford-Waterloo experiment data and used to evaluate the macroscopic dispersion theories of Rehfeldt (1988) and Naff (1989). The results obtained from Rehfeldt's method for spread in the asymptotic transverse horizontal macrodispersivity are quite similar to the results obtained by several researchers based on field studies [see Freyberg, 1986; and Rajaram and Gelhar, 1991]. The results obtained from Naff's time dependent macrodispersion model are found to be quite poor when compared with results from field based studies.

In addition, an analysis of the plume moments for the 1978 Borden tracer experiment are presented. From these moments the solute mass in the plume, the velocity of the centre of mass of the plume, the dispersivity and dispersion, the skew and the kurtosis of the solute concentration in the plume are calculated. Examination of the data shows that the plume splits into two halves each travelling with a different velocity. Due to the relatively poor sampling of the plume only an analysis of the plume in the lower velocity zone is performed. The computed results of the location of the centre of mass, the velocity and the dispersivity for the plume in the low velocity zone are found to be in good agreement with the results of Sudicky et al.

(1983). The computed transverse macrodispersivity results are found to be in excellent agreement with those of Freyberg (1986) and Rajaram and Gelhar (1991) for the 1986 Stanford-Waterloo experiment. The results also show the plume to be positively skewed and platykurtic at early time, appearing to tend towards a normal distribution at later time. This is in agreement with the theoretical work of Gelhar et al. (1979) for perfectly stratified aquifers.

Acknowledgments

This thesis has been the product of one and a half years of work. Although it has one author many people have contributed in one form or another to its production and as a result I would like to take this chance to thanks them all. First and foremost I would like to thank my advisor Dr. Allan Woodbury for taking a chance in offering me this opportunity to expand my horizons. The many discussions we had were very helpful and enlightening. In addition his cheerful disposition and positive attitude made this work more a pleasure than a chore. My only regret is that we didn't get to try everything we discussed. I would like to thank Dr. E. A. Sudicky of the Centre for Groundwater Research, University of Waterloo for his advice on numerous occasions and for providing part of the funding for this work as well as the 1978 Borden Tracer data. Special thanks are also extended to Dr. M. Rivett of the Centre for Groundwater Research, University of Waterloo for providing the waterlevel data used in this work. In addition I would like to thank the faculty and staff of the Department of Geological Engineering and the Department of Geological Sciences for all the assistance they provided. In particular I would to thank Dr. E. Lajtai for allowing me to have unlimited access to the computer facilities of the Rock Mechanics Group; as well as Ingrid Trestrail and Elizabeth Ross for being constant sources of information. I also wish to thank all of the students who shared Rm. 312c with me for all the advice, support and good times we shared during the course of this work.

Special thanks are extended to my parents, Lionel and Audrey Farrell, my brothers, Robert and Kevin, my many relatives and friends who provided the emotional

support and encouragement needed to make this work successful. My success is your success.

Finally I would like to dedicate this work to the memory of my grandmother, Irene Farrell without whom none of this would have been possible. It is unfortunate that you only saw the start of this work and not the final product.

Table of Contents

Abstract	i
Acknowledgments	iii
Table of Contents	v
List of Figures	vii
List of Tables	xi
Chapter 1	1
Introduction	1
1.1 Relevance	1
1.2 The Problem	5
1.3 Objectives and Scope	9
References	11
Chapter 2	15
A Geostatistical Analysis of Fluctuating Waterlevels at the Borden Aquifer	15
2.1 Introduction	15
2.2 Theory	17
2.2.1 Asymptotic Analysis of Dispersion	17
2.2.2 Harmonic-Moment Evolution Model	23
2.3 Waterlevel Data Analysis	27
2.3.1 Field Data	27
2.3.2 Trend Surface Analysis	33
2.3.2.1 Model Discrimination Tests	35
2.3.2.2 Generalized Least Squares Analysis	40
2.3.3 Gradient and Flow Direction Time Series	47
2.4 Geostatistical Analysis of Time Series	48
2.5 Macrodispersion Analysis	64
2.5.1 Application of Geostatistical Results to the Asymptotic Model	67
2.5.2 Harmonic Analysis of Borden Data	70
2.5.3 Application of Harmonics to the Time Dependent Model	72
2.6 Discussion and Conclusions	81
References	83

Chapter 3 86

The 1978 Borden Tracer Experiment;
Analysis of the Spatial Moments 86
3.1 Introduction 86
3.2 Theory 88
3.2.1 Spatial Moments 88
3.3 The Field Data 93
3.4 Methodology 97
3.4.1 Vertical Integration of the Plume 101
3.4.2 Horizontal Integration of the Plume 102
3.5 Results 105
3.5.1 The Vertically Integrated Plume 105
3.5.2 Full Plume Analysis 109
3.5.2.1 Recovered Mass Estimates 109
3.5.2.2 Motion of the Centre of Mass and Plume Velocity Estimates 114
3.5.3.3 Second Moment, Spatial Covariance and Macrodispersivity Estimates 114
3.5.3 Plume in Lower Hydraulic Conductivity Zone 119
3.5.3.1 Recovered Mass Estimates 121
3.5.3.2 Motion of Centre of Mass and Plume Velocity Estimates 121
3.5.3.3 Second moments, Spatial Covariance and Macrodispersivity Estimates 124
3.5.3.3 Third Moment and Skew Estimates 135
3.5.3.4 Fourth Moment and Kurtosis Estimates 140
3.6 Discussion and Conclusions 143
References 146

Chapter 4 150

Discussion and Conclusions 150
4.1 Introduction 150
4.2 Discussion of Stationarity Assumption 150
4.3 Early Time Plume Behavior 151
4.4 Practical Implications 152
4.5 Further Research 153
References 156

Appendix 1 158

Derivation of the Expression for the Unsteady Component of the Macrodispersivity 158

List of Figures

Figure #		Page #
1.1	Plot of longitudinal dispersivity (α_L) versus sample volume (after Dominico and Schwartz, 1990).	3
2.1.	Map of the Borden Tracer-Test site.	18
2.2.	Schematic of the flow field at the Borden site.	22
2.3	Observed watertable elevation time series at piezometer P2.	28
2.4	Observed watertable elevation time series at piezometer P13.	29
2.5	Observed watertable elevation time series at piezometer P24.	30
2.6	Watertable contour map for the emplaced source site on 02/03/1990.	31
2.7	Watertable contour map for the emplaced source site on 28/08/1990.	32
2.8	First order OLS polynomial surface superimposed on the observed hydraulic head contour map for 02/03/1990.	39
2.9	Classical Semi-variogram estimates for residuals of OLS surface fit; 03/01/1990.	43
2.10	Classical Semi-variogram estimates for residuals of OLS surface fit; 13/03/1990.	44
2.11	Classical Semi-variogram estimates for residuals of OLS surface fit; 04/07/1990.	45
2.12	Classical Semi-variogram estimates for residuals of OLS surface fit; 07/09/1990.	46
2.13	North-south hydraulic head gradient time series.	49
2.14	East-west hydraulic head gradient time series.	50
2.15	Hydraulic head gradient magnitude $\lvert J \rvert$ time series.	51

2.16	Flow angle time series (Ω).	52
2.17	Classical Semi-variogram and Jackknife estimates for the flow angle (Ω) time series.	54
2.18	Classical Semi-variogram and Jackknife estimates for the flow angle (Ω) time series (112 - 539 days).	55
2.19	Classical Semi-variogram and Jackknife estimates for the gradient magnitude $\|J\|$ time series.	56
2.20	Classical Semi-variogram and Jackknife estimates for the gradient magnitude $\|J\|$ time series (112 - 539 days).	57
2.21	Cressie-Hawkins variogram and Jackknife estimates for the flow angle (Ω) time series.	58
2.22	Cressie-Hawkins variogram and Jackknife estimates for the flow angle (Ω) time series (112 - 539 days).	59
2.23	Cressie-Hawkins variogram and Jackknife estimates for the gradient magnitude $\|J\|$ time series.	60
2.24	Cressie-Hawkins variogram and Jackknife estimates for the gradient magnitude $\|J\|$ time series (112 - 539 days).	61
2.25	Observed gradient magnitude $\|J\|$ time series compared to the observed maximum and minimum gradient magnitudes given by MacFarlane et al. (1983) and Sudicky (1986).	65
2.26	Observed flow angle time series with 14° range superimposed.	66
2.27	Transverse horizontal asymptotic model results fitted to the transverse horizontal moment data of Freyberg (1986).	69
2.28	Observed gradient perpendicular to the mean flow direction (a_2) vs time.	71
2.29	Frequency spectrum of a_2 gradient time series.	73
2.30	Comparison of time series based on 15 harmonics to the observed a_2 gradient time series.	74
2.31	Results of the harmonic model fitted to the transverse horizontal	

	moment data of Freyberg (1986) for the Borden site.	76
2.32	Extended a_2 gradient time series (7 - 904) days.	77
2.33	Frequency spectrum for extended a_2 gradient time series.	78
2.34	Comparison of time series based on 15 harmonics to the extended a_2 gradient time series.	79
2.35	Results of the harmonic model (extended time series) fitted to the transverse horizontal moment data of Freyberg (1986) for the Borden site.	80
3.1	Map of the Borden Tracer-test site.	94
3.2	Plan view of the injection wells and multilevel sampler array.	95
3.3	Vertical concentration profile after one day (along line A).	96
3.4	Vertical concentration profiles after 5 days along (i) line 3; (ii) line 7.	98
3.5	Vertical concentration profiles after 12 days along (i) line 3; (ii) line 7.	99
3.6	Vertical concentration profiles after 29 days along (i) line 3; (ii) line 7.	100
3.7	Vertically integrated plume using Freyberg extrapolation scheme and inverse square distance interpolation scheme.	106
3.8	Vertically integrated plume using Freyberg extrapolation scheme and kriging interpolation scheme.	107
3.9	Vertically integrated plume using Rajaram and Gelhar extrapolation scheme and inverse square distance interpolation scheme.	108
3.10	Motion of the centre of mass of the entire plume (all of the data used).	115
3.11	Motion of the centre of mass of the entire plume (reduced data set used).	116

3.12	Scheme diagram showing the plume orientation with respect to the field coordinate system and the rotated coordinate system.	118
3.13	Vertically integrated plume in the lower hydraulic conductivity zone.	120
3.14	Motion of the centre of mass of the plume in the lower hydraulic conductivity zone (all the data used).	123
3.15	Motion of the centre of mass of the plume in the lower hydraulic conductivity zone (reduced data set).	125
3.16	Variance in the longitudinal direction for the plume in the lower hydraulic conductivity zone (all the data used).	130
3.17	Variance in the longitudinal direction for the plume in the lower hydraulic conductivity zone (reduced data set used).	131
3.18	Variance in the transverse horizontal direction for the plume in the lower hydraulic conductivity zone (all the data used).	132
3.19	Variance in the transverse horizontal direction for the plume in the lower hydraulic conductivity zone (reduced data set used).	133
3.20	Longitudinal and transverse skew in the plume concentration vs time.	136
3.21	Plot of normalized variance, skewness, and kurtosis for large stratification as functions of dimensionless time (after Naff, 1990).	139
3.22	Longitudinal and transverse kurtosis in the plume concentration vs time.	141

List of Tables

Table #		Page #
2.1	Over-Determination Test: 2nd Order Coefficients.	38
2.2	Transverse Dispersivity Results.	62
2.3	Transverse Dispersivity Results (112 --> 539 days).	63
2.4	Longitudinal Dispersivity Results.	63
2.5	Watertable Data for the Borden Aquifer.	64
2.6	Computed Macrodispersivities.	68
3.1	Estimates of Mass in Solution, Location of Centre of Mass, and Spatial Covariance for the 1978 Tracer Plume [Freyberg extrapolation scheme used; interpolation performed using kriging].	110
3.2	Estimates of Mass in Solution, Location of Centre of Mass, and Spatial Covariance for the 1978 Tracer Plume [Freyberg extrapolation scheme used; interpolation performed using inverse square distance].	111
3.3	Estimates of Mass in Solution, Location of Centre of Mass, and Spatial Covariance for the 1978 Tracer Plume [Rajaram and Gelhar (1991) extrapolation scheme used; interpolation performed using inverse square distance].	112
3.4	Estimates of Mass in Solution, Location of Centre of Mass, and Spatial Covariance for the 1978 Tracer Plume [plume in the lower hydraulic conductivity zone].	122
3.5	Estimated Plume Veolocity for the 1978 Tracer Experiment [plume in the lower hydraulic conductivity zone].	124
3.6a	Second Moments for Field and Rotated Coordinate Systems [rotation angle=-2.078°].	126
3.6b	Second Moments for Field and Rotated Coordinate Systems [rotation angle=-4.574°].	127

3.7 Time Dependent Dispersivity Estimates for the 1978 Tracer Experiment. [plume in the lower hydraulic conductivity zone]. 128

3.8 Dispersion and Macrodispersivity Estimtes for the 1978 Tracer Plume [plume in the lower hydraulic conductivity zone]. 129

3.9 Computed Skew for the Plume [plume in the lower hydraulic conductivity zone]. 137

3.10 Computed Kurtosis for the Plume [plume in the lower hydraulic conductivity zone]. 140

Chapter 1

Introduction

1.1 Relevance

Groundwater contamination has become an area of concern due to public health issues (e.g. in cases where the contaminant has been shown to be or is suspected of being toxic or carcinogenic), environmental issues (particularly where groundwater discharges into lakes, streams and wetlands) and economic factors. Concern is greatest in areas where communities rely on aquifers as their source of drinking water. Contamination of drinking water supplies in such communities may pose severe health and economic problems, especially if water has to be imported from distant sources. The sources of groundwater contamination have been found to vary widely. For example, Guerera (1981) reports the contamination of groundwater by pesticides, Elder et al. (1981) report the contamination of groundwater by leachate from a landfill, and O'Connor and Bouchout (1983) report the contamination of groundwater by gasoline from an underground storage tank spill. As both the development of new chemical substances and the demand for disposal sites increases, it is probable that the number of groundwater contaminated sites will continue to grow.

One alternative in rectifying a contamination problem involves the use of an appropriate remediation scheme. Adequate and cost effective remediation of a contaminated site often requires that the problem be properly modelled. This modelling is usually performed numerically. Numerical modelling of the migration of contaminants in the subsurface requires a good understanding of the physics governing the flow of the various types of contaminants (e.g. miscible and immiscible liquids). Currently, there is much debate about the fundamental processes governing the transport of these substances. Much of the debate centres on how to pass from the macroscopic continuum level of a Representative Elementary Volume (REV) to some appropriate field scale. The REV gives an indication of the range in a sample volume across which the transport parameters, such as porosity, are correlated (see Figure 1.1). For example, Gelhar et al. (1985) point out that much further from a contamination source the spreading of a solute plume is larger than one would expect based on laboratory measurements of hydrodynamic dispersion[1]. The hydrodynamic dispersion is controlled by local fluctuations in the groundwater velocity which cause mechanical mixing of the transported solute and molecular diffusion. The local fluctuations in the groundwater velocity under natural gradient conditions (i.e. in the absence of pumping wells) are caused, in large part, by the variability of the hydraulic conductivity of the porous medium. However, it is common practice to quantify hyrodynamic dispersion by a parameter termed the dispersivity[2]. As mentioned earlier, theory must be validated by observations. The use of field data as opposed to laboratory data provides a better approach to validating theory since the field data fully incorporates the effects of the

[1] The term "hydrodynamic dispersion" refers to the tendency of a solute to spread out from the path that it would be expected to follow based on the bulk average motion of the groundwater flow.

[2] The dispersivity is traditionally assumed to be a unique property of the geologic medium at a particular scale of continuum description (Bear, 1972).

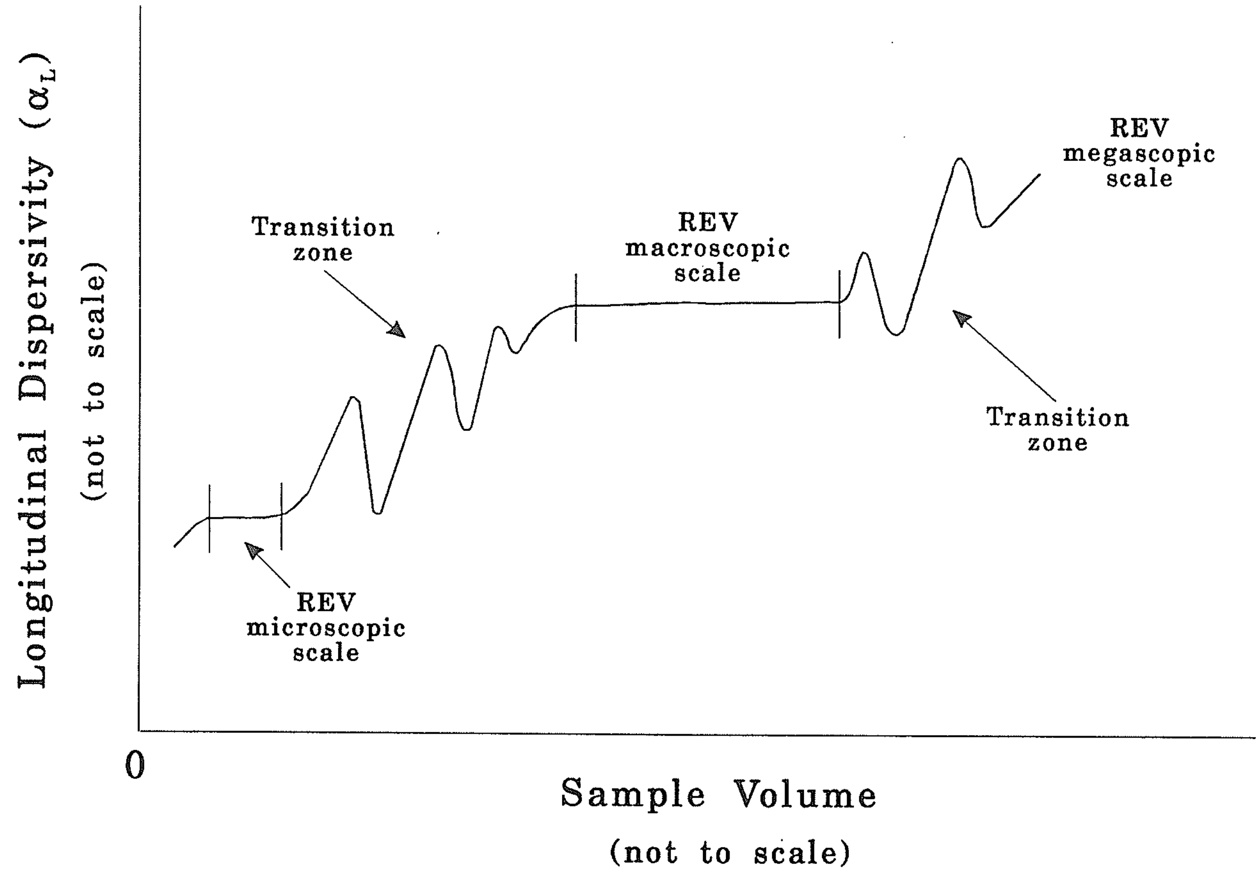

Figure 1.1 An example of the relationship between longitudinal dispersivity (α_L) and sample volume with the REVs defined at the microscopic and macroscopic scale (after Dominico and Schwartz, 1990).

variability of the hydraulic conductivity field. However, as pointed out by Mackay et al. (1986), the use of data from known contaminated sites is often not feasible since:

1. It is difficult to quantify the initial mass of contaminant that entered the groundwater and to locate the contaminant source precisely in time and space;
2. Practical constraints (e.g. cost and time) usually result in relatively sparse monitoring data for the plume which only allow approximate delineation of contaminant distribution as a function of space and time.

As a result, carefully conducted field experiments provide the best method for validating theory and for gaining insight into the behavior of contaminants in the subsurface. Due to the long duration of these tests (particularly natural gradient tests) and, environmental and financial constraints, large scale field experiments cannot be carried out routinely. Fortunately, during the last two decades a small number of natural gradient field experiments have been conducted by various research groups. Among the experimental sites are the Borden aquifer (Sudicky et al., 1983; see also Mackay et al., 1986), the Columbus Airforce Base site (Rehfeldt, 1988; see also Gelhar et al., 1992) and the Cape Cod site (LeBlanc et al., 1991). The aim of these field experiments was to provide a detailed data base describing the transport, transformation and fate of a variety of contaminants in the saturated zone. The results obtained from these experiments have confirmed that:

1. Dispersivity is influenced by the distance travelled (Sauty, 1980) and increases with time (Dieulin, 1980);

2. The dependence of the longitudinal asymptotic macrodispersivity[3] on aquifer heterogeneity (Gelhar and Axness, 1983);

Results obtained from these experiments have also revealed that none of the stochastic theories of transport based on steady state flow accurately predict solute spread in the transverse direction. In addition, it is found that the three-dimensional time dependent moment model of Dagan (1988) over predicts the longitudinal spread and under predicts the transverse spread (see Woodbury and Sudicky, 1991). These issues, and in particular the former issue, will be discussed in more detail in the following section.

1.2 The Problem

Application of the stochastic transport theory of Gelhar and Axness (1983) by Sudicky (1986) to Stanford-Waterloo experiment data at the Borden aquifer resulted in a transverse horizontal asymptotic macrodispersivity[4] value of 0.0m. Based on a spatial moment analysis performed by Freyberg (1986) on actual chloride and bromide plume data collected as part of the experiment, a value of 0.039m was obtained for the apparent asymptotic transverse horizontal macrodispersivity. This estimate is supported by the apparent transverse horizontal asymptotic macrodispersivity value of 0.05m computed as part of an independent review of the bromide plume data by Rajaram and Gelhar (1991).

---

[3] The term "longitudinal asymptotic macrodispersivity" refers to the asymptotic value of the field scale dispersivity along the mean flow direction.

[4] The term "transverse horizontal asymptotic macrodispersivity" refers to the asymptotic value of the field scale dispersivity in the plane which is perpendicular to the mean flow direction.

Application of three-dimensional moment models by Naff (1990), Zhang and Neuman (1990), and Woodbury and Sudicky (1991) all produce less than satisfactory results, particularly in the transverse direction, when compared to the moments computed by Freyberg (1986) from the tracer plumes. A number of researchers have suggested that this transverse dispersion, particularly at the Borden site, may in part be due to the presence of known flow transients (see Sykes et al., 1982; and Sudicky, 1986). The stochastic transport theories of Gelhar and Axness (1983) and Dagan (1982, 1984, 1987 and 1988) do not take transients in the flow field into consideration. Kinzelbach and Ackerer (1986), and Goode and Konikow (1990) have shown from a deterministic perspective that variations in the groundwater flow direction cause an enhancement of transverse horizontal dispersion. Sudicky (1986) suggested that the main features of the enhanced dispersion caused by flow transients might be handled in a practical way by incorporating the unsteady flow behavior into a coupled fluid/transport model in which the macrodispersivities are estimated using steady state flow expressions. In this approach the stochastic theories of Gelhar and Axness (1983) are used to account for the material heterogeneity. Rehfeldt (1988) pointed out a number of potential problems with this approach.

1. The transients can be represented as a stochastic process in time and are composed of a number of components of various amplitudes and frequencies. To model the high frequency components one would have to use a small time step in say, a classic finite element scheme. A short time step coupled with long simulation time would yield a computationally intensive exercise.

2. Low frequency components of the transients could be treated as deterministic while high frequency components could be treated as random. How does one differentiate the deterministic from the random components in the model?
3. Does unsteady behavior cause dispersion?

The work of Gelhar and Axness has been extended by Rehfeldt (1988) to account for the presence of transients in the flow field. Rehfeldt's work does show that unsteady flow behavior can result in an enhanced dispersion. However, his work examines only the asymptotic macrodispersivity, at which time the dispersion process is Fickian[5]. Under the Fickian assumption the concentration distribution within the plume displays a normal distribution. To account for spread at pre-asymptotic times, Naff et al. (1989) proposed a deterministic time-dependent model for predicting the spreading moments under unsteady flow conditions. Both approaches have been applied to the Stanford-Waterloo tracer data using crude estimates of the necessary flow field parameters (see Rehfeldt, 1988; Naff et al., 1989). The results obtained using both models are encouraging; however, it should be noted that the model parameters relating to the flow transients were chosen on an ad hoc basis for illustrative purposes because detailed waterlevel data were unavailable at the time.

A further feature of standard modelling practice of contaminant plumes is the use of a transport model which assumes that the contaminant flux is Fickian and constant.

---

[5] The term "Fickian" refers to the case where the dispersive mass flux is proportional to the concentration gradient (Gelhar et al., 1992).

Naff (1990), based on a theoretical study of the dispersive flux in saturated porous media, suggests that this approach is reasonable provided that the prediction of the mean concentration is at distances from the source equivalent to at least 20 length scales, λ of the hydraulic conductivity. Points separated by a distance less than λ will have similar hydraulic conductivities and those separated by a distance greater than λ can be expected to have significantly differing hydraulic conductivities. Within a distance of 20 λ from a source Naff (1990) points out that two deviations from Fickian behavior will occur. First, the second moments[6] of the plume will be overestimated and second, the plume shape will be platykurtic (flatter than a normal distribution). Also, the observed skew will be negative. Based on a theoretical study of macrodispersion in perfectly stratified aquifers Gelhar et al. (1979), also found that plumes tend to be platykurtic at early times. However, Gelhar et al. (1979) found that the skew at early times was positive and was an important feature in the deviation of the plume from a normal distribution. This latter result contradicts the findings of Naff (1990). From a volumetric averaging perspective Tompson (1988) also showed small positive skews for a transport problem posed at the local level, and this result supports the theoretical findings of Gelhar et al. (1979). It should be emphasized that the approaches applied by Gelhar et al. (1979), Tompson (1988) and Naff (1990) were different. These approaches will be described later in this thesis. To date, little work has been done with regards to examining the skew and kurtosis of plumes for any of the tracer experiments discussed even though adequate data bases exist for such a study. As a result, the theoretical result of Gelhar et al. (1979) and

---

[6] The term "second moment" refers to second spatial moment of a contaminant plume that had an initial condition of a pulse.

Naff (1990) have not been field validated.

1.3 Objectives and Scope

The first part of this thesis will address the former problem as outlined above. Specifically, the influence of flow transients on the transverse spread of a plume will be looked at. Waterlevel data for the Borden site has been collected during the period July 25, 1989 to January 15, 1991. Using least squares methods, the mean spatial hydraulic gradient at each waterlevel sample period is computed. The hydraulic gradient time series is used as inputs to the Naff et al. (1989) model. Using geostatistical methods the necessary statistical parameters relating to the hydraulic gradient needed for the model of Rehfeldt (1988) are estimated. Assuming stationarity in time and space, the result obtained from these two models is compared with the observed asymptotic macrodispersivity estimates obtained for the Stanford-Waterloo experiment. This comparison provides a means of determining whether the proposed models explain the enhanced plume dispersion in the horizontal transverse direction at the Borden site.

In the second part of this thesis the latter problem as outlined in the previous section is addressed. Specifically, to perform this analysis the concentration data collected for the 1978 Borden tracer experiment are used. An approach similar to that employed by Freyberg (1986), and Rajaram and Gelhar (1991) is carried out. Due to truncation of the plume by the sampling devices and the irregular spacing of these devices, both interpolation and extrapolation of the concentration data will be required in order to perform the moment estimates. In this work, the fourth and lower order moments are emphasized. From these moments the solute mass, macrodispersivity, and skew and kurtosis of the concentration distribution in the plume as a function of time are estimated. Particular attention will be placed on the following aspects:

1. Sensitivity of the moment estimates to the various interpolation and extrapolation schemes used;
2. Comparison of the velocity and macrodispersivity estimates to those of Sudicky et al. (1983) for this experiment. In addition these values are compared to those of Freyberg (1986) and Rajaram and Gelhar (1991) for the Stanford-Waterloo experiment;
3. Comparison of the computed skew and kurtosis with the theoretical results of Gelhar et al. (1979) and Naff (1990).

In addition, the estimated transverse horizontal asymptotic macrodispersivity for the 1978 Borden tracer experiment is compared to the transverse horizontal asymptotic macrodispersivity computed for Stanford-Waterloo experiment (see Freyberg, 1986; also Rajaram and Gelhar, 1991). Note that if the transverse dispersion at both Borden sites is caused by transients in the flow field then the two transverse horizontal asymptotic macrodispersivities computed at each site should agree. Therefore, this comparison provides an estimation as to whether or not the flow field at the Borden site is stationary in time.

References

Bear, J., Dynamics of Fluids in Porous Media, Elseiver Science, New York, 1972.

Dagan, G., Stochastic modelling of groundwater flow by unconditional and conditional probabilities, 2, The solute transport, Water Resour. Res., 18(4), p. 835-848, 1982.

Dagan, G., Solute transport in heterogeneous porous formations, J. Fluid Mech., 145, p. 151-177, 1984.

Dagan, G., Theory of solute transport in groundwater, Ann. Rev. Fluid. Mech., 19, p. 183-215.

Dagan, G., Time-dependent macrodispersion for solute transport in anisotropic heterogeneous aquifers, Water Resour. Res., 24(9), p. 1491-1500, 1988.

Dieulin, A., Propagation de pollution dans un aquifère alluvial: l'effet de parcours, D. Ing. Thesis, University of Sciences and Medicine of Grenoble, Grenoble, 1980.

Elder, V. A., B. L. Proctor, and R. A. Hites, Organic compounds found near dump sites in Niagara Falls, New York, Environ, Sci. Technol., 15(10), p.1237-1242, 1981.

Freyberg, D. L., A natural gradient experiment on solute transport in a sand aquifer; 2. Spatial moments and the advection and dispersion of nonreactive tracers, Water Resour. Res., 22(13), p. 2031-2046, 1986.

Garabedian, S. P., D. R. LeBlanc, L. W. Gelhar, and M. A. Celia, Large scale natural gradient tracer test in sand and gravel, Cape Cod, Massachusettes: 2. Analysis of spatial moments for a non-reactive tracer, Water Resour. Res., 27(5), p. 911-

924, 1991.

Gelhar, L. W., and C. L. Axness, Three-dimensional stochastic analysis of macrodispersion in aquifers, Water Resour. Res., 19(1), p. 161-180, 1983.

Gelhar, L. W., A. L. Gutjahr, and R. L. Naff, Stochastic analysis of macrodispersion in a stratified aquifer, Water Resour. Res., 15(6), p. 1387-1397, 1979.

Gelhar, L. W., A. Montoglou, C. Welty, and K. R. Rehfeldt, A review of field-scale physical solute transport processes in saturated and unsaturated porous media, Final Proj. Rep. EPRI EA-4190, Elec. Power Res. Inst., Palo Alto, Calif., 1985.

Gelhar, L. W., C. Welty, and K. Rehfeldt, A critical review of data on field-scale dispersion in aquifers, Water Resour. Res., 28(7), p. 1955-1974, 1992.

Guerera, A. A., Chemical contamination of aquifers on Long Island, New York, J. Am. Water Works Assoc., 73, p. 190-199, 1981.

Goode, D. J. and Konikow, L. F., Apparent dispersion in transient groundwater flow, Water Resour. Res., 26(10), 2339-2351, 1990.

Kinzelbach, W. and Ackerer, P., Modelisation de la propagation d'un contaminant dans un champ d'ecoulement transitoire, Hydrogeologie, 2, 197-205, 1986.

LeBlanc, D. R., S. P., Garabedian, K. M. Hess, L. W. Gelhar, R. D. Quadri, K. G. Stollenwerk, and W. W. Wood, Large-scale natural gradient tracer test in sand and gravel, Cape Cod, Massachusetts, 1, Experimental design and observed tracer movement, Water Resour. Res., 27(5), p. 895-910, 1991.

Mackay, D. M., D. L. Freyberg, P. V. Roberts, J. A. Cherry, A natural gradient experiment on solute transport in sand a aquifer, 1. Approach and overview of plume movement, Water Resour. Res., 22(13), p. 2017-2029, 1986.

Naff, R. L., On the nature of the dispersive flux in saturated heterogeneous porous media, Water Resour. Res., 26(5), p. 1013-1026, 1990.

Naff, R. L., Yeh, J. T. -C. and Kemblowski, M. W., Reply, Water Resour. Res., 25(12), p. 2523-2525, 1989.

O'Connor, M. J., and L. W. Bouchout, Gasoline spills in urban areas: A comparison of two case histories, Seminar on Groundwater and Petroleum Hydrocarbons, Protection, Detection, Restoration, Ottawa, Proc.: Petroleum Assoc. for Conservation of the Canadian Environment, p. VIII-1 to VIII-34.

Rajaram, H., and L. W. Gelhar, Three-dimensional spatial moments analysis of the Borden tracer test, Water Resour. Res., 27(6), p. 1239-1251, 1991.

Rehfeldt, K. R., Prediction of macro-dispersivity in heterogeneous aquifers, Ph. D. dissertation, MIT, 1988.

Sauty, J. P., An analysis of hydrodispersive transfer in aquifers, Water Resour. Res., 16, p. 145-158, 1980.

Sudicky, E. A., A natural gradient experiment on solute transport in a sand aquifer: Spatial variability of hydraulic conductivity and its role in the dispersion process, Water Resour. Res., 22(13), p. 2069-2082, 1986.

Sudicky, E. A., J. A. Cherry, and E. O. Frind, Migration of contaminants in groundwater at a landfill: A case study: 4. A natural gradient dispersion test, Journal of Hydrology, 63, p. 81-108, 1983.

Sykes, J. F., S. B. Pahwa, R. B. Lantz, S. D. Ward, Numerical simulation of flow and contaminant migration at an extensively monitored landfill, Water Resour. Res., 18(6), p. 1687-1704, 1982.

Tompson, A. F. B., On a new functional form for the dispersive flux in porous media, Water Resour. Res., 24(11), p. 1939-1947, 1988.

Woodbury, A. D., and E. A. Sudicky, The geostatistical characteristics of the Borden aquifer, Water Resour. Res., 27(4), p. 533-546, 1991.

Zhang, Y. -K., and S. P. Neuman, A quasi-linear theory of non-Fickian and Fickian subsurface dispersion, 2, Application to anisotropic media and the Borden site, Water Resour. Res., 26(5), p. 903-913, 1990.

Chapter 2

A Geostatistical Analysis of Fluctuating Waterlevels at the Borden Aquifer

2.1 Introduction

As part of the overall Stanford-Waterloo tracer experiment, Sudicky (1986) applied the stochastic theories of Gelhar and Axness (1983) and Dagan (1986) in order to predict the dispersion of the injected tracer which had been measured over a three year period. Based on a geostatistical analysis of the hydraulic conductivity field and field observed hydraulic gradients, Sudicky (1986) estimated the asymptotic horizontal transverse macrodispersivity to be 0.0m and the asymptotic longitudinal macrodispersivity to be 0.61m, keeping in mind that these values must be augmented by the corresponding components of the local scale dispersivity. However, a moment analysis performed by Freyberg (1986) on the actual chloride and bromide plume data collected at the site yielded an asymptotic horizontal transverse macrodispersivity equal to 0.039m, and an asymptotic longitudinal macrodispersivity equal to 0.36m. An independent re-analysis of the bromide plume data performed by Rajaram and Gelhar (1991) yielded an asymptotic horizontal transverse macrodispersivity equal to 0.05m, thus confirming Freyberg's calculations. In addition, attempts at applying three-dimensional moment models by Woodbury and Sudicky (1991), Naff et al. (1988, 1989), and Zhang and Neuman (1990) all produced less than satisfactory results, particularly in the transverse direction, when compared to the moments computed by Freyberg (1986) from the tracer plumes. Sudicky (1986) suggested that the enhancement to the observed horizontal transverse dispersion could be due to the presence of groundwater flow transients at the site. Sudicky's conjecture was supported by the earlier work of Sykes et al. (1982), who suggested that much of the observed horizontal transverse dispersion at the Borden landfill was caused by a time-varying potentiometric surface. In addition, Kinzelbach and Ackerer (1986) and Goode and Konikow (1990) have shown from a deterministic perspective that variations in the groundwater flow direction cause enhancement of horizontal transverse dispersion. The presence of such flow transients are not accounted for in the stochastic models of Dagan [1986 (unpublished manuscript) and 1988] and Gelhar and Axness (1983).

Recently, Rehfeldt (1988) extended the work of Gelhar and Axness (1983) to account for the enhanced asymptotic macrodispersivity which results from the presence of transients in a flow field. To account for spread at pre-asymptotic times, Naff et al. (1989) proposed a deterministic time-dependent model for predicting the spreading moments at a site where flow transients are observed. Both approaches have been applied to the Borden tracer test data to model the observed transverse spread using crude estimates of the necessary flow field parameters (see Rehfeldt, 1988; Naff et al., 1989). The results of both approaches compare reasonably well to Freyberg's data for the Borden plume; however, it should be noted that model parameters relating to the flow transients, in particular those of Naff et al. (1989), were chosen on an ad hoc basis for illustrative purposes because detailed waterlevel data were unavailable at the time.

Recent work at the Borden aquifer involving an emplaced source experiment (Figure 2.1) has resulted in the regular collection of watertable elevation data in a part of the aquifer for the period July 25, 1989 to January 15, 1991. The aim of this thesis is to use this waterlevel data to investigate whether the models proposed by Rehfeldt (1988) and Naff et al. (1989) explain the enhanced plume dispersion in the horizontal transverse direction at the Borden site. Specifically the approach proposed will be to:

1. Outline which parameters are required by the two models;
2. Use the waterlevel data to obtain the parameters required by the two models and their relative uncertainties;
3. Substitute these parameters into the models;
4. Assume stationarity and compare the results of point 3 above to the published results for the Borden plume.

2.2 Theory

2.2.1 Asymptotic Analysis of Dispersion

Rehfeldt's (1988) approach assumes that the macrodispersive flux is Fickian in nature. In addition, the hydrogeologic properties along with the concentration of the solute,the specific discharge, and the hydraulic head are treated as random variables. These quantities are decomposed into mean components and perturbations about the mean. The perturbed terms are assumed to have zero expectation. As a result

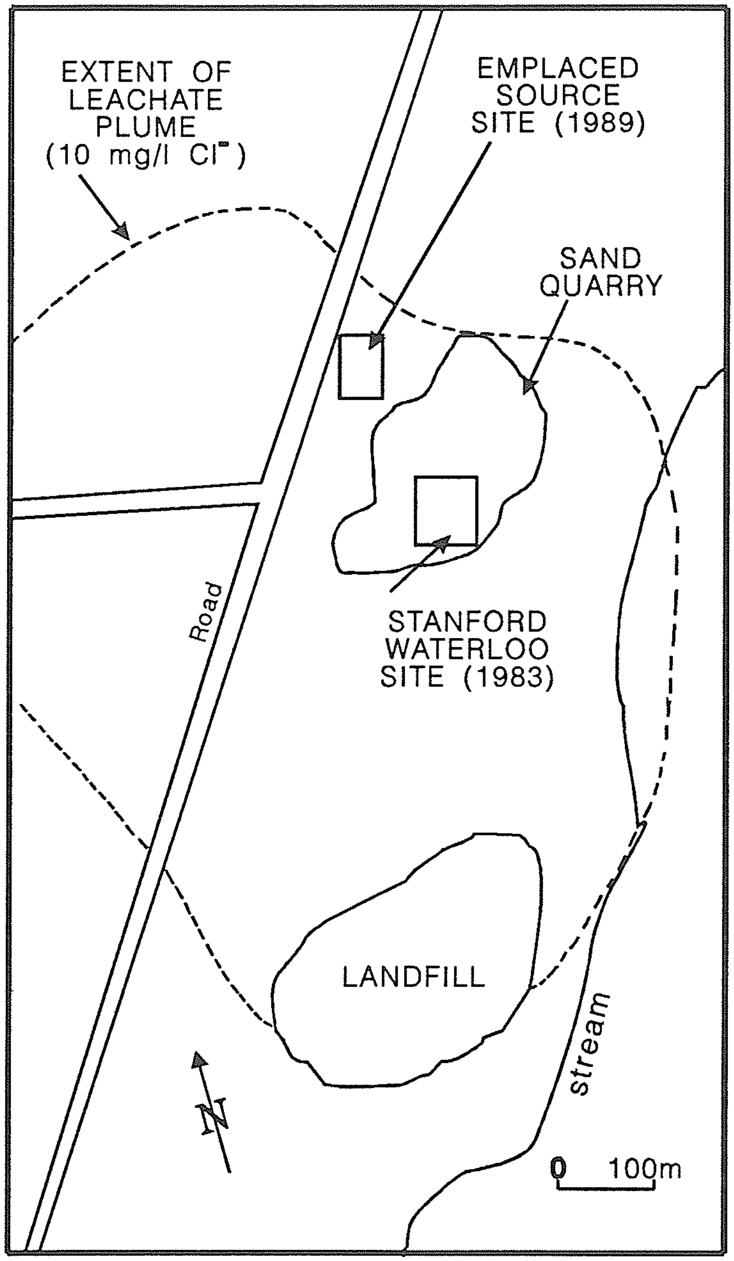

Figure 2.1. Map of the Borden Tracer-Test site.

$$c=\bar{c}(x_i,t)+c'(x_i,t) \qquad \ldots(2.1)$$

$$q=\bar{q}(x_i,t)+q'(x_i,t) \qquad \ldots(2.2)$$

$$ln(K)=F+f, \quad F=E[lnK], \quad E[f]=0 \qquad \ldots(2.3)$$

$$\phi(x,t)=\bar{H}(x,t)+H'(x,t)+h(x,t) \qquad \ldots(2.4)$$

where c represents the solute concentration, q is the specific discharge and K is the hydraulic conductivity. In Rehfeldt's approach, ϕ is the observed hydraulic head, $\bar{H}$ represents the slowly varying ensemble mean hydraulic head in space and time, H' is a temporal perturbation about the mean hydraulic head, and h represents local perturbations in space and time. Therefore,

$$H(x,t)=\bar{H}(x,t)+H'(x,t) \qquad \ldots(2.5)$$

In the above H(x,t) combines the slowly varying ensemble mean hydraulic head in time and space as well as the temporal perturbation about the mean hydraulic head. As a result, H(x,t) represents the ensemble mean hydraulic head in space at any time. The analysis in this chapter principally revolves around determining $H(x,t_1,t_2,\ldots)$ over a discrete set of time samplings $t_1,t_2,\ldots$. It will be shown in this chapter that at the Borden site h(x,t) is uncorrelated in space and time. H(x,t) however, is correlated in time and it is the statistical properties of this variable that will be shown to principally control the spread of the Borden tracer mass in the horizontal transverse direction. The hydraulic gradient is represented as

$$-\frac{\partial \bar{H}}{\partial x_i}=\bar{J}_i \qquad \ldots(2.6a)$$

and

$$-\frac{\partial H'}{\partial x_i}=J_i' \qquad \ldots(2.6b)$$

The perturbation J′ is assumed to be random in time, but on the local scale (because of its planar like features) constant in space. Note also $J=\bar{J}+J'$.

The approach used by Rehfeldt (1988) to determine an expression for the form of the component of macrodispersivity due to the unsteady mean behaviour of the flow field is outlined in Appendix A. The approach is similar in principle to the small perturbation method used by Gelhar and Axness (1983). However, Rehfeldt's method differs from that of Gelhar and Axness (1983) in that it treats the specific discharge spectrum as being a function of time and space. The method is able to reproduce the result of Gelhar and Axness (see Gelhar and Axness 1983, equation 62; see also Rehfeldt 1988, equation 2-39) plus an additional term which gives the mean unsteady form of the macrodispersivity (see Appendix A). The unsteady term is reduced to

$$A_{ij}^{(u)}=\frac{1}{\gamma^2}\frac{q\pi}{n\bar{J}_1^2}S_{J_iJ_j}(0) \qquad (2.7)$$

where $A_{ij}^{(u)}$ represents the unsteady component of the macrodispersivity tensor, $\bar{J}_1$ is the mean gradient magnitude in the flow direction, γ is the flow factor term defined by Gelhar and Axness (1983), and $S_{J_iJ_j}(0)$ is the gradient spectrum evaluated at zero frequency. The unsteadiness in the flow field is contained in the gradient spectrum. By making use of the spectra-covariance transform and assuming that the cross- and auto-covariance functions are exponential in form, the gradient spectrum reduces to

$$S_{J_iJ_j}(0)=\frac{1}{\pi}\sigma^2_{J_iJ_j}\ \lambda_{J_iJ_j} \qquad \ldots(2.8)$$

Here $\sigma_{J_iJ_j}{}^2$ represents the covariance and $\lambda_{J_iJ_j}$ represents the correlation or integral scale of the time variation of J. Finally, the unsteady component of the macrodispersivity tensor can be expressed as

$$A_{ij}^{(u)}=\frac{1}{\gamma^2}\frac{q}{n}\frac{\sigma^2_{J_iJ_j}}{\bar{J}_1^2}\lambda_{J_iJ_j} \qquad \ldots(2.9)$$

Rehfeldt (1988) has shown that equation (2.9) results in an enhanced horizontal transverse asymptotic macrodispersivity while contributing little to the longitudinal direction.

In order to apply equation (2.9) to the Borden tracer data, additional assumptions have been made to reduce equation (2.9) to a more manageable form. Freyberg (1986) showed that the mean angular offset $\bar{\Gamma}$ (see Figure 2.2), between the mean gradient direction and the horizontal trajectory of the tracer plumes is less than 2°. For the purpose of this analysis we shall then set $\bar{\Gamma}$ equal to zero due to its small magnitude. The gradient data given by Sudicky (1986) shows that the maximum angular deviation Γ_{max}, between the horizontal trajectory of the plumes and the maximum gradient deflection is approximately 9°. Sudicky (1986) indicates that the vertical gradient at the tracer site is

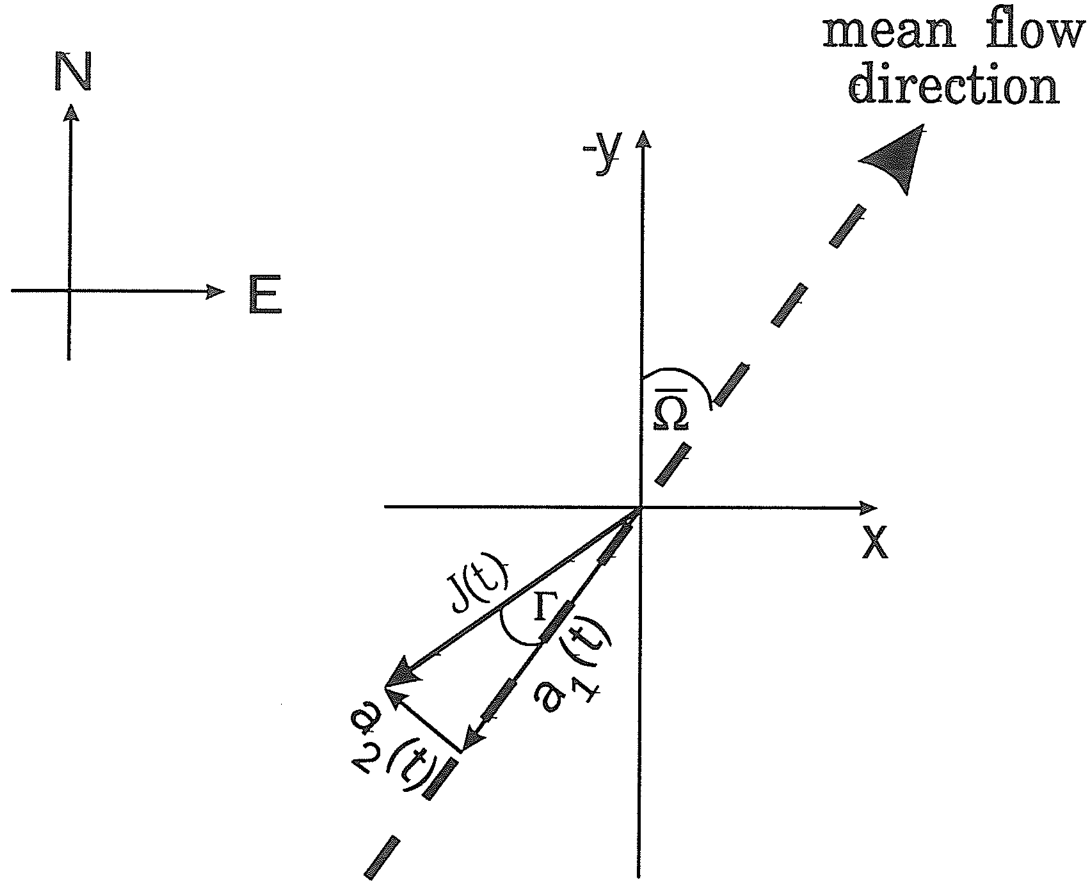

a1(t) = component of hydraulic head parallel to the mean flow path.
a2(t) = component of hydraulic head perpendicular to the mean flow path.
J(t) = hydraulic head gradient at time t.
x, y = cartesian coordinate axes.
Ω = mean flow angle.
Γ = angle between mean flow direction and the hydraulic gradient.

Figure 2.2. Schematic of the flow field at the Borden site.

approximately two orders of magnitude smaller than the horizontal gradient. Therefore, the contribution of the vertical gradient can be considered to be negligible (i.e. $J_3=0$). These assumptions along with the small size of Γ_{max}, allow equation (2.9) (see also Rehfeldt (1988), equations 2-53 and 2-62) to be reduced to

$$A_{11}^{(u)}=\frac{1}{\gamma^2}\frac{q}{n}\frac{\sigma_J^2}{\bar{J}^2}\lambda_J \qquad \text{...(2.10)}$$

$$A_{22}^{(u)}=\frac{1}{\gamma^2}\frac{q}{n}\sigma_\Gamma^2\lambda_\Gamma \qquad \text{...(2.11)}$$

where $A_{11}^{(u)}$ and $A_{22}^{(u)}$ give the longitudinal and horizontal transverse asymptotic macrodispersivities which result from the mean flow transients and the subscripts J and Γ indicate gradient magnitude and flow angle parameters respectively. For the Borden site the variance and integral scale for both the flow angle and the gradient magnitude data are unknown parameters which must be determined from observed watertable data.

2.2.2 Harmonic-Moment Evolution Model

As described above, Rehfeldt's (1988) approach only addressed dispersion behaviour at asymptotic time and, of course is only valid after a tracer plume has been effectively averaged over a number of hydraulic conductivity and non-steady gradient integral scales. The reader should recall that attempts to model the early time behaviour of Freyberg's (1986) second moment data using approaches such as Dagan's (1988) three dimensional model, have produced poor results (see Woodbury and Sudicky, 1991). Naff et al. (1988) have proposed a deterministic moment model which accounts for an unsteady mean flow field. However, their model ignores the effects of variations in the hydraulic conductivity field on the dispersion process. The unsteadiness in the flow field is represented deterministically as the sum of a series of harmonic functions. The most important harmonics are at the long wavelengths (low frequencies).

A general form of the velocity equation given by Naff et al. (1989, equation 2) is

$$U_i(x,t) = \frac{K_i}{n}\left[\delta_{1i}\bar{J}_1 + g_i(t)\right] \qquad \ldots(2.12)$$

where $U_i(x,t)$ is the velocity field in the i^{th} direction, $\bar{J}_1$ is the mean gradient in the x_1 direction (along mean flow path), K_i is the hydraulic conductivity in the i^{th} direction, n is the porosity and $g_i(t)$ represents the unsteady mean behaviour in the i^{th} direction of the gradient field. The model requires that $g_i(t)$ be expressed as the sum of a series of harmonic functions. Hence a harmonic analysis on an observed time signal must be performed to find the wavelengths and amplitudes present in $g_i(t)$.

Let $G_i(f)$ be the frequency spectrum of $g_i(t)$. Then the following relationships, given by Brigham (1974, chap.2), can be applied

$$g_i(t) = \int_{-\infty}^{\infty} G_i(f) e^{i\omega_f t} df \qquad \ldots(2.13)$$

$$G(f) = A(f) e^{i\alpha(f)} \qquad \ldots(2.14)$$

where A(f) is the amplitude at frequency f, α(f) is the phase at frequency f, and ω is the angular frequency. Combining (2.13) and (2.14) gives

$$g_i(t)=\int_{-\infty}^{\infty} A_i(f)e^{i[\omega_i t+\alpha_i(f)]}df \qquad \text{...(2.15a)}$$

or

$$g_i(t)=\int_{-\infty}^{\infty} A_i(f)\{\cos[\omega_i(t)+\alpha_i(f)]+i\ \sin[\omega_i(t)+\alpha_i(f)]\}df \qquad \text{...(2.15b)}$$

The second integrand in equation (2.15b) is an odd function and hence its contribution to the integral is zero. Using a discrete representation equation (2.15b) reduces to

$$g_{im}(t)=\sum_{m=1}^{N} A_{im}\cos(\omega_{im}t+\alpha_{im}) \qquad \text{...(2.16)}$$

where m represents the mth frequency harmonic and N represents the total number of harmonics present. The ω_{im} term can be shown to be of the form

$$\omega_{im}=2\pi\bar{U}_1\frac{t}{l_{im}} \qquad \text{...(2.17)}$$

where Naff et al. (1989) defined l_{im} to be the attendant travel length associated with the mth harmonic and $\bar{U}_1$ as the mean velocity in the x_1 direction. Equation (2.16) is similar in form to the integrand in Naff et al. (1989, equation 6) with the difference being the addition of a phase shift term.

The displacement $X_i(t)$ and spatial variance σ_{ii} of a tracer plume in the ith direction due to a time-varying flow direction is given by Naff et al. (1989) as

$$X_i(t) = B_i \overline{U}_1 \int_0^t \sum_{m=1}^{N} A_{im} \cos(2\pi \overline{U}_i \frac{t}{l_{im}} + \alpha_{im})\ dt \qquad ...(2.18)$$

$$\sigma_{ii} = t^{-1} \int_0^t [X_i(t)]^2\ dt \qquad ...(2.19)$$

where $B_i = (\bar{J}_1 K_i)/(\bar{U}_1 n)$. Equation (2.19) is integrated numerically since X(t) is generally a complicated function.

As mentioned earlier, the harmonics needed for this model are unknown and must be determined by conducting a harmonic analysis on the watertable gradient data. For the purpose of this work, the interest is in assessing the horizontal transverse spread of the tracer at the Borden site. As a result it will be necessary to compute the harmonics present in the a_2 gradient component (see Figure 2.2).

In the next section a decomposition of the watertable data measured at the Borden site will be performed in order to determine the parameters needed for the proposed models. The proposed approach will be to:

1. Determine the spatial trend in the waterlevel data;
2. Use the trend information to compute the mean gradient magnitude and the mean flow direction time series for the data;
3. Perform a geostatistical analysis on the time series computed in point 2 above, to determine the variance and integral scales present;
4. Compute the harmonics present in the gradient data.

2.3 Waterlevel Data Analysis

2.3.1 Field Data

The watertable data used for this study were collected at the site of an emplaced source experiment conducted in the Borden aquifer from July 25, 1989 to January 15, 1991. The experiment site is located about 150m north of the 1986 tracer test site (Figure 2.1). Piezometers were installed at the site to measure the watertable elevation in the vicinity of a migrating plume (associated with the emplaced source experiment). Initially only two piezometers were used, but as the plume evolved, additional piezometers were installed with the final number increasing to 34. Watertable elevations in each piezometer were recorded on average once a week. Figures 2.3, 2.4 and 2.5 show the watertable elevation time series recorded by three piezometers (P2, P13 and P24) at the site.

The observed watertable elevation time series at each piezometer (Figures 2.3, 2.4 and 2.5) displays a cyclic character, with short wavelength features being superimposed on a much longer wavelength feature. The period of this long wavelength feature appears to be between 340 and 370 days at all the piezometers. The maximum magnitude of the watertable fluctuations is approximately 0.8m. When an observed time series for individual piezometers located in different parts of the site are compared, an obvious correlation is apparent. This suggests that the watertable surface at the emplace source site may be decomposed into simple forms in time and space.

Contour maps of the watertable elevations at each recording time for a portion of the domain (for example, Figure 2.6 and 2.7) show that the watertable surface is approximately planar. These maps indicate that the general flow direction is

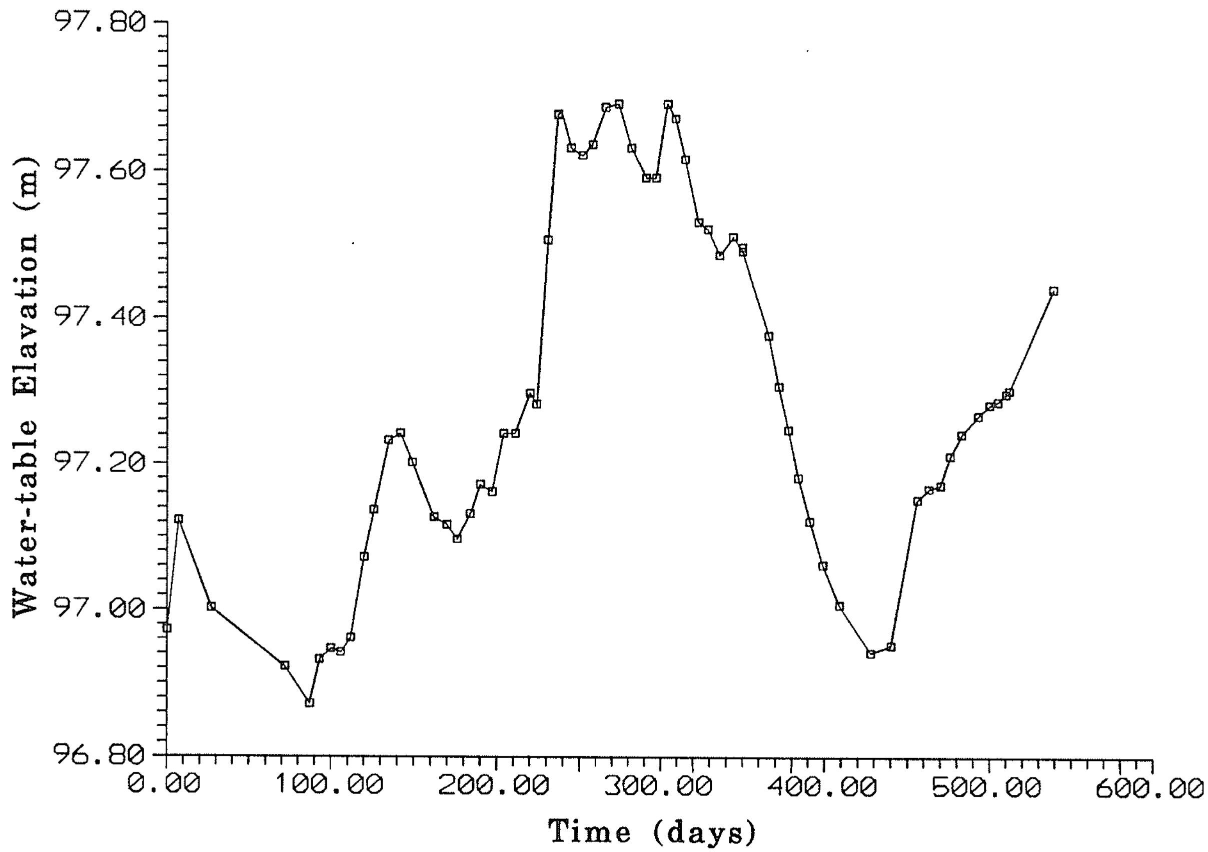

Figure 2.3 Observed water-table elevation time series at piezometer P2.

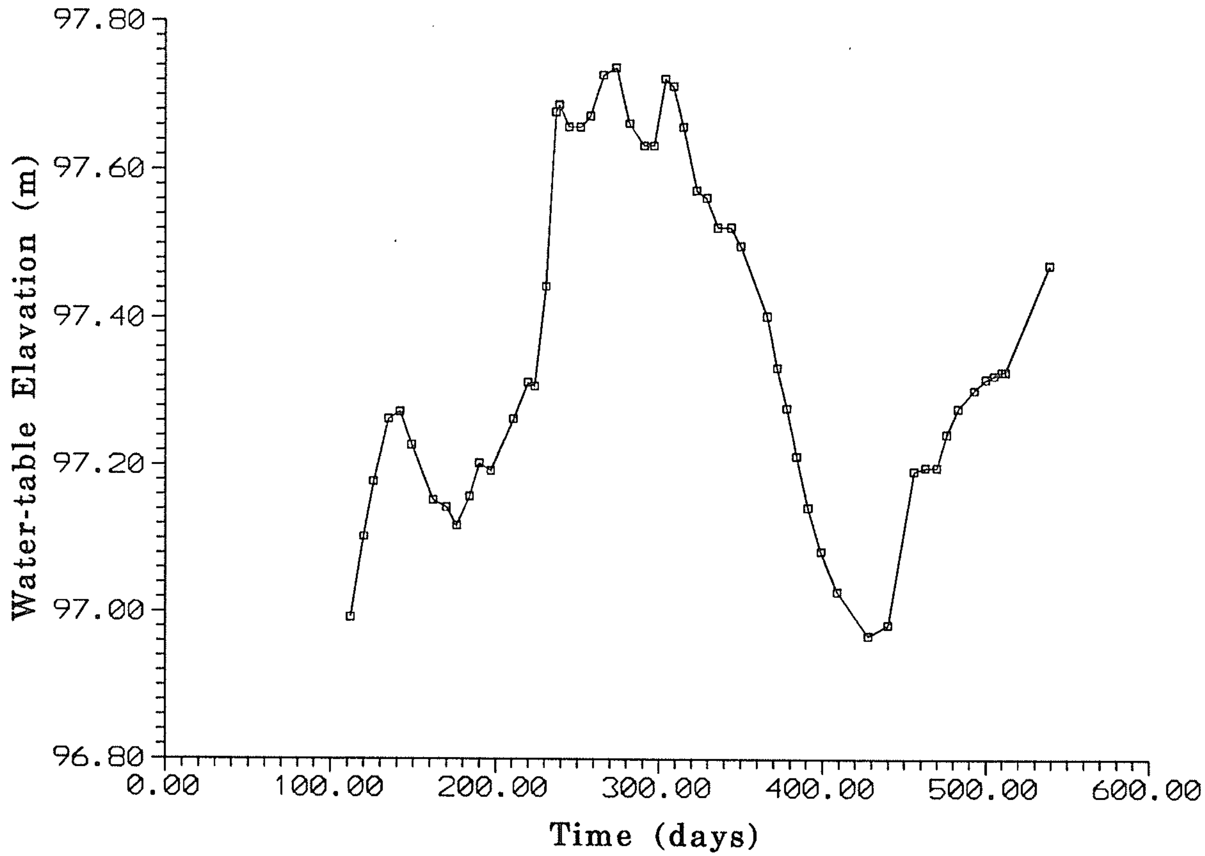

Figure 2.4 Observed water-table elevation time series at piezometer P13.

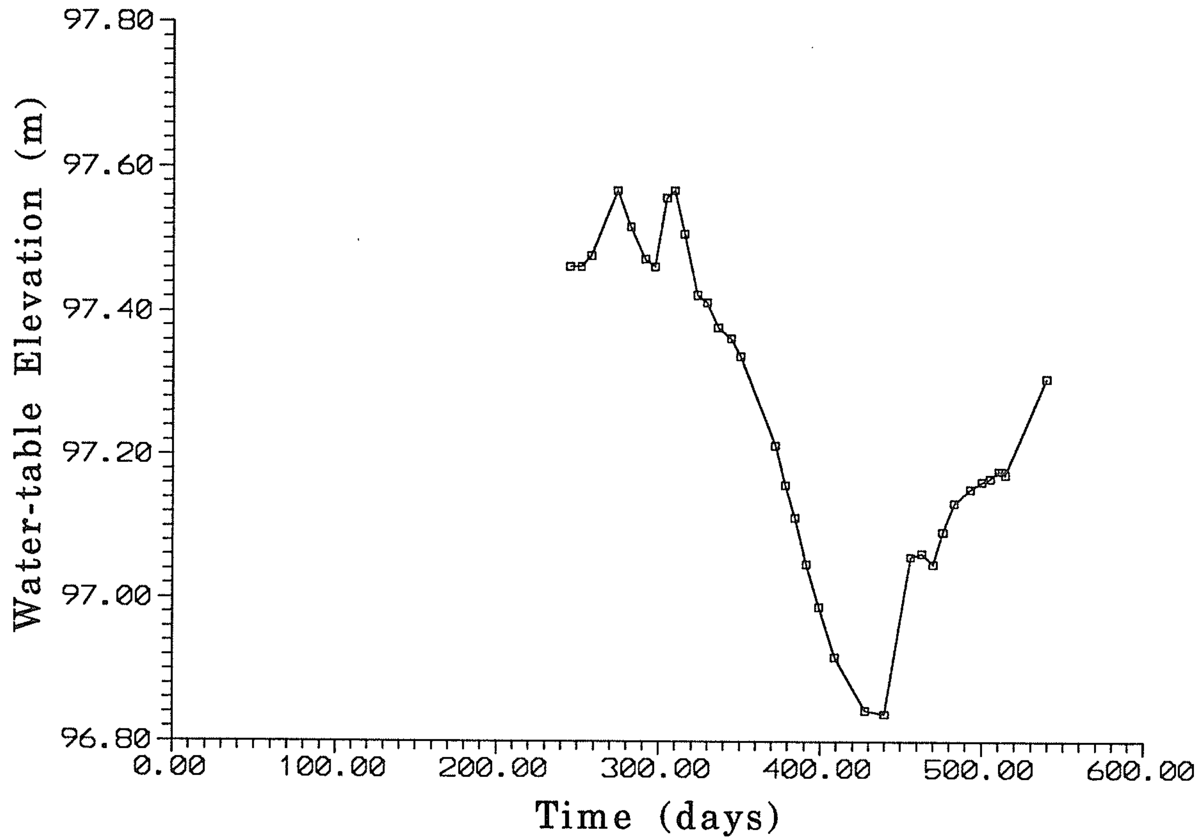

Figure 2.5 Observed water-table elevation time series at piezometer P24.

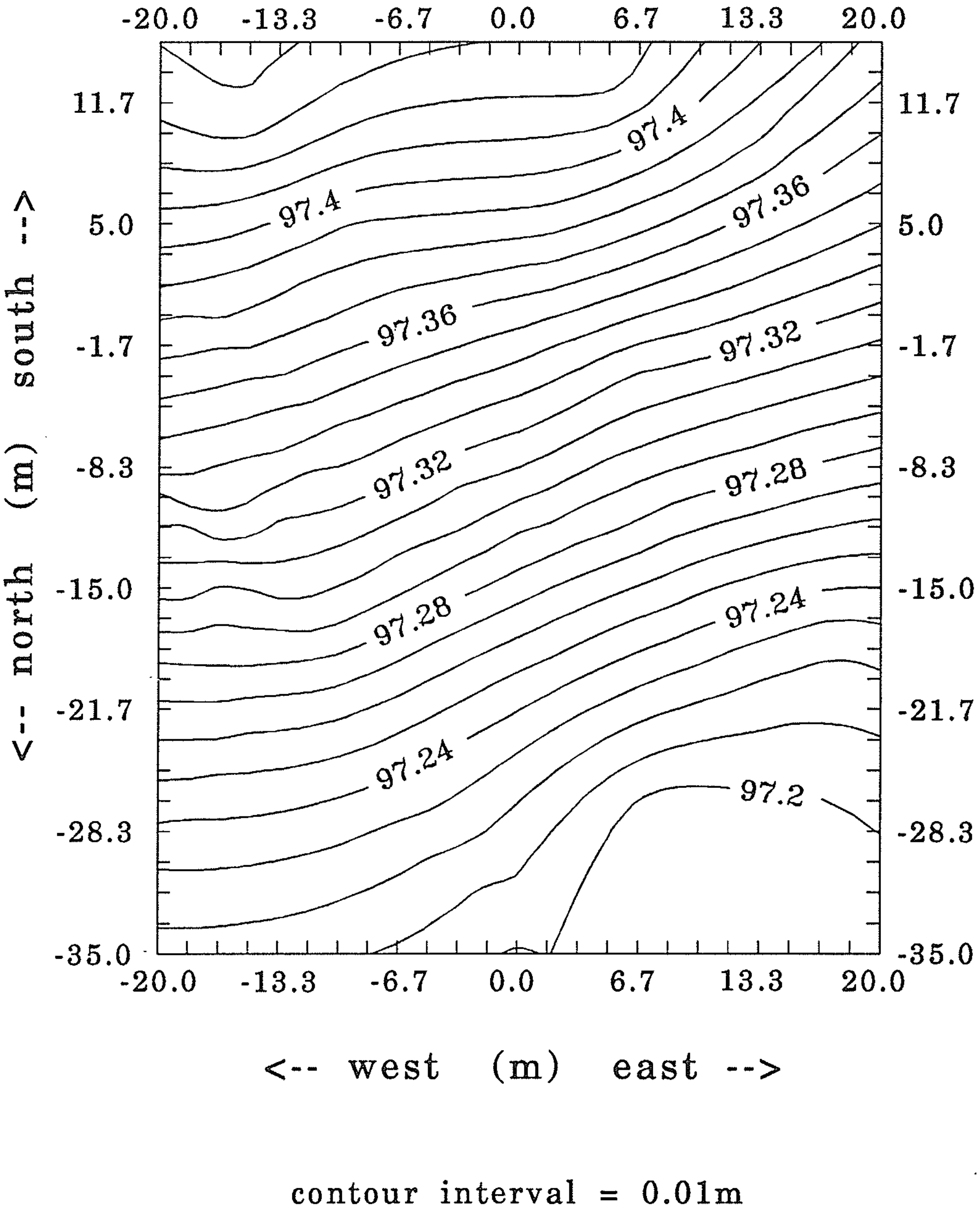

Figure 2.6. Watertable contour map for the emplaced source site on 02/03/1990.

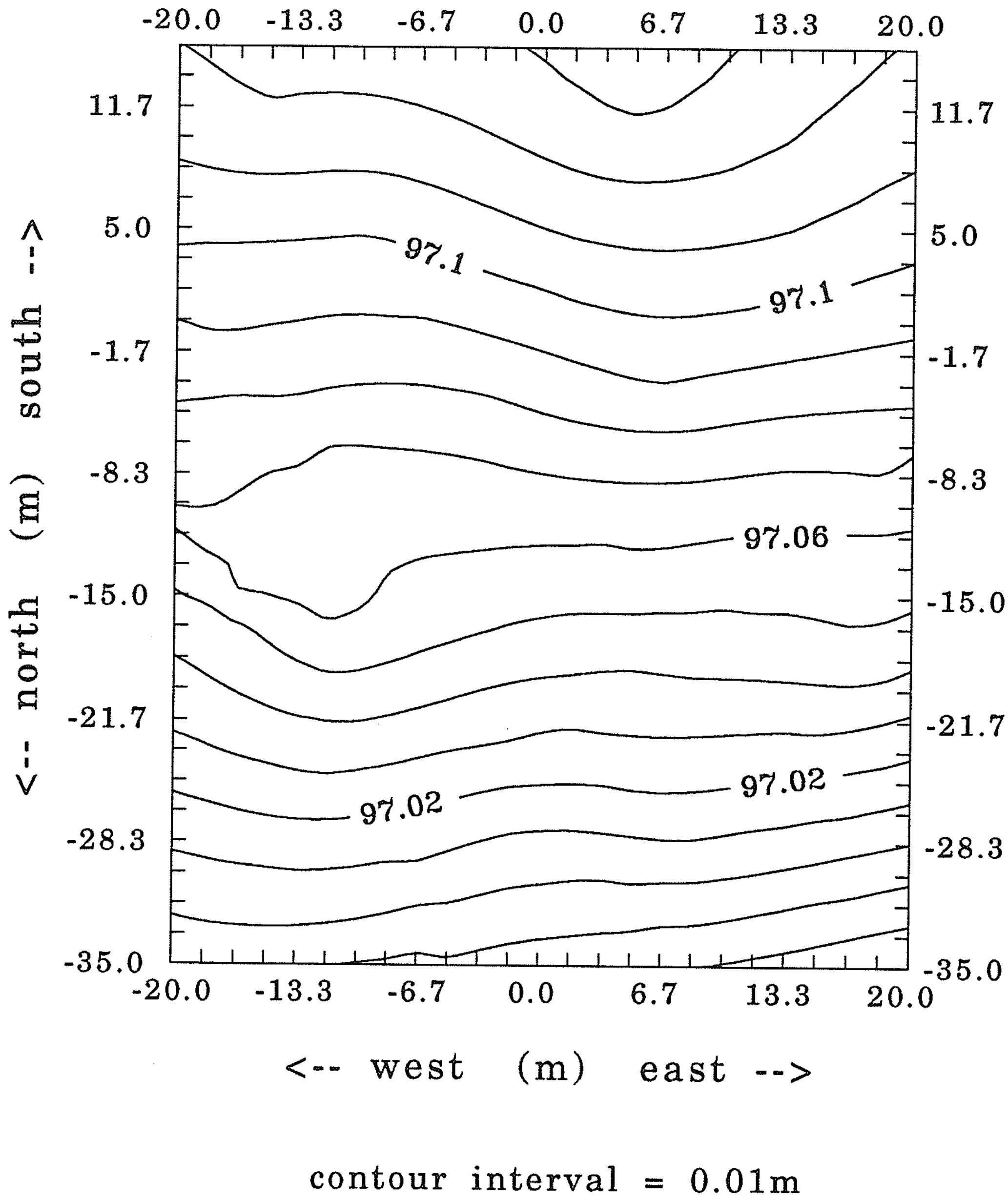

Figure 2.7. Watertable contour map for the emplaced source site on 28/08/1990.

predominantly towards the north with the direction rotating eastward for short periods in response to recharge conditions. This general flow direction is consistent with the earlier observations of MacFarlane et al. (1983) and Sudicky (1986) who both described predominantly north-easterly flows at the site. In addition, the gradient magnitude fluctuates in time with the highest gradients being observed during the recharge periods.

In the development of Rehfeldt's model, the hydraulic head was assumed to be planar over the region of interest (Rehfeldt 1988). It is therefore necessary to first determine whether the hydraulic head over our area of interest at the Borden aquifer satisfies this criterion and, if so, to determine the necessary coefficients for predicting the influence of the flow transients on the macrodispersion process.

2.3.2 Trend Surface Analysis

An examination of the watertable elevation contour maps at different times indicates that spatial trends over the area are simple in form and can be adequately represented by a polynomial surface in space of first or second order. For example:

1st Order Polynomial Surface

$$H(x,y)=m_1+m_2x+m_3y \qquad \text{...(2.20)}$$

2nd Order Polynomial Surface

$$H(x,y)=m_1+m_2x+m_3y+m_4x^2+m_5xy+m_6y^2 \qquad \text{...(2.21)}$$

where x and y give the spatial coordinates of piezometers, H(x,y) represents the watertable trend surface and m_i gives the model coefficients. Note that the coefficients, m_i, are time dependent.

In each case, the 'data' and the model parameters are linearly related and the model coefficients can be estimated by a standard least squares approach, by minimizing the following functional (Lawson and Hanson, 1974)

$$F=(\mathbf{d}^*-G\mathbf{m})^T V^{-1} (\mathbf{d}^*-G\mathbf{m}) \qquad ...(2.22)$$

where

$$E(\vartheta)=0 \qquad ...(2.23a)$$

and

$$E(\vartheta\vartheta^T)=V \qquad ...(2.23b).$$

Here $\mathbf{d}^*$ is a (p*1) vector of observed watertable elevations at each time sampling, $\mathbf{m}$ is a (n*1) vector of model coefficients, G is a (p*n) matrix of Kernals, ϑ is a (p*1) vector of residuals ($\mathbf{d}^*$-Gm) and V is a (p*p) covariance matrix of the residuals. The solution vector, $\mathbf{m}$, to equation (2.22) is computed using the Singular Value Decomposition (SVD) technique (Lawson et al., 1974; see also Woodbury, 1989).

If the covariance matrix is set equal to the identity matrix, then the model coefficients for the Ordinary Least Squares (OLS) surface are obtained. The model coefficients for the Generalized Least Squares (GLS) surface are obtained when correlation among the residuals is present, and V must in principle be defined as a full matrix.

As mentioned earlier, equations (2.20) and (2.21) are possible representations of the spatial trend in the data at each time sampling. However, it is desirable to determine the surface which optimally fits the data and therefore the spatial trend. To estimate the optimal surface representation for any trends present, model discrimination tests are used. These discrimination tests are described in the next section.

2.3.2.1 Model Discrimination Tests

An over-parameterization test allows one to examine whether the addition of an independent variable into a model significantly improves the prediction of a model when the other independent variables of the model are present. In this work both the Partial F-test (see Kleinbaum et al., chap. 2, 1987) and the Akaike Information Criterion (AIC) (see Hipel, 1981) will be used to perform over-parameterization tests on the OLS models proposed to represent the trend.

The Partial F-test allows the significance of an independent variable in a model to be statistically tested in the presence of the other model parameters. For example, the significance of the variable $\mathbf{x}^*$ in the following model (see equation 2.24) may be tested.

$$y(x_1,x_2,\dots,x_p,x^*)=a_0+a_1x_1+\dots+a^*x^*+E \qquad \dots(2.24)$$

The F statistic used to perform the partial F-test is given by (Kleinbaum et al., chap. 2, 1987) as

$$F(x^*|x_1,x_2,\dots,x_p)=\frac{SS(x^*|x_1,x_2,\dots,x_p)}{MS\ residual\ (x_1,x_2,\dots,x_p,x^*)} \qquad \dots(2.25)$$

where

$$SS(x^* | x_1,x_2,..,x_p) = regression\ SS(x_1,x_2,..,x_p,x^*) - regression\ SS(x_1,x_2,..,x_p) \quad \ldots(2.26)$$

The F statistic has an F distribution with 1 and n-p-2 degrees of freedom under the null hypothesis, H_o; where n represents the number of observations and p represents the number of parameters in the model. The null hypothesis for this test states: x^*, does not significantly improve the prediction of the model, y, given that x_1, x_2,...., x_p are already in the model. The null hypothesis H_o is rejected if the computed F exceeds $F_{1,n-p-2,1-\alpha}$ where α is a critical value used to define the confidence limit of the test; for this work the 95% confidence level will be used, hence α will be set to 0.05.

Like the Partial F-test the AIC method attempts statistically to determine the optimal set of parameters needed to fit a model. The optimal set of parameters are the parameters which result in the minimum computed AIC value. The AIC value is computed using the following expression

$$AIC = 2(L+k) \quad \ldots(2.27)$$

where k is the number of independent variables in the model and L is the negative log-likelihood function given by (see Hoeksema and Kitanidis, 1985)

$$L = \frac{1}{2}[n\ln(2\pi) + n\ln(\sigma^2) + X^2] \quad \ldots(2.28)$$

where n is the number of data points and X^2 represents the Chi squared distribution. For the analysis to be performed the AIC value for the full model (i.e. the model with all the independent variables being present; refer to equation 2.24) will be computed. This value will then be compared to the AIC value computed for a reduced model (i.e. the model with the x^* independent variable set to zero; refer to equation 2.24). If the AIC value computed for the reduced model is less than the AIC value computed for the full model then the variable x^* is not needed in the model since it results in an over-parameterization.

As pointed out earlier, both the first order OLS surface and the second order OLS surface are possible candidates for the spatial trend present in the data. Therefore, as a starting estimate for the optimal polynomial surface to represent the trend the second order OLS surface is used. The significance of the second order terms in the model are then computed using both the AIC and the partial F test techniques described above. The results of some of these tests are shown in Table 2.1. The table shows that on 24/10/1990 the smallest AIC value was obtained when the m_4x^2 term was ignored; this is supported by the partial F test which shows that the m_4x^2 term does not significantly improve the prediction of the model. In general, both tests showed that the x^2 and the y^2 terms were needed to optimally model the spatial trend present in the data. However, Rehfeldt's model requires that the spatial trend present in the data be modelled by a planar surface. Figure 2.8 shows the first order OLS surface super-imposed on the observed hydraulic head map for the aquifer at the emplaced source site on 02/03/1990. From this figure it can be seen that the first order OLS surface provides a good representation of the trend present with the deviation between the two surfaces being on average about 1.0 cm. Likewise, the deviation between the first order OLS surface and the optimal polynomial trend surface is quite small.

Based on the above observations it appears that the use of the first order OLS

Table 2.1

Over-Determination Test : 2nd Order Coefficients

Date	2nd Order Coefficients m_4	m_5	m_6	F-value	T-value
11/01/90	-1.788×10^{-5}	0.0	0.0	1.3297	-1.1570
	0.0	5.842×10^{-6}	0.0	1.3528	0.2591
	0.0	0.0	-5.519×10^{-6}	1.8287	-1.6321
13/03/90	-6.180×10^{-5}	0.0	0.0	1.2715	-0.5855
	0.0	-1.292×10^{-4}	0.0	1.2646	-0.9712
	0.0	0.0	-2.991×10^{-5}	1.4513	1.0385
12/05/90	-2.004×10^{-5}	0.0	0.0	1.0231	-0.9964
	0.0	2.595×10^{-5}	0.0	1.0702	0.3975
	0.0	0.0	-7.832×10^{-6}	1.0138	-1.6463
10/07/90	3.956×10^{-6}	0.0	0.0	1.0091	0.1301
	0.0	2.496×10^{-5}	0.0	1.2815	0.2427
	0.0	0.0	-1.678×10^{-5}	1.9016	-2.6825*
07/09/90	-3.003×10^{-6}	0.0	0.0	1.0545	-0.2506
	0.0	7.722×10^{-6}	0.0	1.3487	-0.3066
	0.0	0.0	-3.125×10^{-6}	1.3328	-1.4622
24/10/90	-4.884×10^{-6}	0.0	0.0	1.0790	-0.3132
	0.0	4.083×10^{-6}	0.0	1.0687	-0.1218
	0.0	0.0	-6.891×10^{-6}	2.6141*	-2.7458*
30/11/90	-7.619×10^{-6}	0.0	0.0	1.1307	-0.4121
	0.0	6.645×10^{-6}	0.0	1.1291	-0.1894
	0.0	0.0	-8.632×10^{-6}	3.8410*	-3.0532*
17/12/90	-9.446×10^{-6}	0.0	0.0	1.1919	-0.6238
	0.0	3.199×10^{-6}	0.0	1.0558	-0.0923
	0.0	0.0	-6.838×10^{-6}	2.9676*	-2.8145*

Note: * indicates coefficients which fail test at 95% confidence limit.

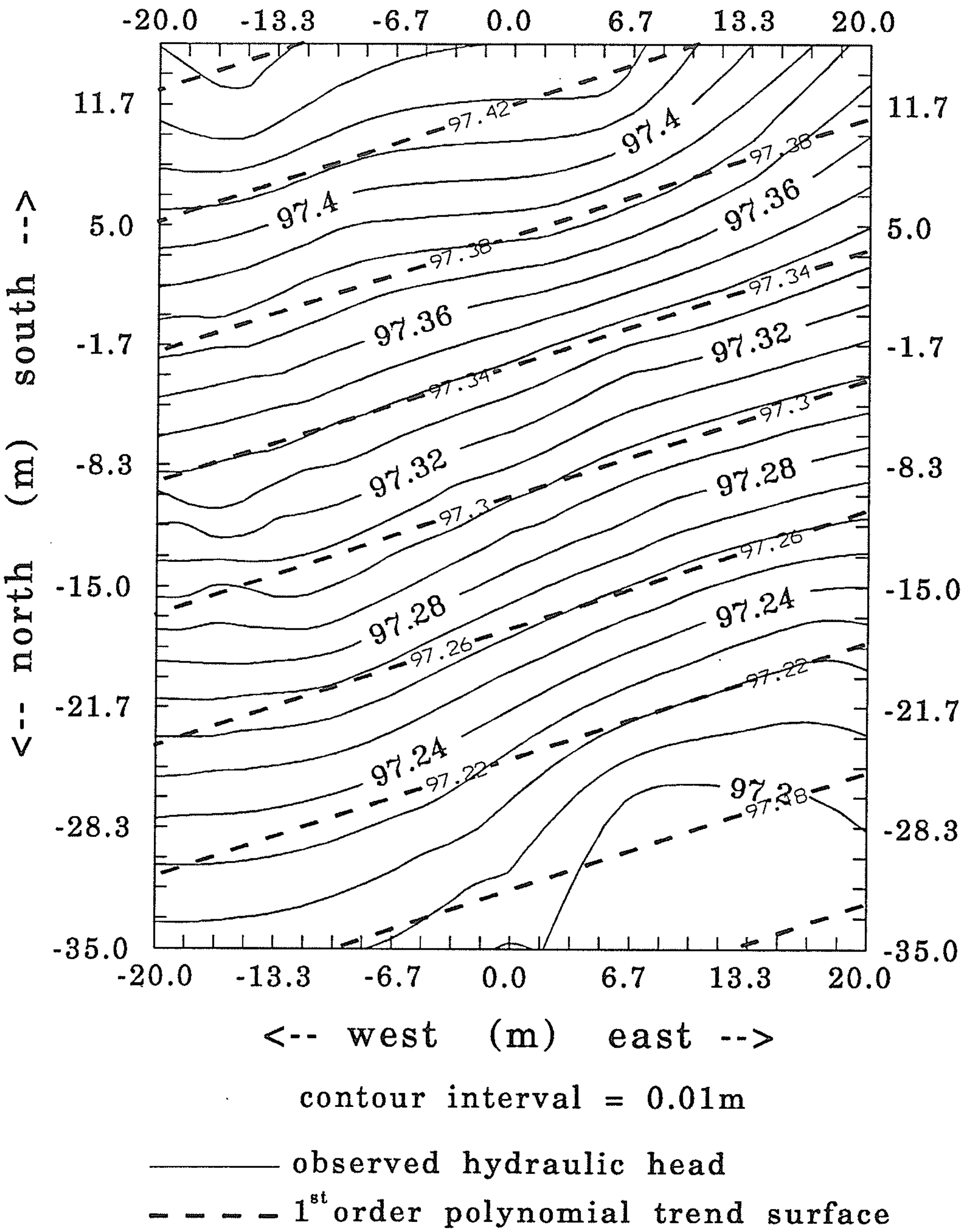

Figure 2.8 First order OLS polynomial surface superimposed on the observed hydraulic head contour map for 02/03/1990.

surface to model the spatial trend present in the data is justified. Therefore, for the proceeding analysis the first order OLS surface will be used to model the spatial trend present in the data.

2.3.2.2 Generalized Least Squares Analysis

It is well known (for example Stedinger and Tasker, 1985) that the OLS method will not identify the optimal parameter estimates of a regression model when the residual errors are not homoscedastic and independently distributed. In addition, Stedinger and Tasker (1985) have pointed out that model parameters estimated using the OLS method can be highly biased. The GLS method attempts to overcome these problems associated with the OLS method by allowing the residual field to be cross-correlated as well as heteroscedastic (Draper and Smith, 1981). The GLS method is applied in this part of the analysis to determine whether the first-order model parameters can be improved.

Equation (2.22) can be used to apply the GLS method to the Borden watertable data; however, the application of this equation requires a priori knowledge of the spatial correlation present in the waterlevel data. For the Borden watertable data, no such information is available a priori. As an alternative, an iterative approach, similar to the method outlined by Neuman and Jacobson (1984) and Loaiciga et al. (1988), is applied to determine the covariance structure. The iterative approach may be summarized as follows:

1. A diagonal matrix of residuals generated from the OLS fit to the data is used as a starting estimate of the covariance matrix; the diagonal matrix is then used

to solve equation (2.22) for the model parameters, m, and the residuals generated by the updated model parameters are computed;

2. The covariance structure of the residuals is determined by geostatistical methods;
3. The updated covariance matrix is then used to re-solve equation (2.22).

This iterative procedure is repeated until the covariance matrix converges, so that no further improvement in the model parameters can be obtained.

The geostatistical analysis mentioned above is performed in two steps. The first step involves the computation of the experimental variogram for the residuals described above. In the second step, the sill (variance), nugget and integral scales are estimated from the computed variogram and the covariance matrix is computed.

The experimental variogram for the residuals is calculated using the following two methods: the "classical" semi-variogram (Matheron, 1963) which provides an optimal estimate of the variogram if the pairs $Y(x_i)$ and $Y(x_i+h)$ are bivariate and normal and the Cressie-Hawkins estimator (Cressie and Hawkins, 1980) which reduces the effects of outliers on the variogram (see Woodbury and Sudicky ,1991, for comparison).

An exponential model for the covariance structure is initially chosen as it is the model often assumed by researchers in stochastic hydrology (e.g. Hoeksema et al., 1985; Sudicky, 1986; Dagan, 1989b; Woodbury and Sudicky, 1991). The terms of the covariance matrix are computed using equation (2.29),

$$C_{ij}=\sigma^2\exp(-\frac{h_{ij}}{\lambda})+\sigma_o\delta_{ij} \qquad \ldots(2.29)$$

where σ^2 is the variance, σ_o^2 is the nugget, h_{ij} (the lag distance) is the distance between the points i and j, and λ is the integral scale.

In practise, the above iterative method is difficult to implement. Journel and Huijbregts (1978 p. 194) suggest that the useful part of the variogram is the portion $|h| < L/2$ and $n(h) > 30$ pairs, where L is the length of the transect sampled and n(h) is the number of pairs at lag h. Using a lag distance of 8m and a transect length of 80m (the longest dimension of our domain) the criteria of Journel and Huijbregts (1978) produces approximately five lags per data set. It is found that varying the lag distance does not increase the number of 30 pair lags in the data. Estimation of the variance and integral scale based on only five lags is difficult (Figures 2.9, 2.10, 2.11 and 2.12) and may lead to substantial bias. After the first iteration of the GLS method the model parameters are usually found to be similar to those obtained from the OLS model. Furthermore, it is observed that the variance of the residual field is quite small (approximately 10^{-5} m^2 to 10^{-4} m^2). This indicates that further iterations may only lead to small changes in the model parameters. These changes are not considered to be significant and their contribution to the trend surface will probably be below measurement error. Therefore it is concluded that the correlation in the residual field is weak and that the residual field is homoscedastic for the purposes of this work. The first-order OLS polynomial surface therefore provides an optimal representation of the spatial trend present the watertable data. Having determined the optimal polynomial

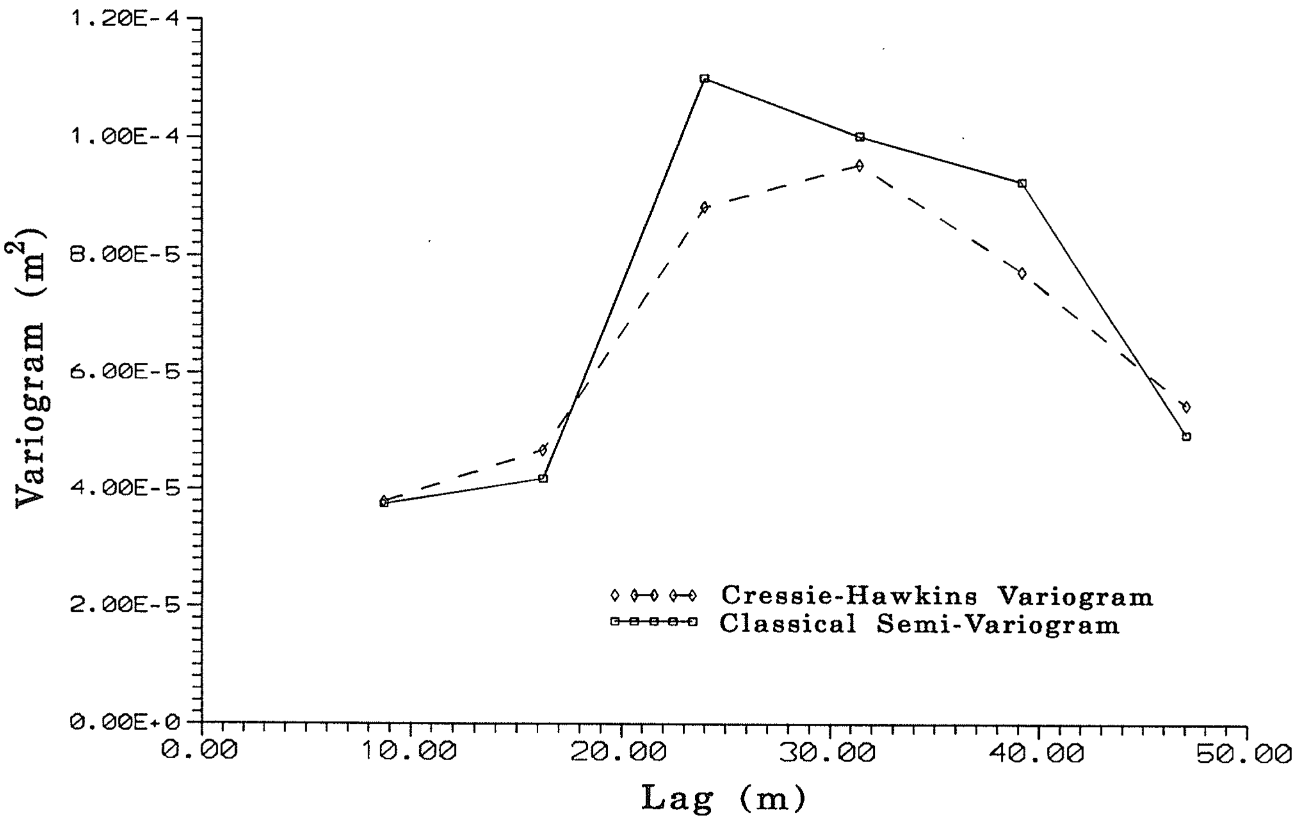

Figure 2.9 Classical Semi-variogram estimates for residuals of OLS surface fit; 03/01/1990.

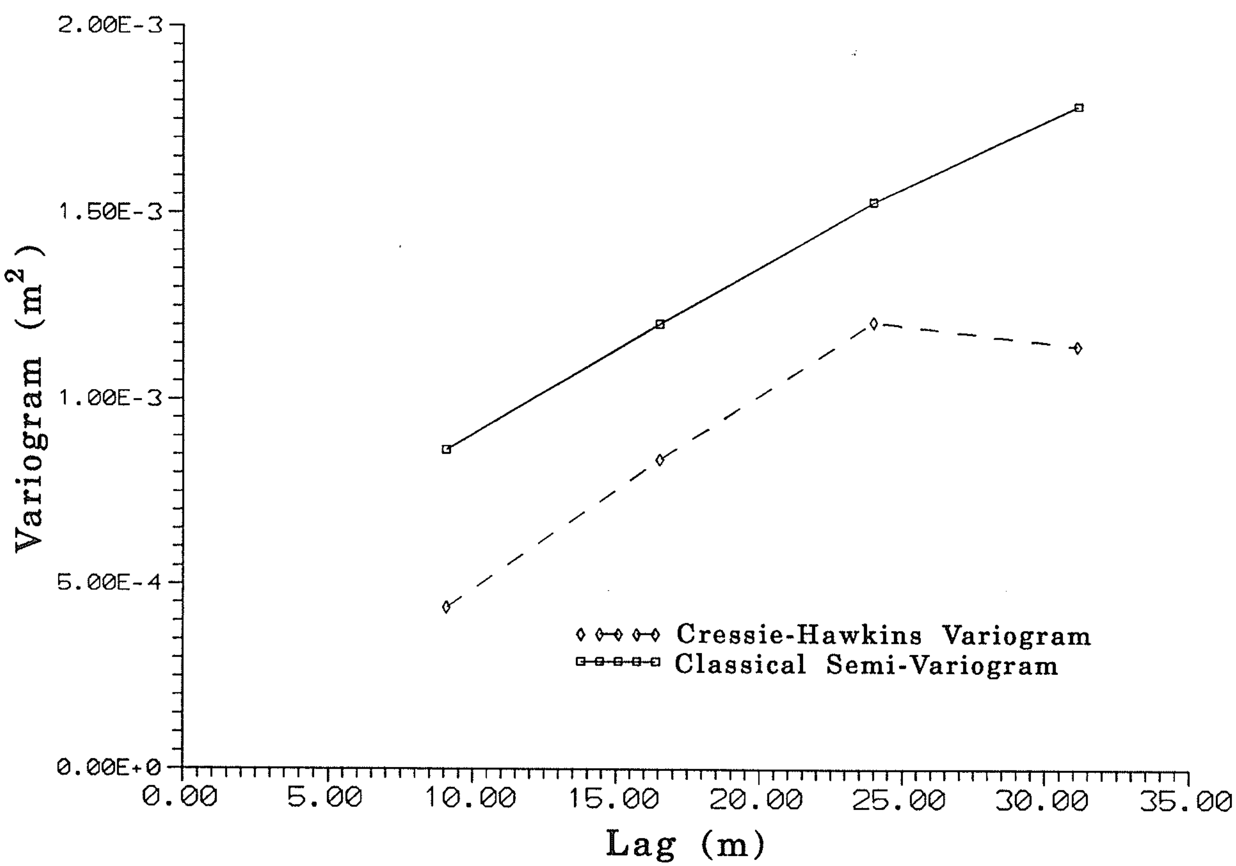

Figure 2.10 Classical Semi-variogram estimates for residuals of OLS surface fit; 13/03/1990.

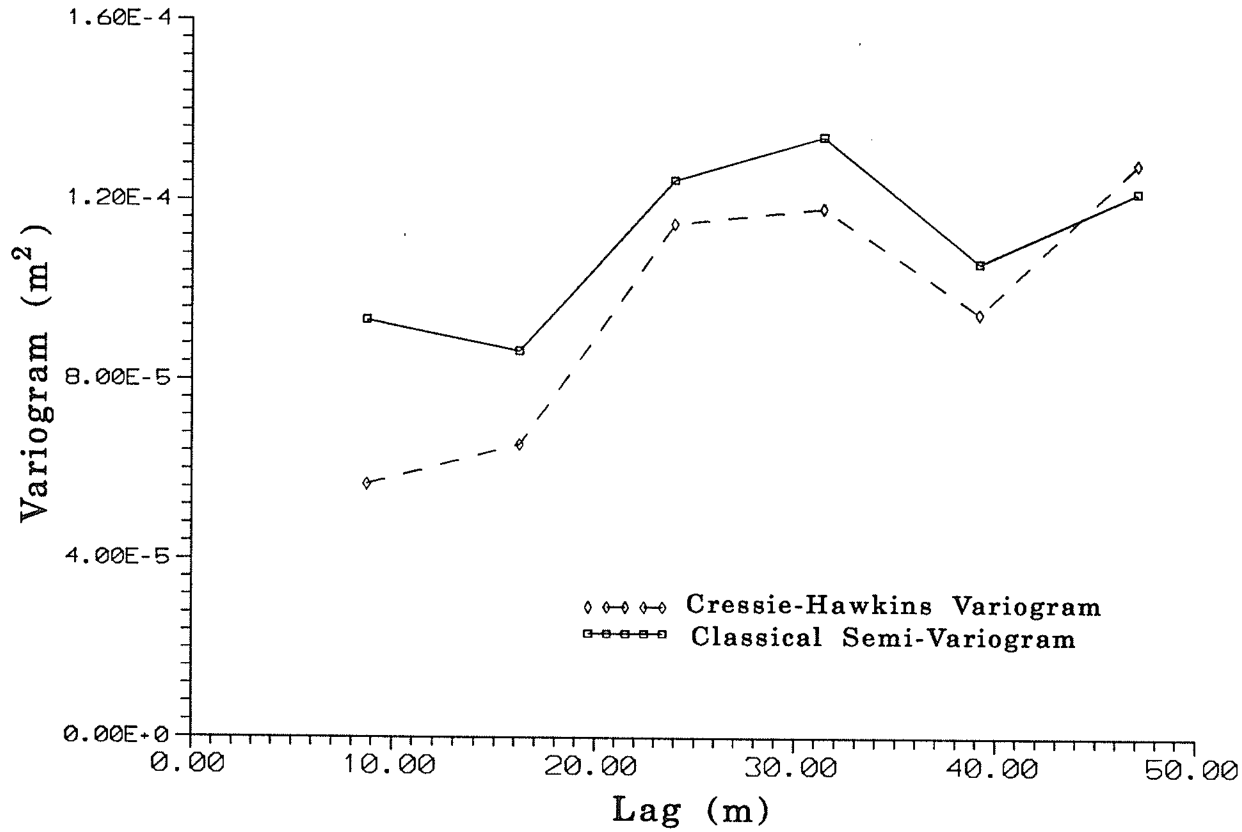

Figure 2.11 Classical Semi-variogram estimates for residuals of OLS surface fit; 04/07/1990.

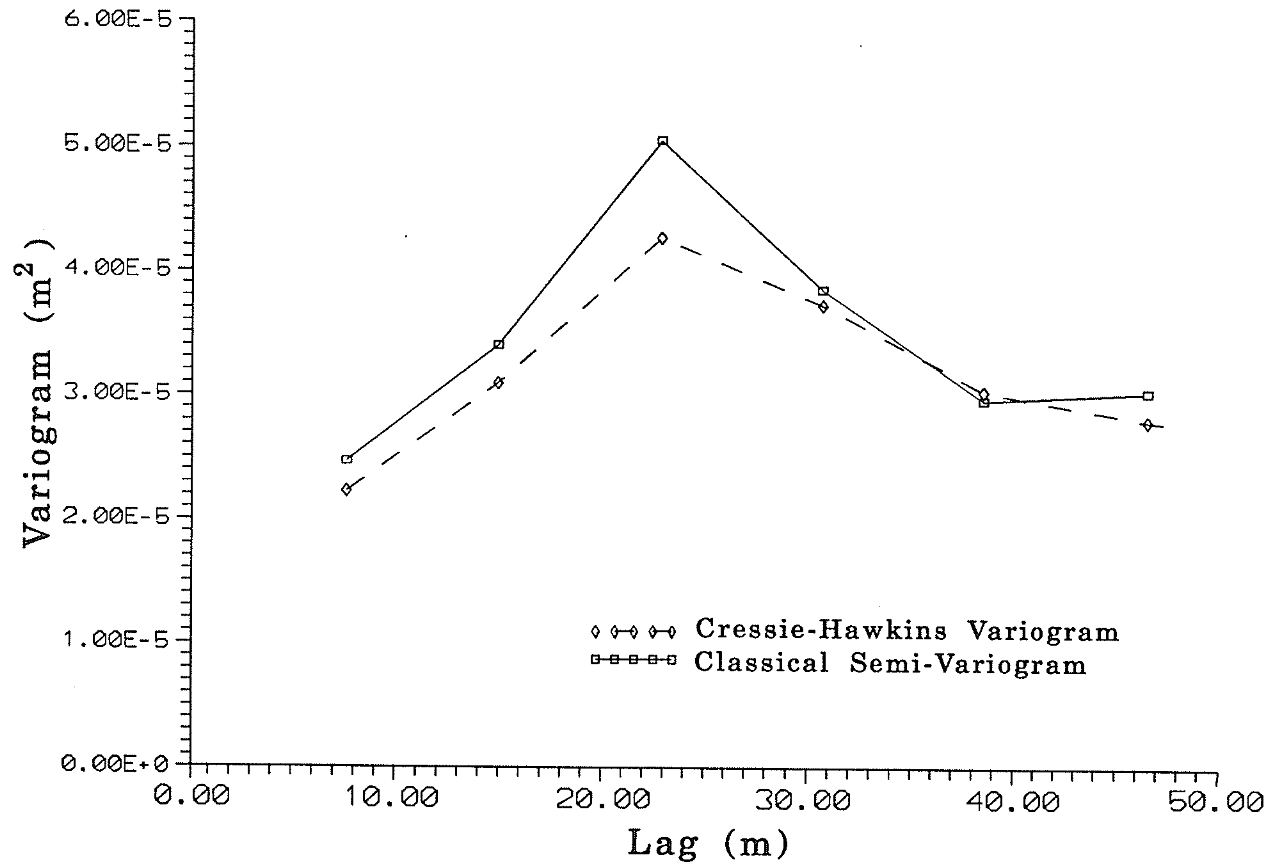

Figure 2.12 Classical Semi-variogram estimates for residuals of OLS surface fit; 07/09/1990.

representation for the trend in the data, each time sampling is represented by a simple set of spatial coefficients which will be analyzed to yield a mean gradient and flow direction.

2.3.3 Gradient and Flow Direction Time Series

As mentioned earlier, the spatial coefficients calculated above are time dependent. As a result the trend surface equation can be expressed in the following form:

$$H(x,y,t) = m_1(t) + m_2(t)x + m_3(t)y \qquad \text{...(2.30)}$$

Partial differentiation of the trend surface equation at each time sampling with respect to the space coordinates, gives the following gradient time series.

$$\frac{dH}{dx}(x,y,t) = m_2(t) \qquad \text{...(2.31)}$$

$$\frac{dH}{dy}(x,y,t) = m_3(t) \qquad \text{...(2.32)}$$

Equation (2.31) gives the east-west time series and equation (2.32) gives the north-south time series. The gradient-magnitude time series is given by:

$$|J(t)| = \left[m_2(t)^2 + m_3(t)^2\right]^{(1/2)} \qquad \text{...(2.33)}$$

and the flow direction measured clockwise from the north is given by

$$\Omega(t)=\tan^{-1}\left[-\frac{m_2(t)}{m_3(t)}\right] \qquad \ldots(2.34)$$

Figure 2.2 displays the various geometric relationships for the flow field.

The gradient- and flow-direction time series are shown in Figures 2.13 to 2.16. Long wavelength periodicities are present in both time series. Superimposed on these long wavelength periodicities are short wavelength fluctuations. The maximum amplitudes of the time series occur in the spring while the minimum amplitudes occur in the autumn, corresponding to the well known recharge cycle at the site.

The north-south gradient component and the total gradient-magnitude time series are similar in appearance, showing the dominance of the north-south gradient component at the site. The amplitudes of the short wavelength fluctuations for both these data sets are smaller than the amplitude of the long wavelength feature.

The east-west gradient component and flow direction time series are also quite similar in appearance, with the flow direction time series simply being a reflection of the east-west time series in the horizontal plane. For these two data sets, it is found that the amplitudes of the short wavelength fluctuations are larger than the amplitude of the long wavelength feature.

2.4 Geostatistical Analysis of Time Series

Rehfeldt's (1988) unsteady analysis requires that the integral scale and the variance of the gradient magnitude and the flow angle time series be known. To obtain estimates of these parameters, a geostatistical analysis similar to that described earlier is

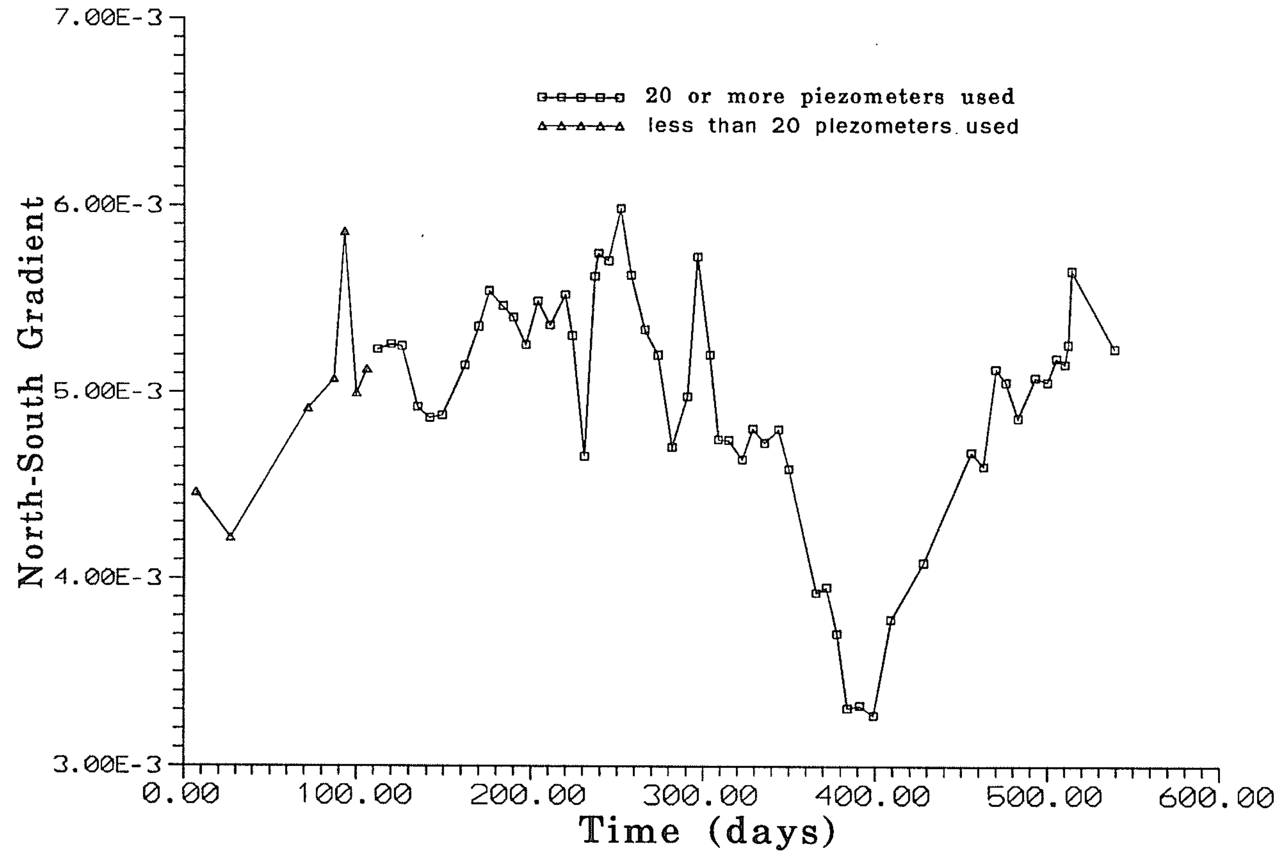

Figure 2.13 North-south hydraulic head gradient time series.

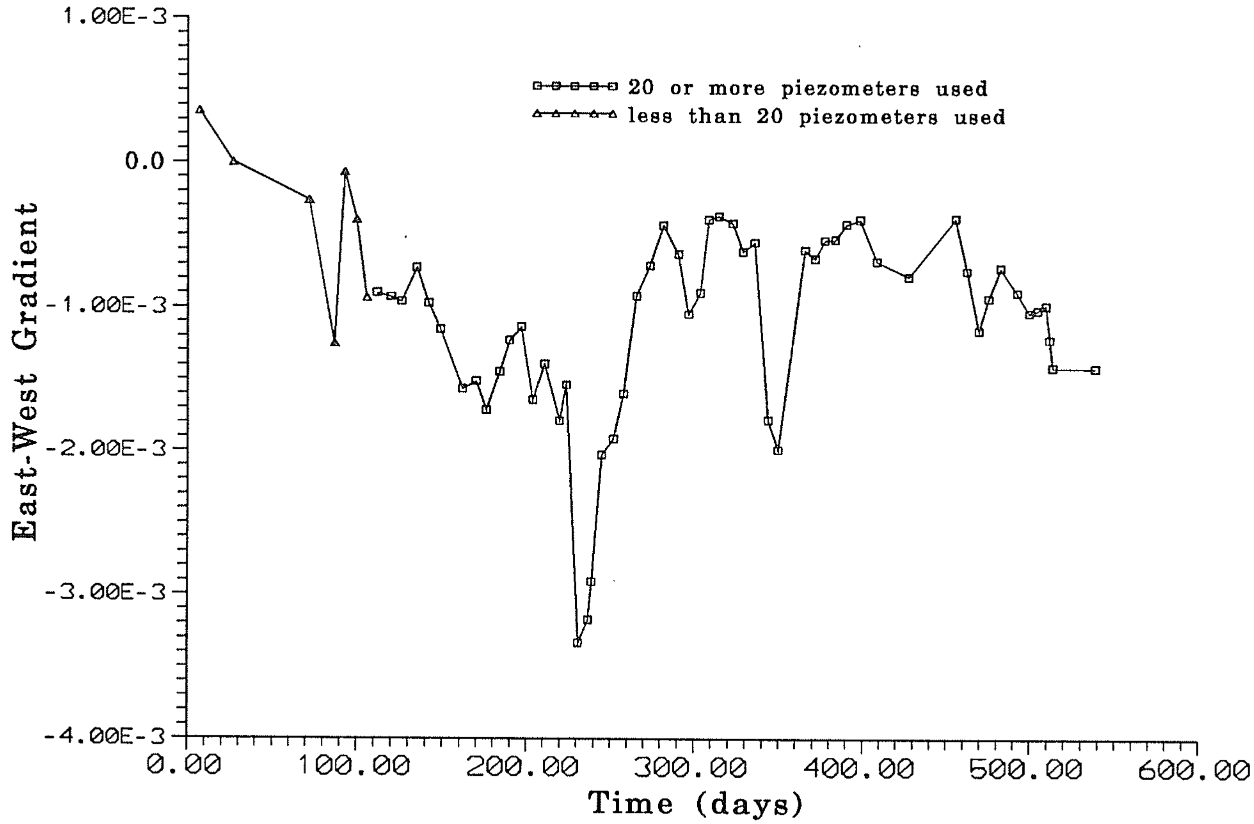

Figure 2.14 East-west hydraulic head gradient time series.

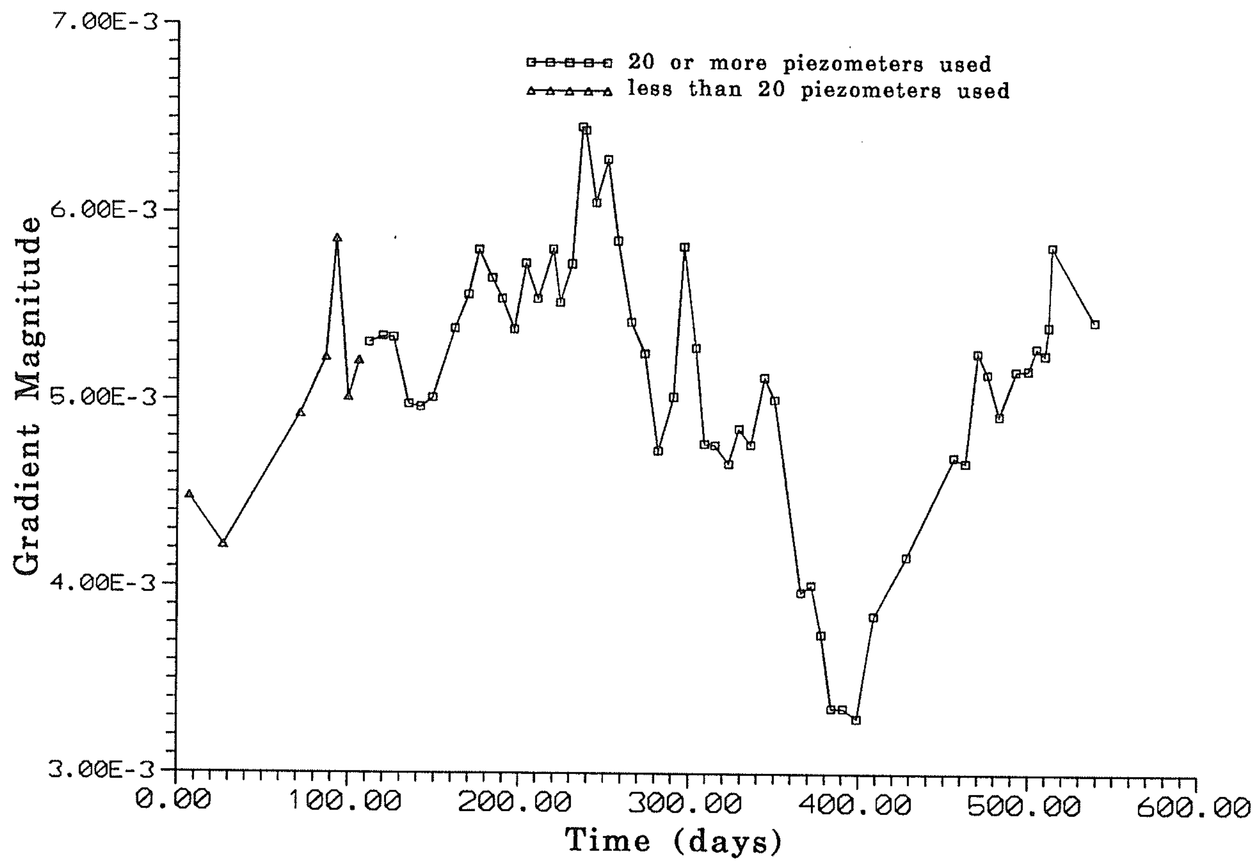

Figure 2.15 Hydraulic head gradient magnitude |J| time series.

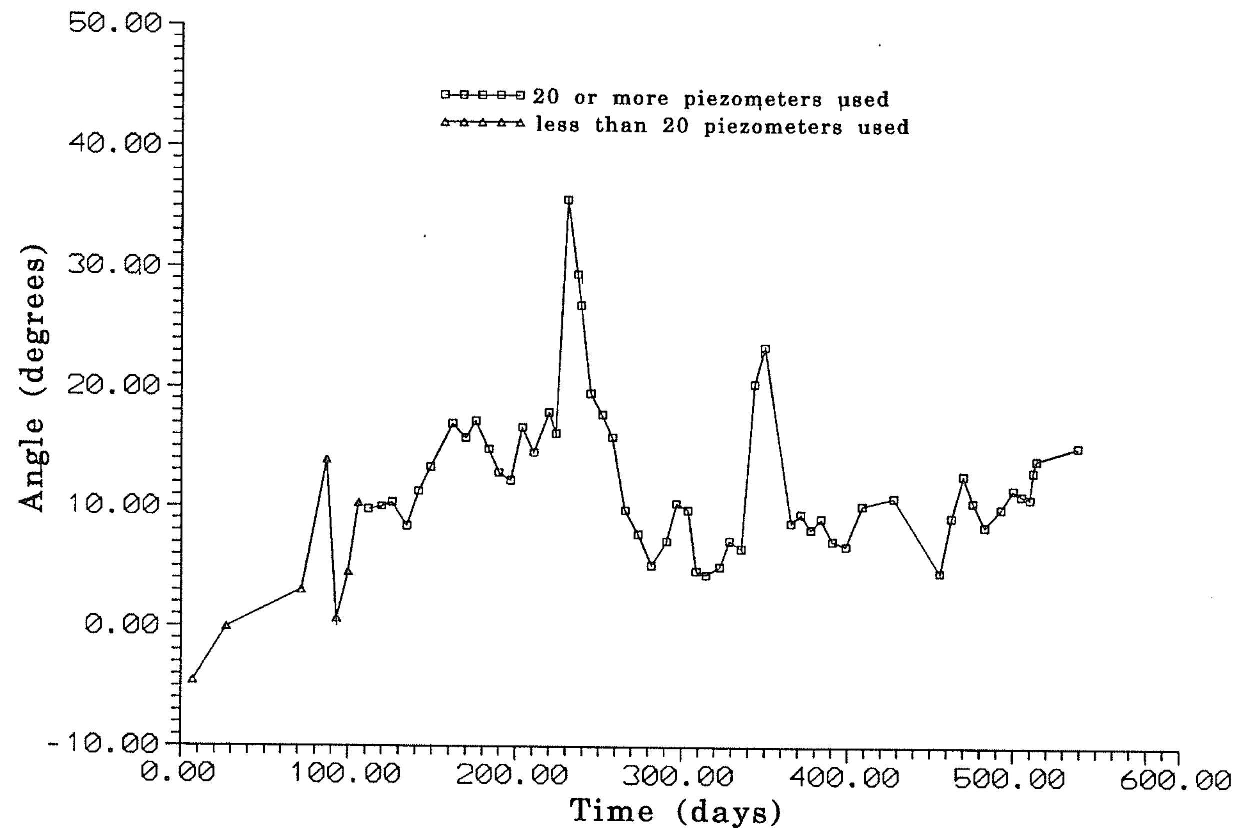

Figure 2.16 Flow angle time series (Ω).

carried out on the time series. The variogram methods previously described are enhanced by the use of the Jackknifing technique (Shafer and Varljen, 1990). This approach allows confidence limits to be placed around the experimental variogram.

At early times, water level measurements were obtained from only two piezometers with the number increasing to 20 after 112 days and finally 34 after 539 days when the experiment ended. Watertable trend surfaces computed at early times using a few piezometers provide relatively poor estimates of the waterlevel trend surface present since the computed surface may be strongly influenced by the presence of an anomaly or measurement error at a piezometer. When incorporated into the time series, these poor estimates may bias the estimates of the integral scale and the variance obtained from the geostatistical analysis. Using the assumption that trend surface estimates based on 20 or more piezometers are representative of the spatial trend, additional flow angle and gradient magnitude time series are generated (Figures 2.13 to 2.16). These two time series are used to examine the effect of the early time data on the integral and variance estimates.

The experimental variograms of the 4 data sets (the flow direction and the gradient magnitude time series for the full data set and the flow direction and the gradient magnitude time series computed described above) are computed using both variogram estimation techniques, (see Figures 2.17 to 2.24). The variograms appear to be exponential in form with zero nugget. The two variogram estimation techniques provide similar results at the 95% confidence level. Hence the choice of variogram technique does not appear to be important.

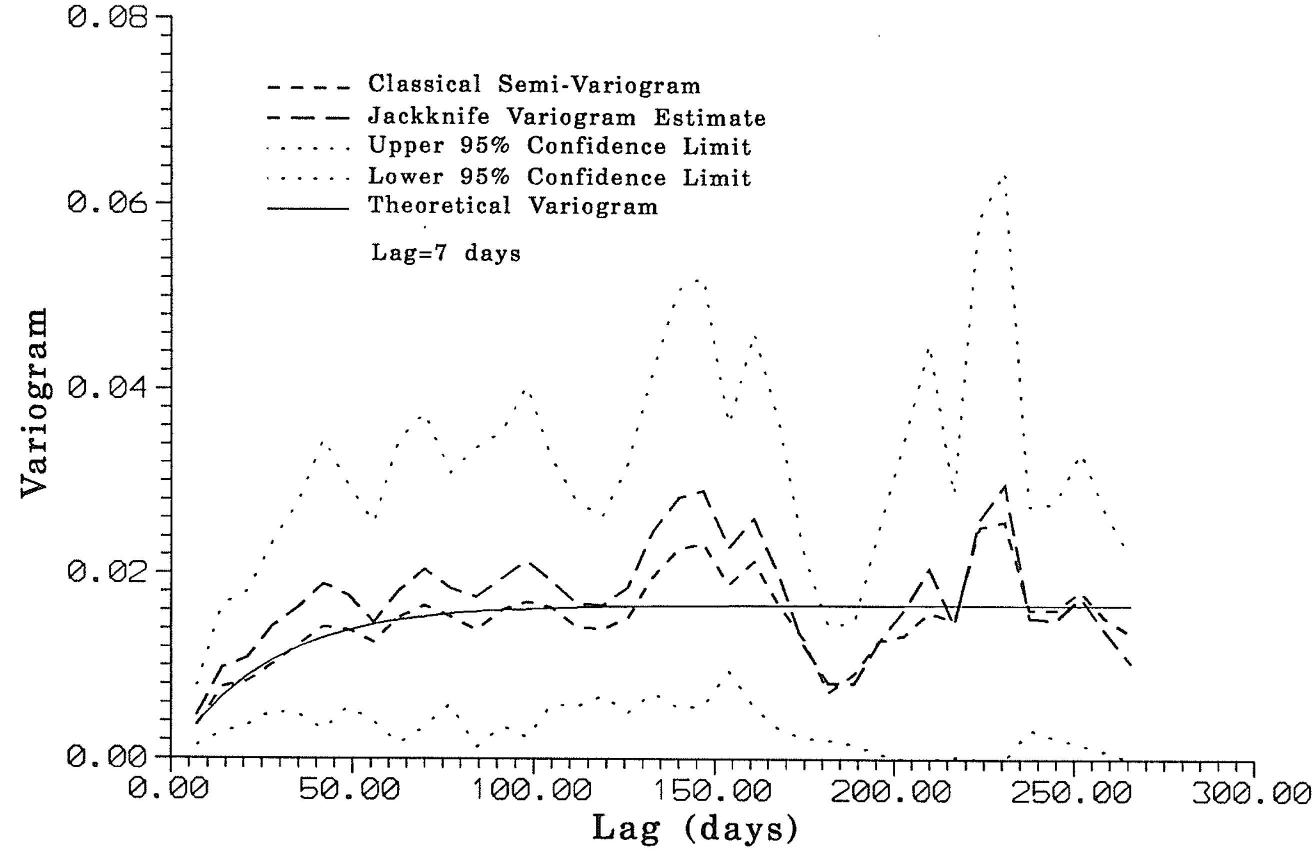

Figure 2.17 Classical Semi-variogram and Jackknife estimates for the flow angle (Ω) time series.

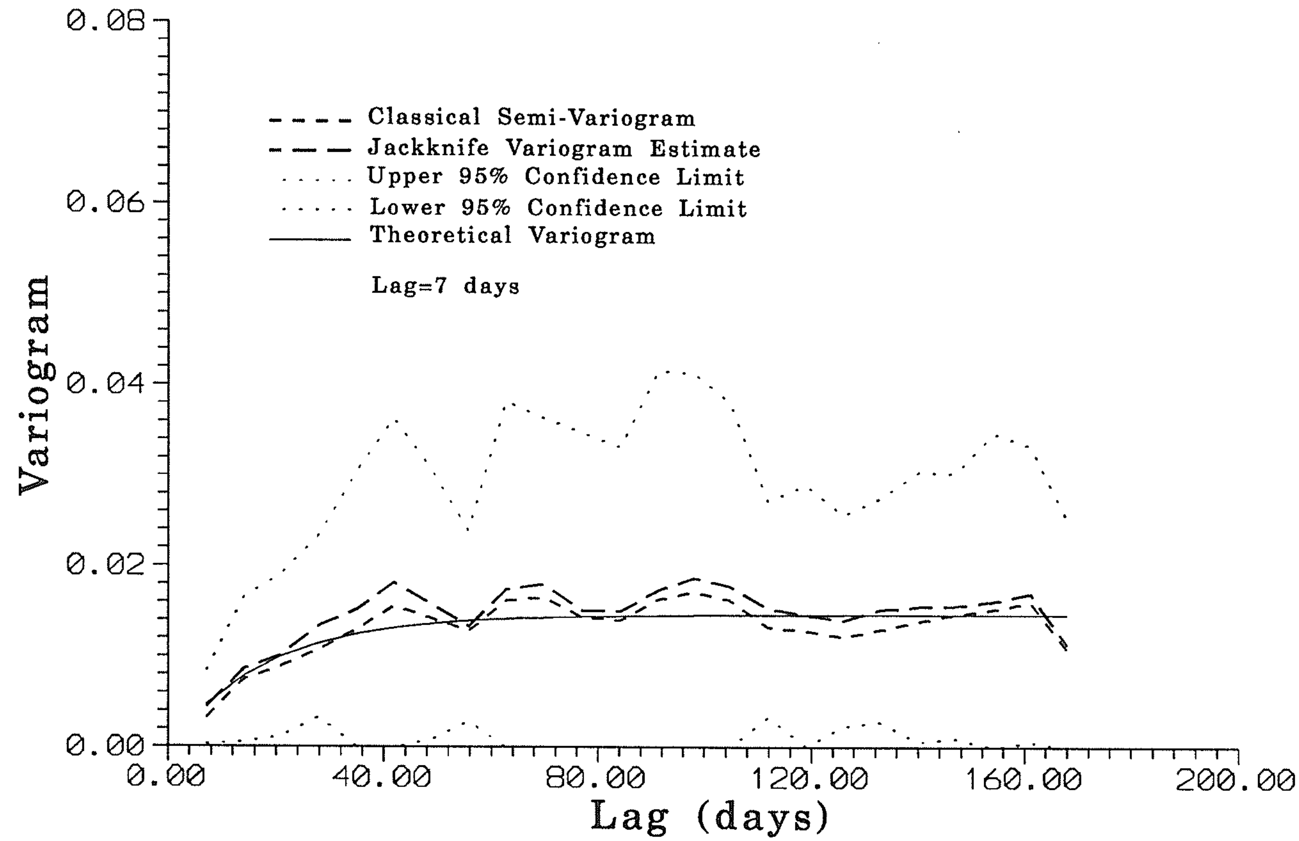

Figure 2.18 Classical Semi-variogram and Jackknife estimates for the flow angle (Ω) time series (112 - 539 days).

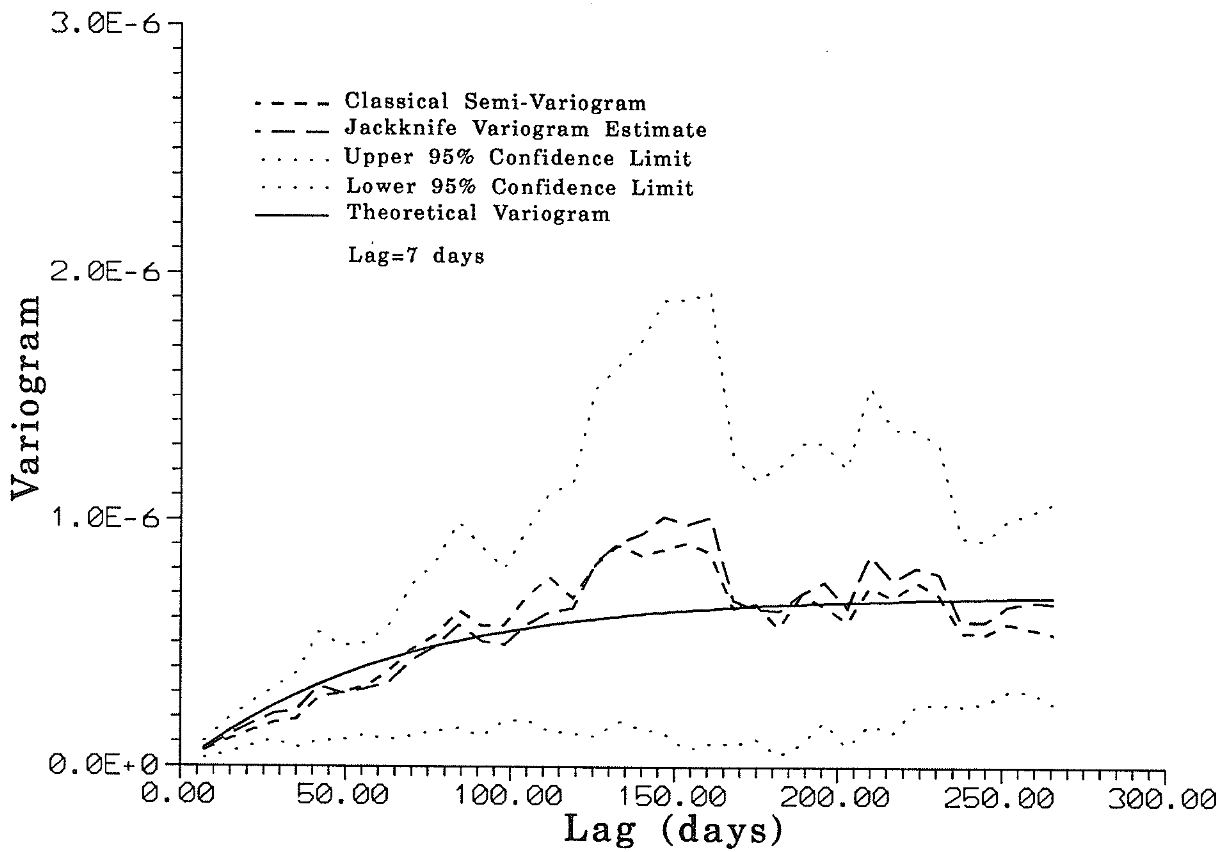

Figure 2.19 Classical Semi-variogram and Jackknife estimates for the gradient magnitude |J| time series.

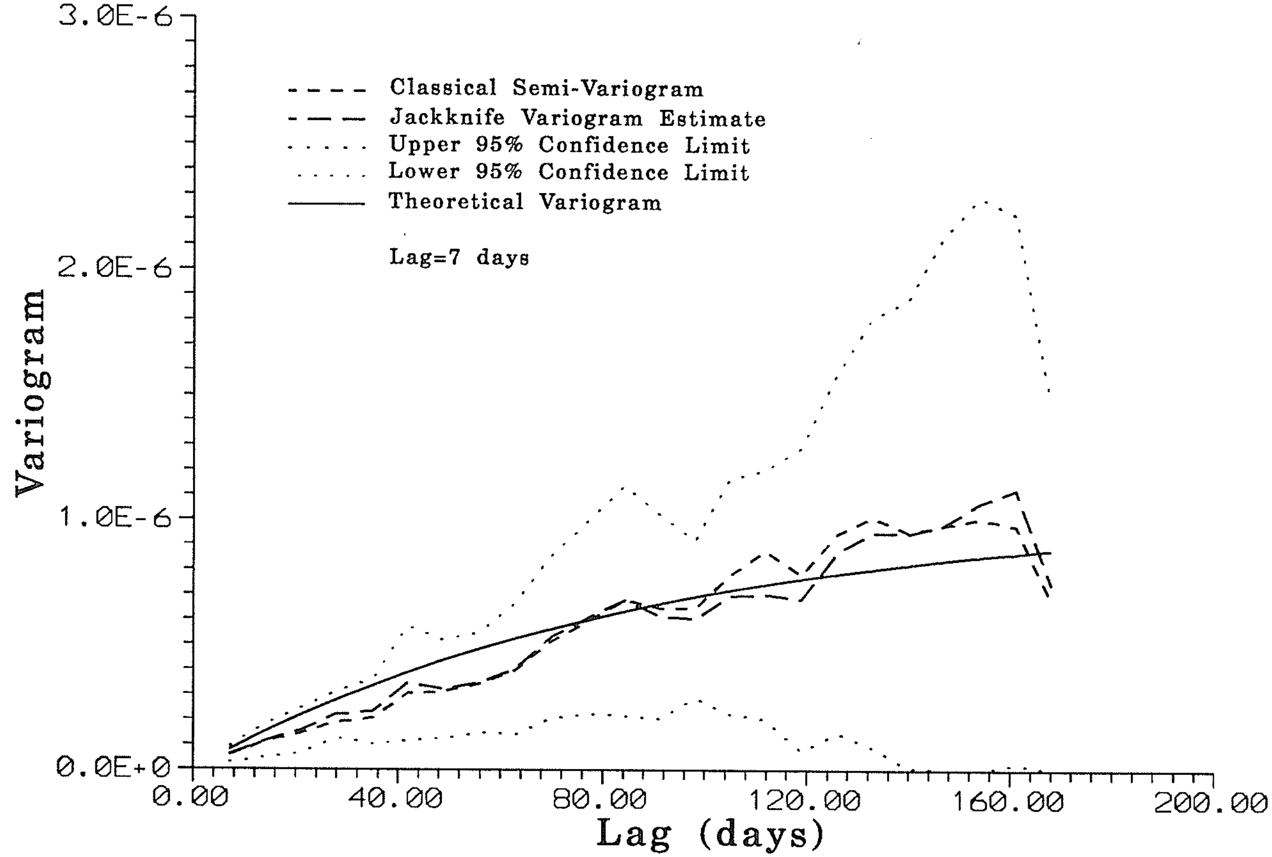

Figure 2.20 Classical Semi-variogram and Jackknife estimates for the gradient magnitude |J| time series (112 - 539 days).

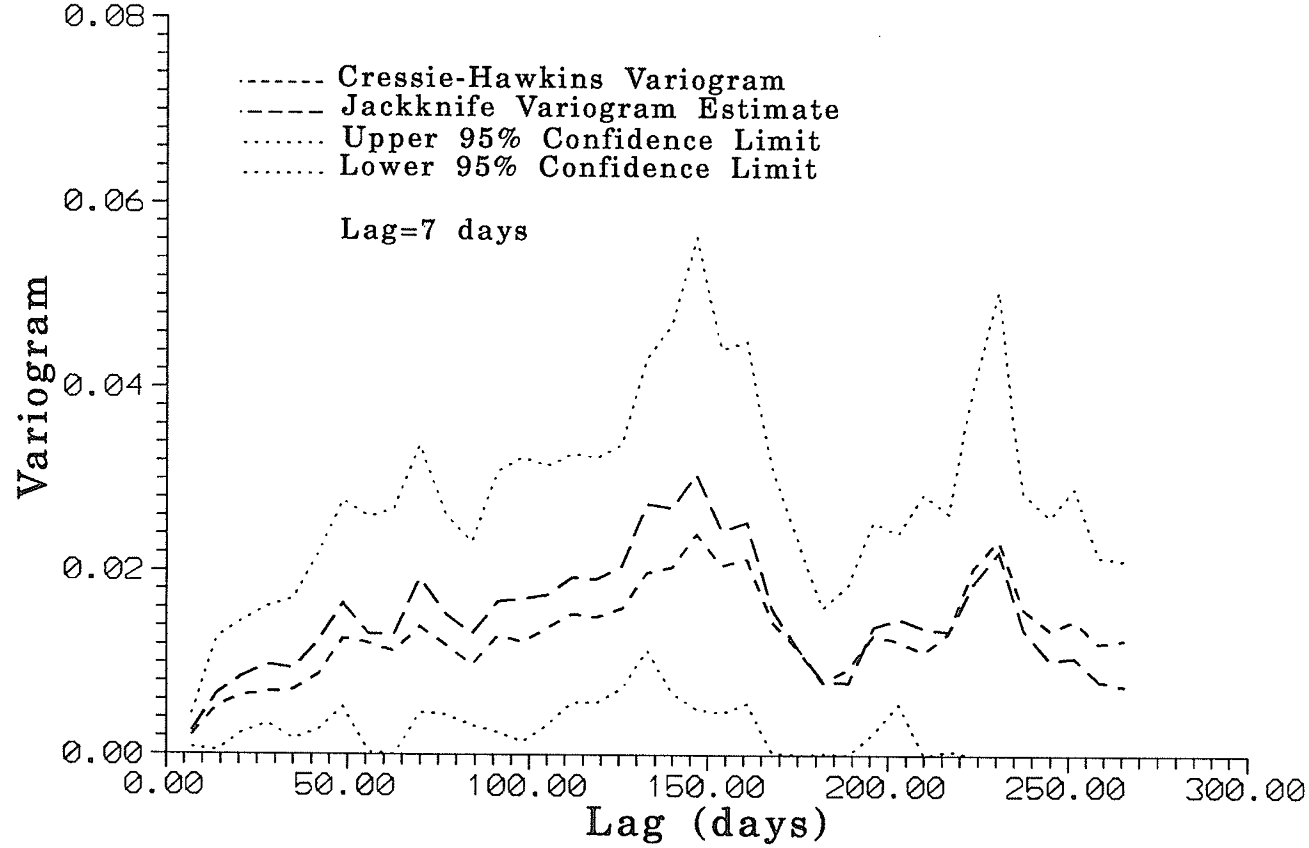

Figure 2.21 Cressie-Hawkins variogram and Jackknife estimates for the flow angle (Ω) time series.

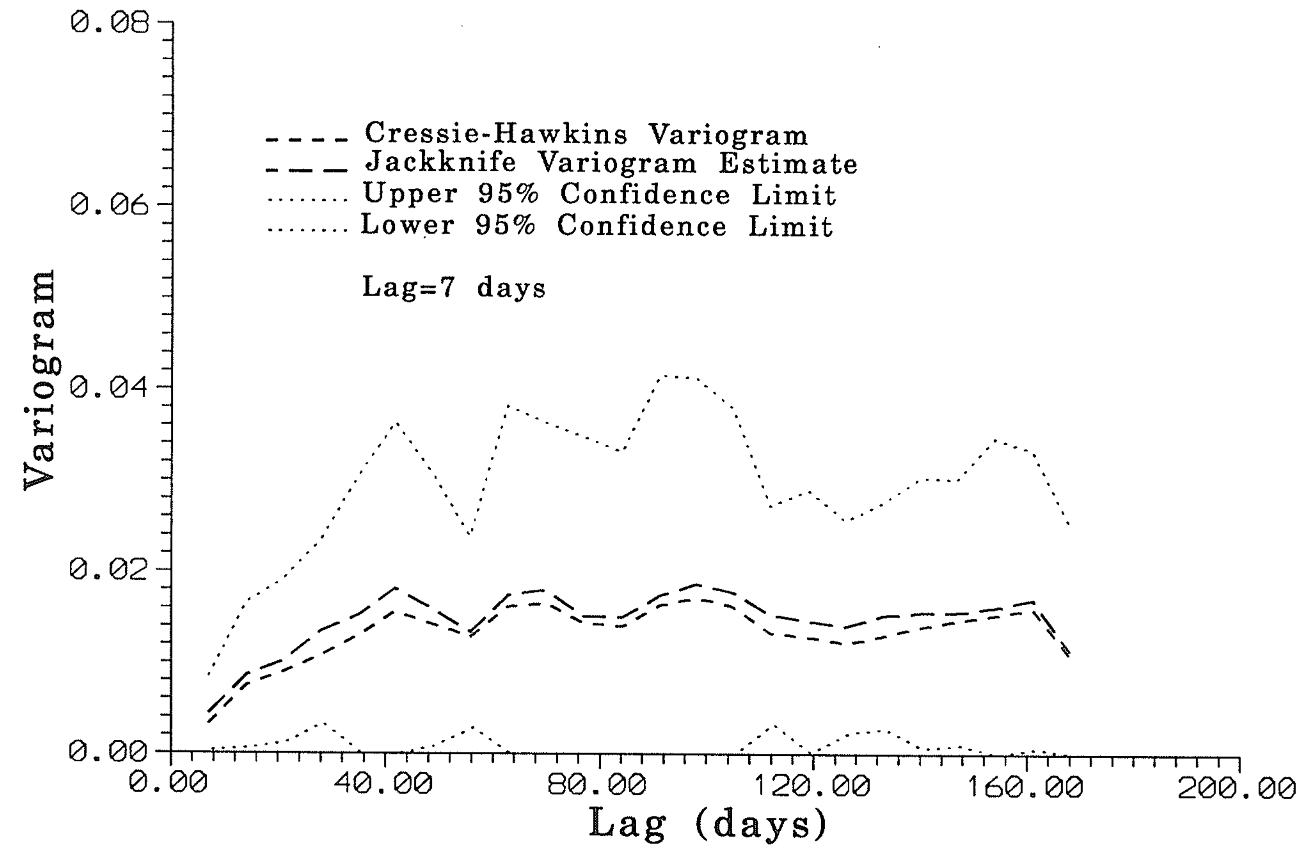

Figure 2.22 Cressie-Hawkins variogram and Jackknife estimates for the flow angle (Ω) time series (112 - 539 days).

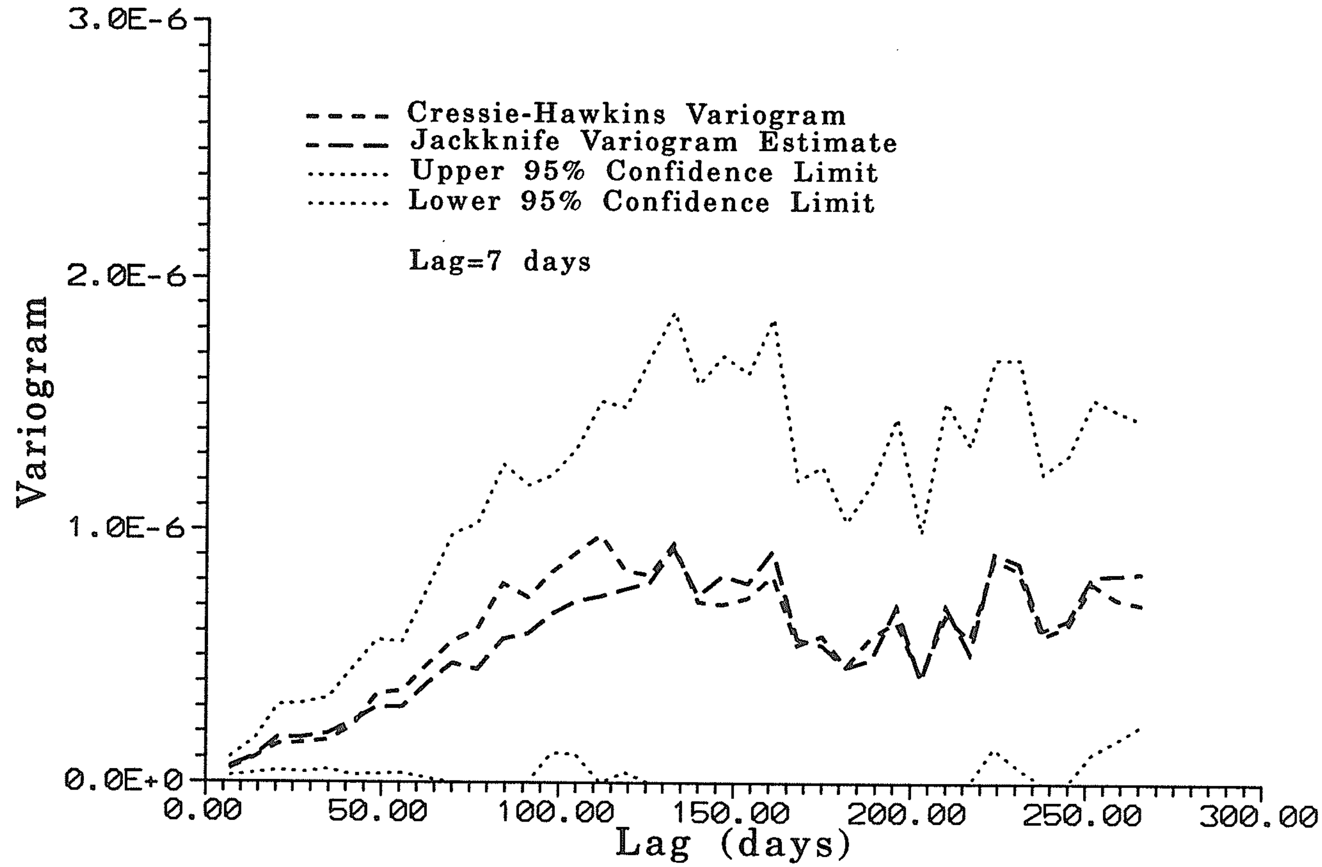

Figure 2.23 Cressie-Hawkins variogram and Jackknife estimates for the gradient magnitude |J| time series.

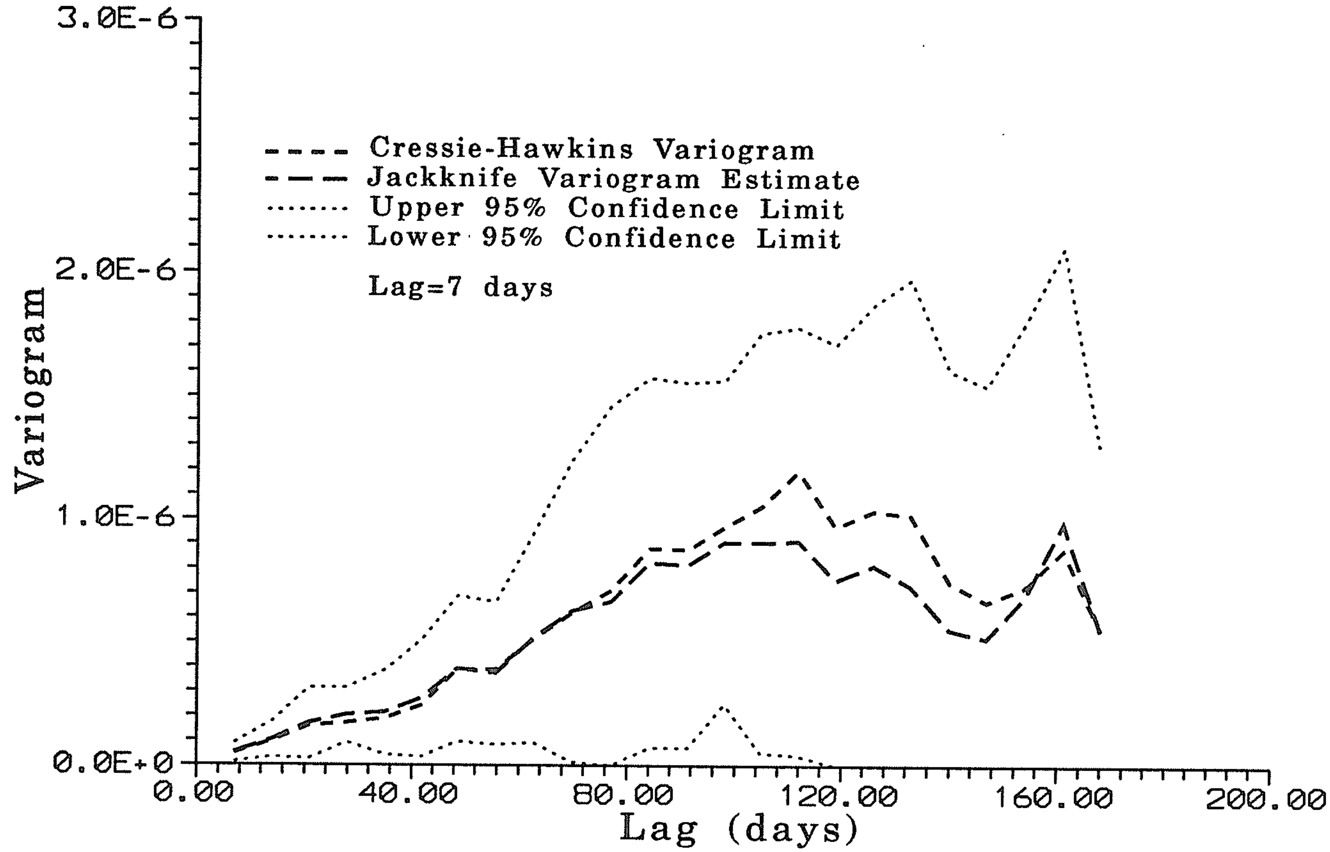

Figure 2.24 Cressie-Hawkins variogram and Jackknife estimates for the gradient magnitude |J| time series (112 - 539 days).

The variograms show the presence of a sill. However the sill estimates for the full time series and the truncated time series differ (see Figure 2.17 to 2.24). This shows that the gradient magnitudes and flow angles computed using less than 20 piezometers influence the variograms.

The parameter estimates for the data sets (i.e. the variances and the integral scales), computed from the classical semi-variograms are shown in Tables 2.2, 2.3 and 2.4. In addition, the upper and lower 95% confidence limits computed for the variograms are used to obtain estimates for these parameters (i.e. the variances and the integral scales) at the 95% confidence limit. These will later be used to estimate the 95% confidence limits for the asymptotic macrodispersivities.

Table 2.2

Transverse Dispersivity Results

	Components of Expected Estimate	Components at 95% Confidence Limit	
		Upper Limit	Lower Limit
σ_r^2 (radians^2)	0.0166	0.0348	0.003
$d\sigma_r^2$ (radians^2)	0.00076	0.00206	0.00004
λ_r (days)	27.2	23.20	6.8
$d\lambda_r$ (days)	11.4	14.20	30.0

Table 2.3

Transverse Dispersivity Results

(112 --> 539 days)

	Components of Expected Estimate	Components at 95% Confidence Limit
		Upper Limit
σ_Γ^2 (radians^2)	0.0146	0.0328
$d\sigma_\Gamma^2$ (radians^2)	0.00089	0.00133
λ_Γ (days)	18.44	18.20
$d\lambda_\Gamma$ (days)	10.64	7.09

Table 2.4

Longitudinal Dispersivity Results

	Components of Expected Estimate	
	(7 -> 539 days) data	(112 ->539 days) data
σ_J^2 (radians^2)	7.0×10^{-7}	1.04×10^{-6}
$d\sigma_J^2$ (radians^2)	4.5×10^{-8}	2.1×10^{-7}
λ_J (days)	65.00	90.00
$d\lambda_J$ (days)	20.00	37.00

2.5 Macrodispersion Analysis

The intention is to apply the watertable data to the dispersion models and then compare the results to the plume moment data given by Freyberg (1986) for the 1983 Borden tracer plumes (chloride and bromide). This requires that the assumption be made that the mean flow field at the Borden site is stationary in time. This allows the emplaced source watertable data to be incorporated into the moment analysis of the 1983 tracer experiment. Some evidence exists to support this assumption of stationarity. Certain similarities are evident between the waterlevel data from the emplaced source site and the data given by MacFarlane et al. (1983) and Sudicky (1986) [see Table 2.5 and Figures 2.25 and 2.26].

Table 2.5

Watertable Data for the Borden Aquifer

	Emplaced Source Experiment 1989	MacFarlane et al. 1983	Sudicky 1986
Range in Water-table Fluctuation (m)	0.8	1.0	--
Range in Flow Angle (degrees)	39	13	14
Minimum Gradient	3.3×10^{-3}	3.5×10^{-3}	3.6×10^{-3}
Maximum Gradient	6.4×10^{-3}	5.4×10^{-3}	5.6×10^{-3}

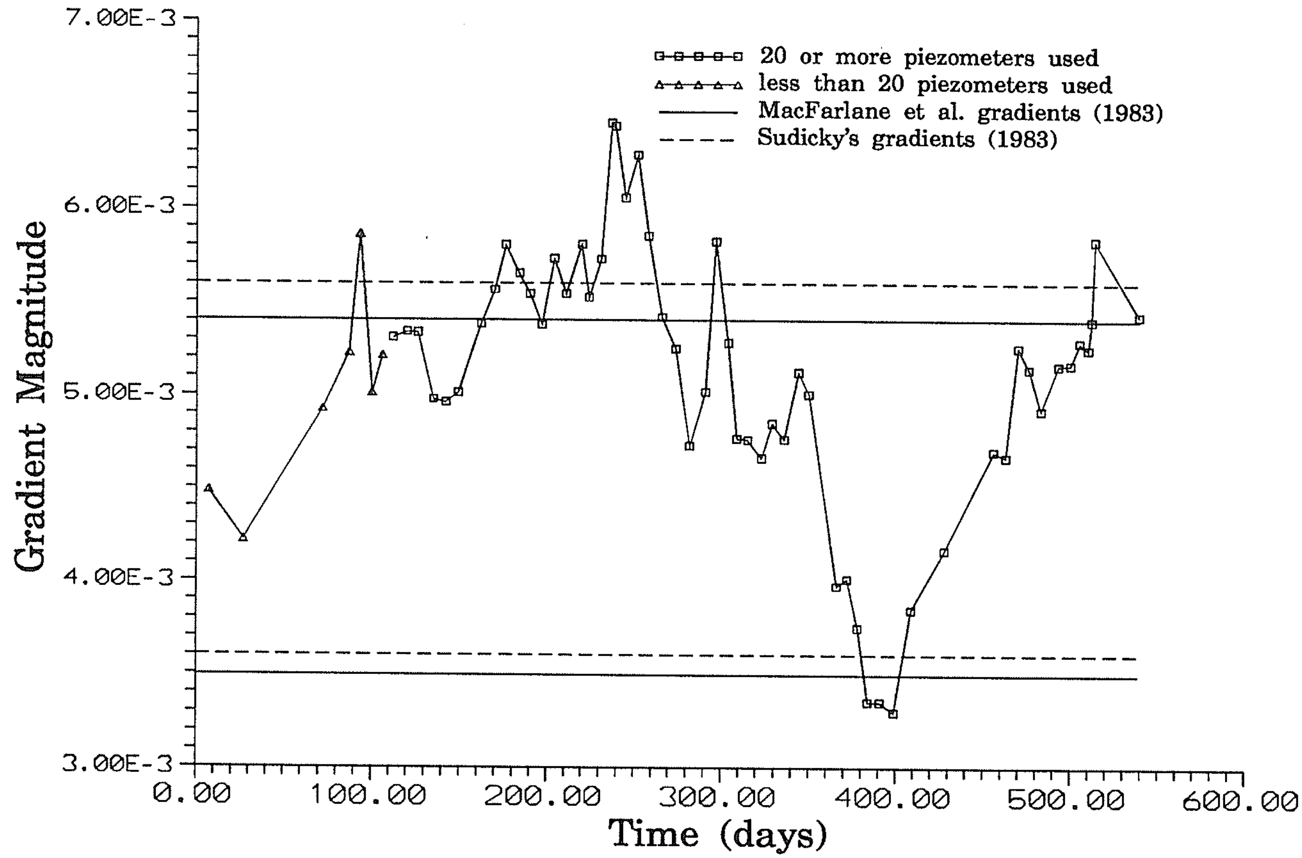

Figure 2.25 Observed gradient magnitude |J| time series compared to the observed maximum and minimum gradient magnitudes given by MacFarlane et al. (1983) and Sudicky (1986).

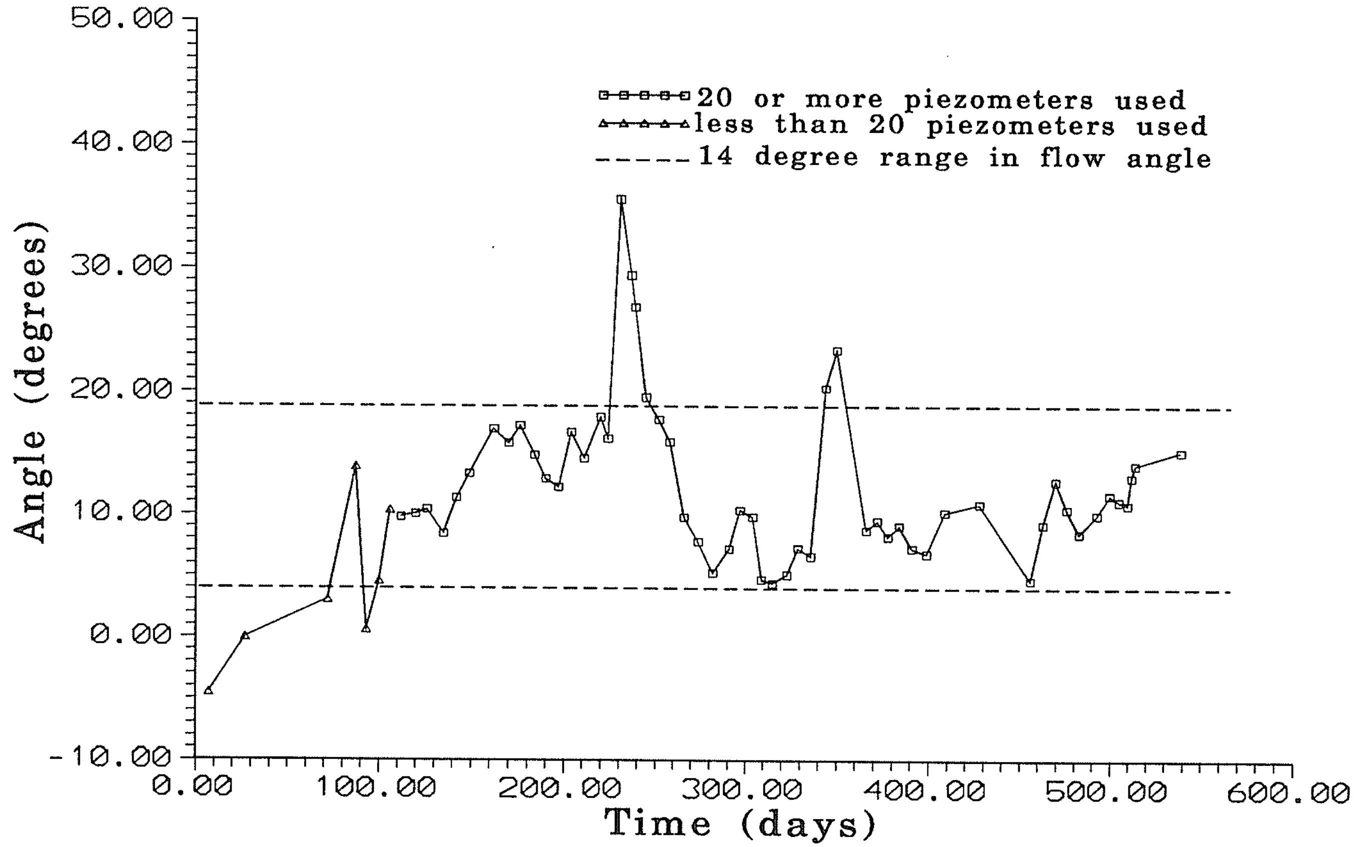

Figure 2.26 Observed flow angle time series with 14° range superimposed.

An examination of Table 2.5 and Figure 2.25 shows that the maximum waterlevel fluctuations and the maximum and minimum hydraulic gradient magnitudes for the waterlevel data from the emplaced source site compare well with the observations of MacFarlane et al. (1983) and Sudicky (1986). However, the deviation in flow angle (39°) for the waterlevel data from the emplaced source site (see Table 2.5) is approximately three times the values reported by MacFarlane et al. (1983) and Sudicky (1986). Figure 2.26 shows the flow angle time series for the waterlevel data from the emplaced source site with a 14° range in flow angle superimposed on it. From this figure it is seen that the majority of the data points for the waterlevel data from the emplaced source site fall within the range observed by MacFarlane et al. (1983) and Sudicky (1986). It is possible that part of the observed difference between the data from the emplaced source site and those of MacFarlane et al. (1983) and Sudicky (1986) is due to differences in sample density. For this waterlevel data recorded at the emplaced source site the sample density was approximate one sample period per week compared to approximately one sample per month for the data set of MacFarlane et al. (1983).

2.5.1 Application of Geostatistical Results to the Asymptotic Model

Substitution of the computed gradient magnitude and flow angle variances and integral scales (refer to Tables 2.2, 2.3 and 2.4) along with the mean gradient magnitude ($|J| = 0.0043$), the flow factor ($\gamma = 1.16149$) and the flow velocity ($\bar{U} = 0.091$ m/day) given by Sudicky (1986) into equations (2.10) and (2.11) yields the asymptotic macrodispersivity results shown in Table 2.6. By replacing the expected values used for the variances and the integral scales in the above calculations with the 95% confidence limit values for these parameters (see Table 2.2 and 2.3) estimates for the asymptotic macrodispersivities at the 95% confidence limit have been obtained (see Table 2.6).

Table 2.6

Computed Macrodispersivities in the Longitudinal and Transverse Directions

	Horizontal Transverse Macrodispersivity (m)			Longitudinal Macrodispersivity (m)		
	Lower	Expected	Upper	Lower	Expected	Upper
7 - 539	0.002	0.031	0.054	--	0.165	--
112 - 539	~ 0.0	0.017	0.040	--	0.341	--

Note: Lower refers to the lower 95% confidence limit.
Upper refers to the upper 95% confidence limit.

In Table 2.6, it can be seen that the computed asymptotic horizontal transverse macrodispersivity and its associated 95% confidence limits are statistically equivalent to those of Freyberg (1986) [0.039m], Rehfeldt (1988) [0.013m] and Rajaram and Gelhar (1991) [0.05m]. The horizontal transverse asymptotic macrodispersivity and its 95% confidence levels for the truncated flow angle time series are also in good agreement with the values of Freyberg (1986) and Rehfeldt (1988). If the transverse spread of the plume is assumed to be Fickian (i.e. $\sigma^2=2Dt$), then Figure 2.27 shows that the expected asymptotic horizontal transverse macrodispersivity presented in Table 2.6 provides a good fit to Freyberg's (1986) transverse second moment data beyond 259 days. In addition, the upper and lower 95% confidence limits for the asymptotic horizontal transverse macrodispersivity are found to enclose Freyberg's (1986) transverse second

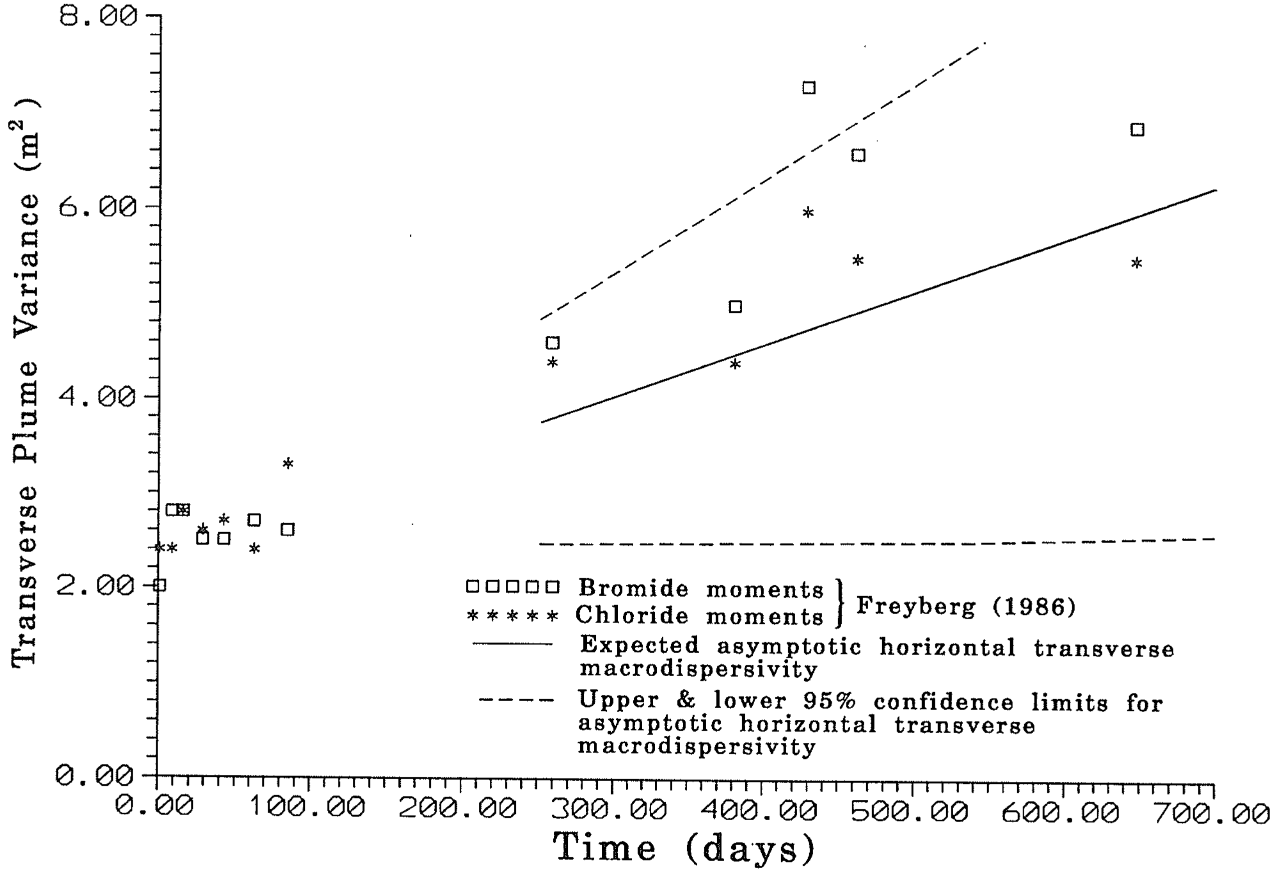

Figure 2.27 Transverse horizontal asymptotic model results fitted to the transverse horizontal moment data of Freyberg (1986).

moment data beyond 259 days quite well.

Estimates for the component due to unsteady flow of the asymptotic longitudinal macrodispersivity are also shown in Table 2.6. Notice the large uncertainty associated with these estimates. These results reflect the uncertainty in the variogram estimates. A more accurate estimate of the variance and integral scale present in the gradient magnitude time series probably requires a longer time series.

2.5.2 Harmonic Analysis of Borden Data

Before the harmonic model can be used to predict the transverse moment data at the Borden site the gradient time series perpendicular to the mean flow direction (the $\mathbf{a}_2$ gradient component, see Figure 2.2) must be computed and a harmonic analysis performed. This latter task is performed using the Fast Fourier Transform (FFT) method.

The $\mathbf{a}_2$ gradient time series is computed using the following expression

$$a_2(t) = |J(t)| * \sin[\Gamma(t)] \qquad \ldots(2.35a)$$

where

$$\Gamma(t) = \Omega(t) - \bar{\Omega} \qquad \ldots(2.35b)$$

where $\bar{\Omega}$ is the mean flow angle, $\Omega(t)$ is the flow angle at time t and $|J(t)|$ is the mean gradient magnitude at time t. Figure 2.28 shows the computed $\mathbf{a}_2$ gradient time series.

The FFT method requires that the sample interval be constant in time. Unfortunately this not the case for the waterlevel data. The time series data must therefore be interpolated onto a regular grid. The linear and the natural cubic spline

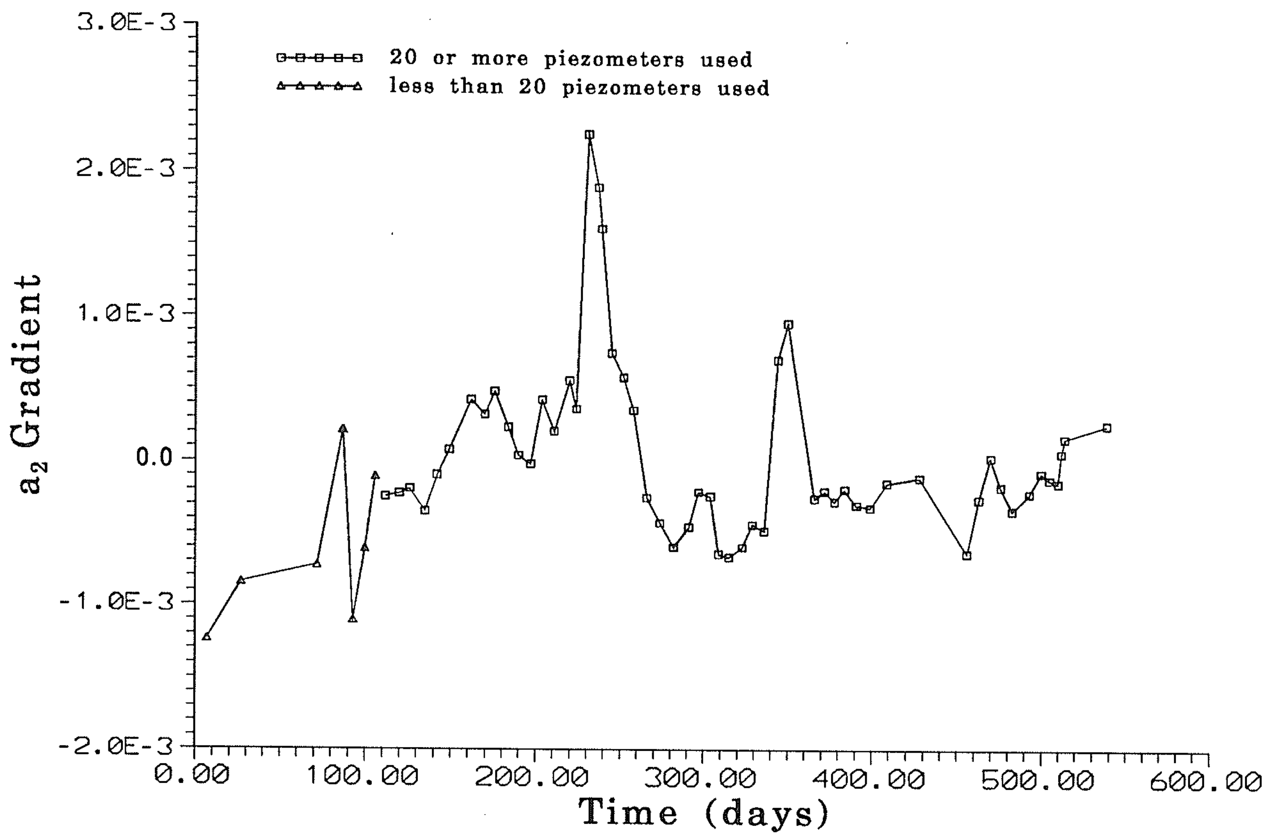

Figure 2.28 Observed gradient perpendicular to the mean flow direction (a_2) vs time.

interpolation methods (Smith, 1986, p.273) are used to interpolate the data onto a 128 point grid with a sample interval of approximately 4 days. A 128 point grid is chosen for two reasons. The first reason is that the FFT method requires that the input data set contain 2^n points. Secondly, 128 points result in a sample interval which is greater than the minimum waterlevel sample interval. Both methods produce similar results with the major differences being at early times when the waterlevel data spacing is much greater than the interpolation interval.

In addition to the precautions used to prevent aliasing in the frequency domain when performing spectral analysis, care must also be taken when interpreting the amplitudes obtained from spectral analysis. Based on the FFT algorithms which have been tested (NLOGN, Robinson) it is found that the FFT method tends to scale the true amplitudes of a signal by a factor of NPTS/2, where NPTS is the number of points in the data set. The length of the data set can be increased by the addition of zeros after the time signal when using the FFT method (Kanasewich, 1981, p.121). The addition of zeros increases the resolution in the frequency domain without altering the observed amplitudes. By using 2^{13} zeros a resolution in the order of 10^{-5} cycles/day has been achieved. Figure 2.29, shows the frequency spectrum of the a_2 gradient data set, while Figure 2.30 shows the reconstructed signal compared to the original signal.

2.5.3 Application of Harmonics to the Time Dependent Model

The harmonics computed from the a_2 gradient time series are substituted into equation (2.18) and the displacement time series, X(t) computed. The value of B used

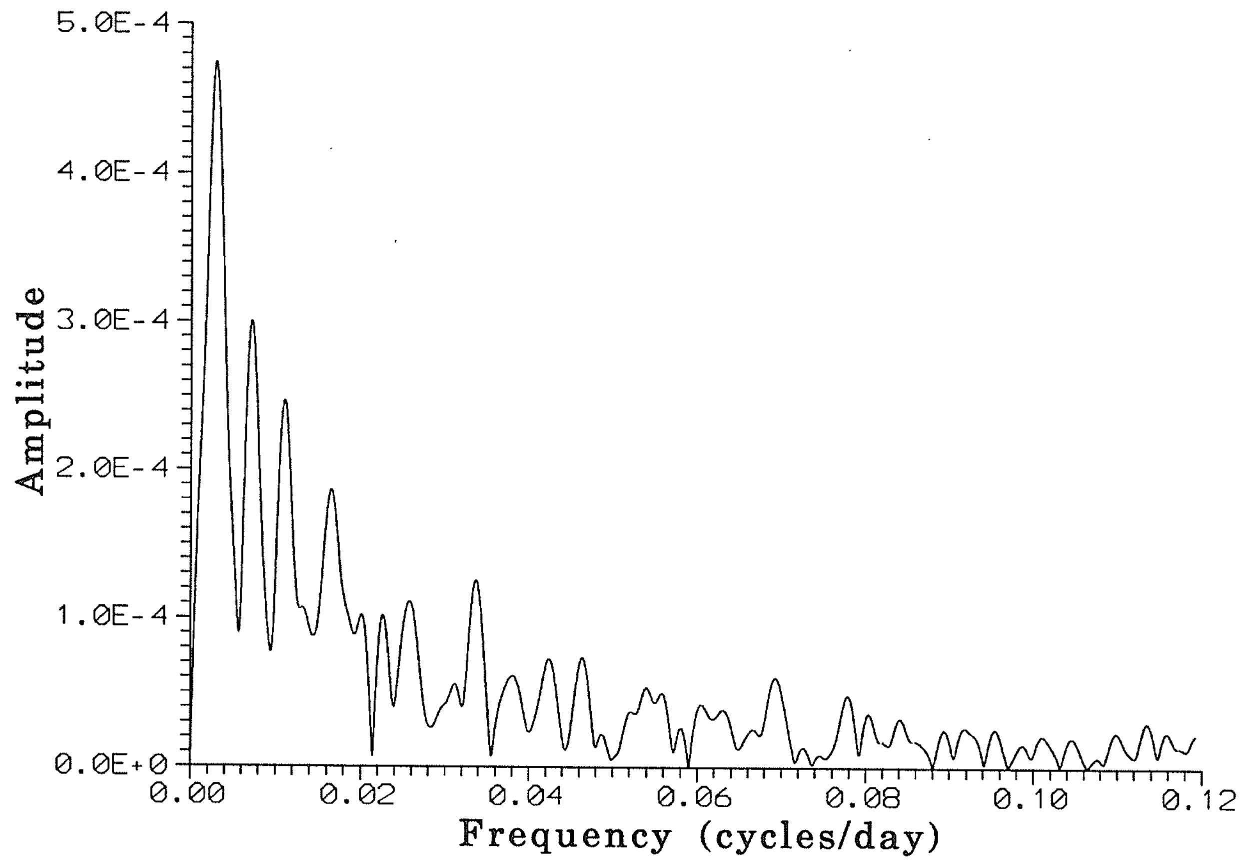

Figure 2.29 Frequency spectrum of $\mathbf{a}_2$ gradient time series.

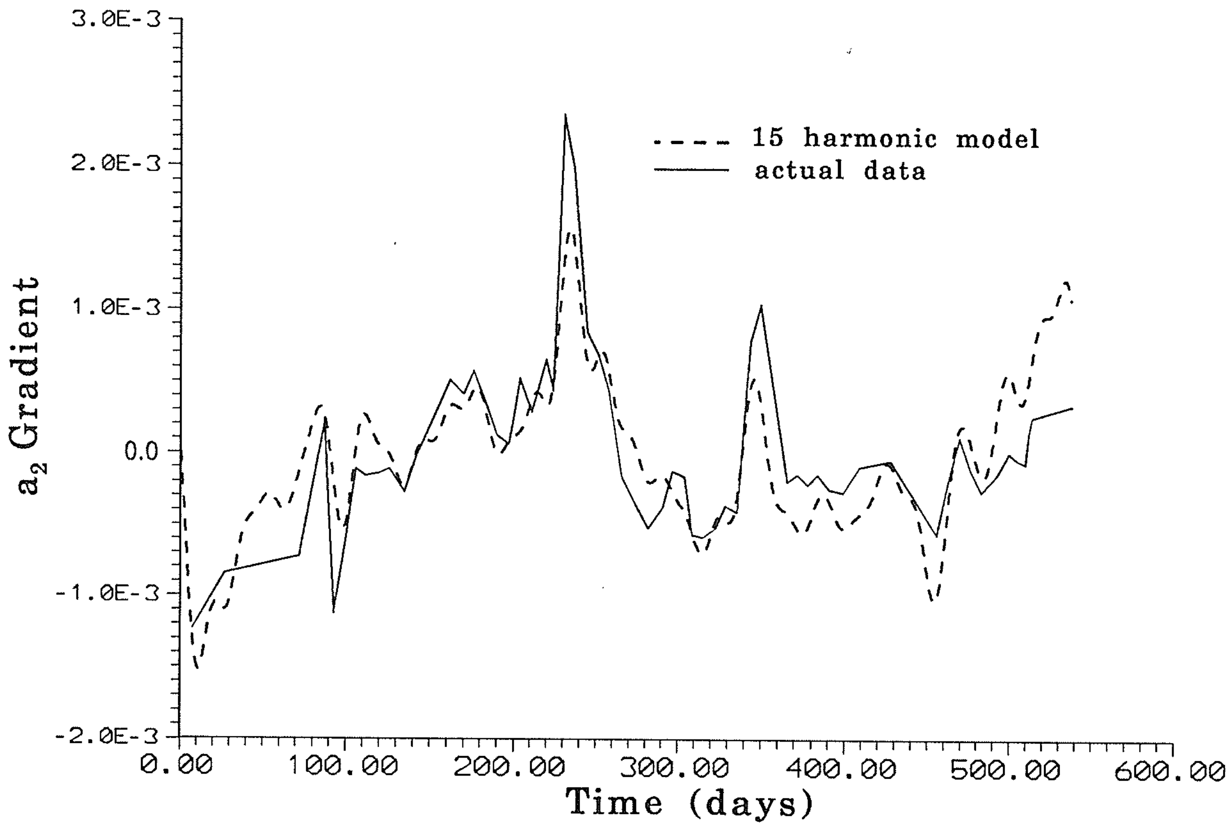

Figure 2.30 Comparison of time series based on 15 harmonics to the observed a_2 gradient time series.

is equal to one since the hydraulic conductivity of the aquifer is constant in the horizontal plane (see Sudicky, 1986). Note that the start time of the displacement time series (August 1, 1989 or seven days after the start of the emplaced source experiment) and the start time for the Borden tracer experiment (August 23, 1982) are different. By making the assumption of stationarity, the first 22 days of the displacement time series must be ignored to obtain the displacement time series for the Borden experiment. If the extra 22 days of data are not removed an enhanced spreading moment will be obtained. The displacement time series is then substituted into equation (2.19) to solve for the temporal variance in the horizontal transverse direction. The results (Figure 2.31) show that the harmonic method produces a poor fit to Freyberg's horizontal transverse second moment data.

Naff et al. (1989) obtained a fit to Freyberg's horizontal transverse second moment data by including a four year harmonic in their model. To test whether the fit to Freyberg's 2nd moment data will be improved by the use of a longer a_2 time series the following experiment is performed. Since the assumption has been made that the flow field is stationary, then it is in principle possible to repeat the time series beyond 539 days using the assumption of a one year period. The extended time series is shown in Figure 2.32. The frequency spectrum for this time series is shown in Figure 2.33 and the reconstructed time series based on 15 harmonics is shown in Figure 2.34 along with the extended time series. The harmonics obtained from the frequency spectrum are inserted into equation (2.18) and the results then substituted into equation (2.19) and the horizontal transverse spreading moments computed (Figure 2.35). The results show that

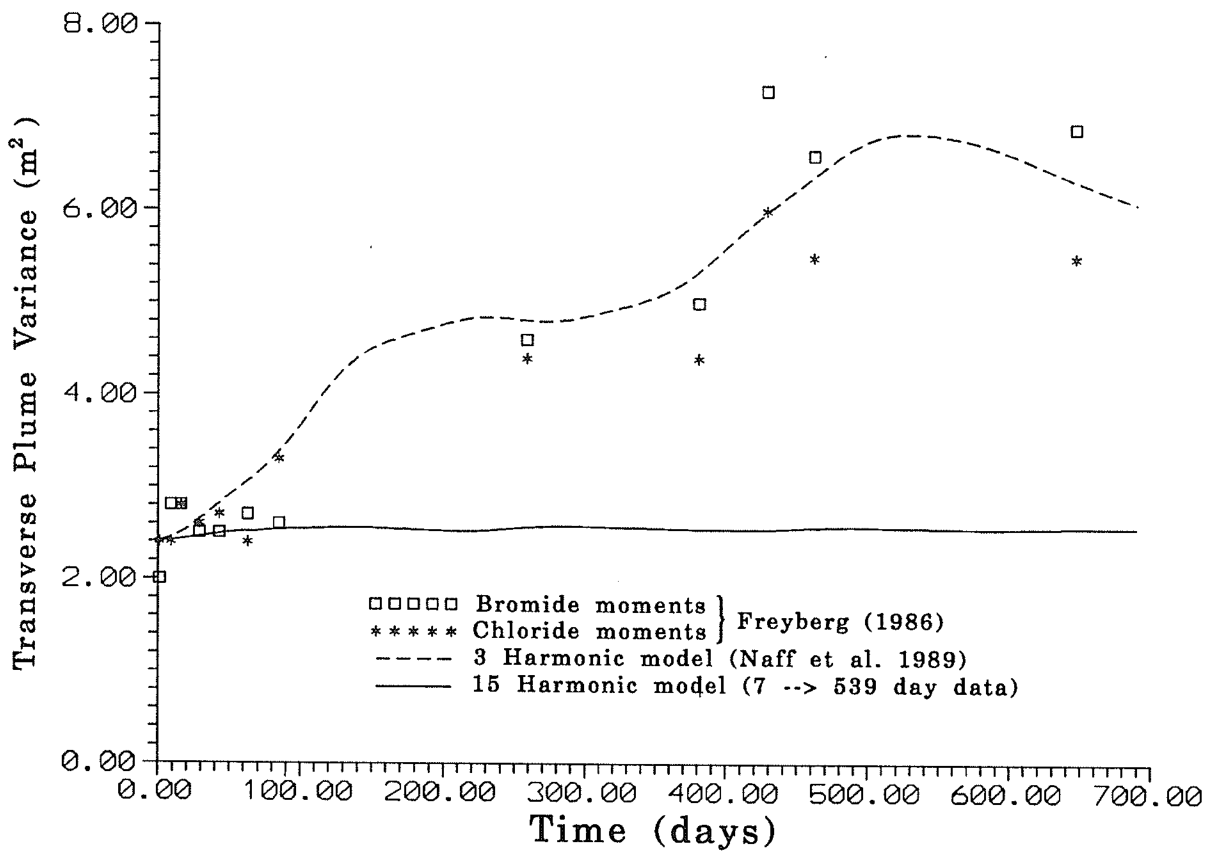

Figure 2.31 Results of the harmonic model fitted to the transverse horizontal moment data of Freyberg (1986) for the Borden site.

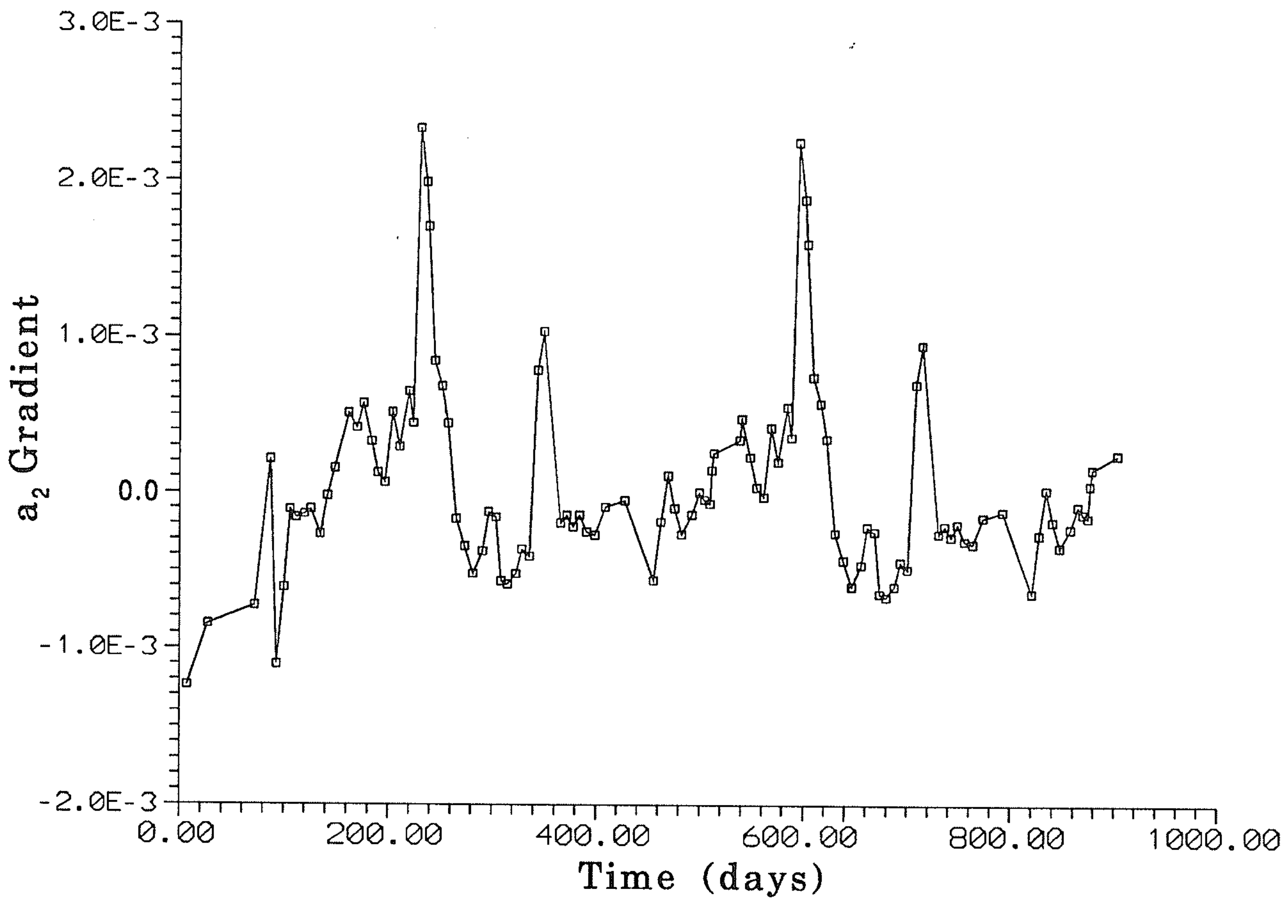

Figure 2.32 Extended a_2 gradient time series (7 - 904) days.

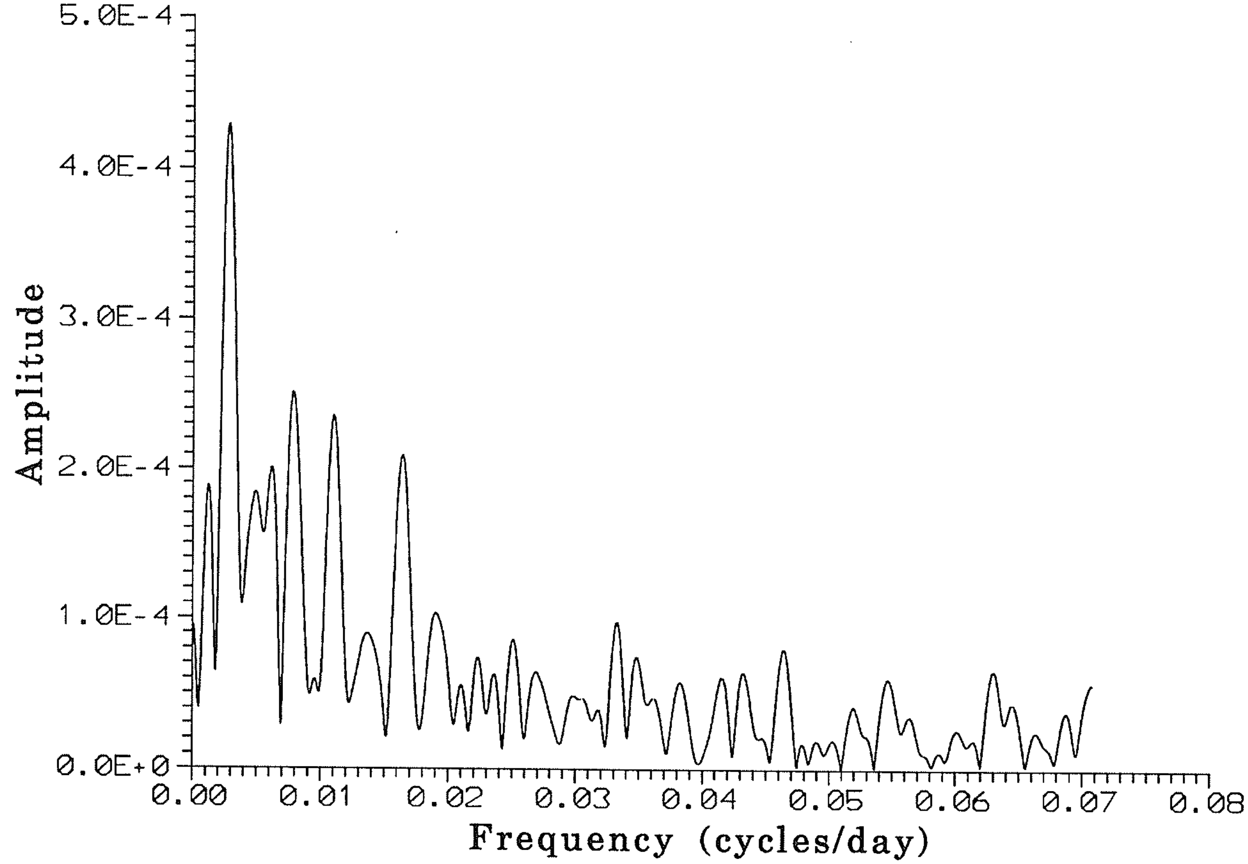

Figure 2.33 Frequency spectrum for extended a_2 gradient time series.

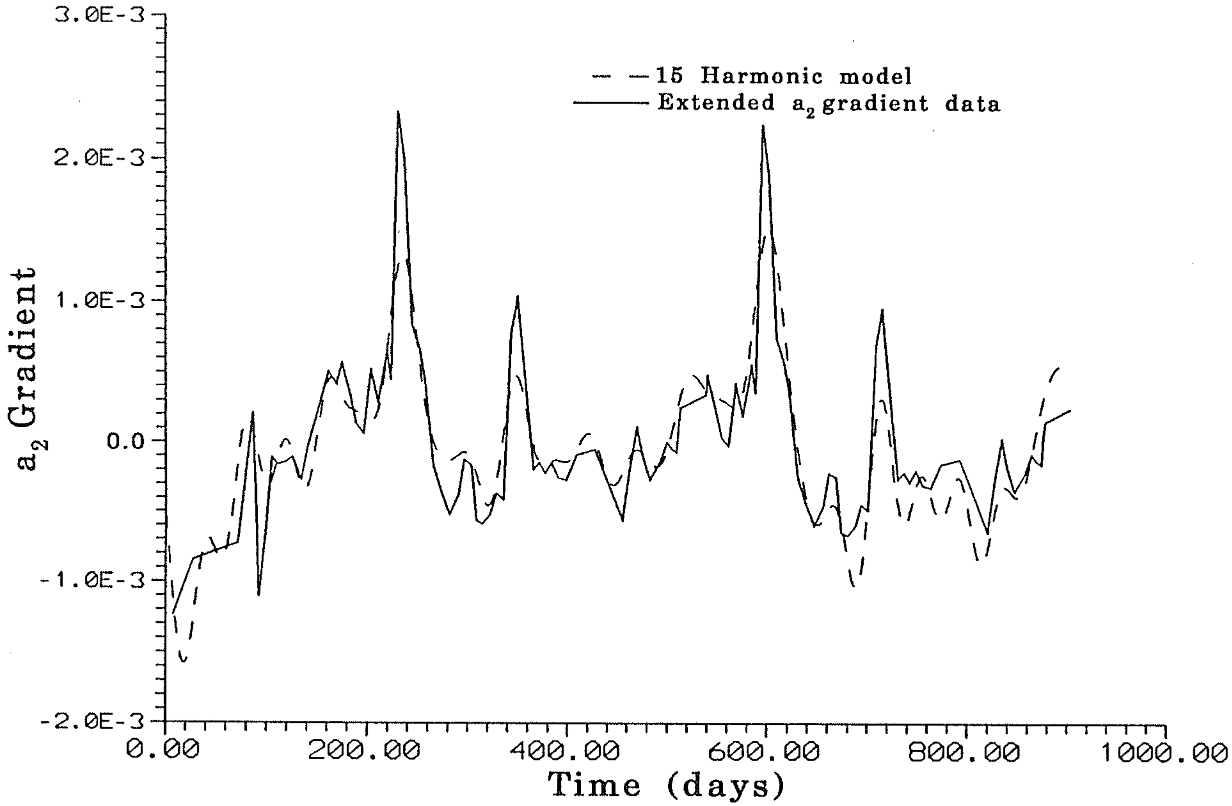

Figure 2.34 Comparison of time series based on 15 harmonics to the extended a_2 gradient time series.

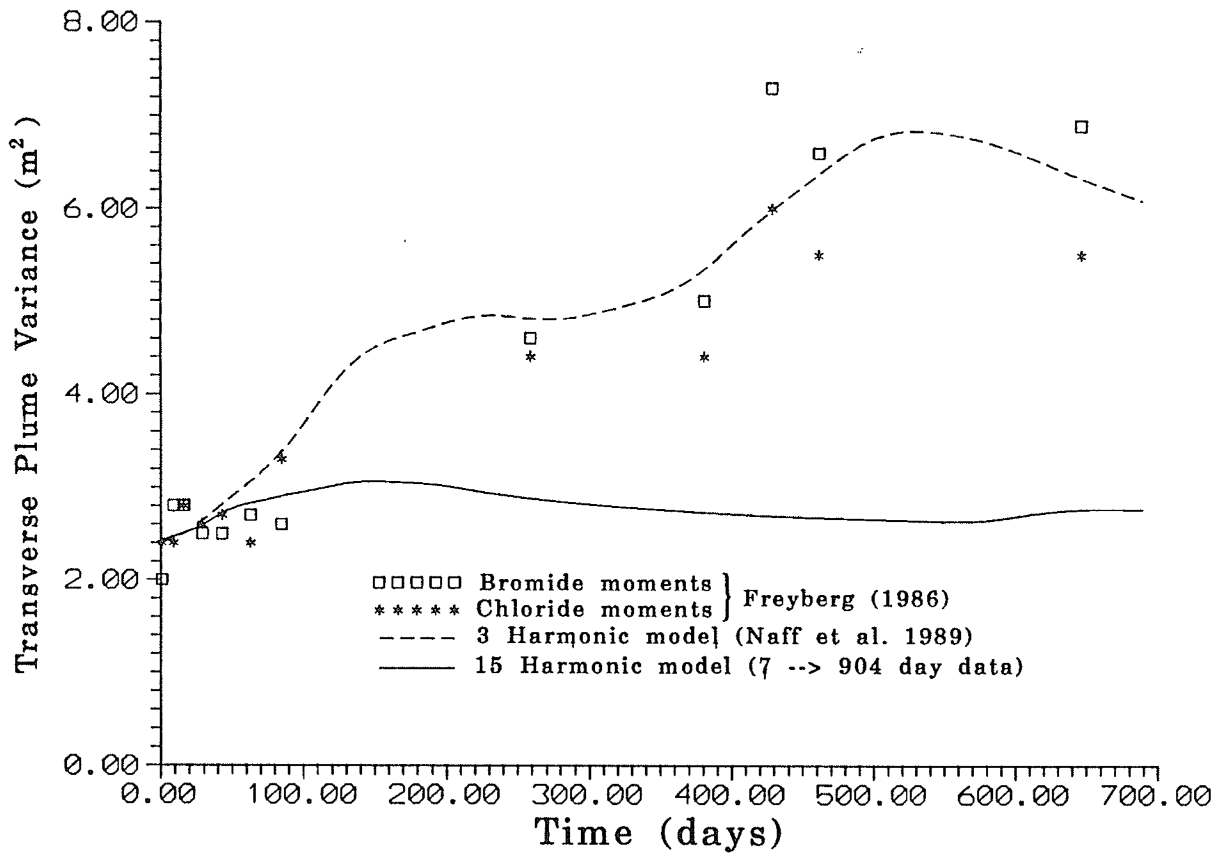

Figure 2.35 Results of the harmonic model (extended time series) fitted to the transverse horizontal moment data of Freyberg (1986) for the Borden site.

the increased time series slightly improves the fit to Freyberg's data; however the fit is still quite poor.

2.6 Discussion and Conclusions

The computation of the macrodispersivity in this paper is based on the assumption that the flow field at the Borden site is stationary in both space and time. It is found that if the geostatistical parameters (variances and integral scales) derived from the 1989 watertable data are used to evaluate the 1983 tracer data, then the asymptotic horizontal transverse macrodispersivity computed using Rehfeldt's (1988) theory is in statistical agreement with the asymptotic horizontal transverse moment estimates of Freyberg (1986) and Rajaram et al. (1991). This indicates that waterlevel fluctuations play an important role in the spreading of contaminants in the horizontal transverse direction at the Borden site, and confirms the results of deterministic analyses such as that of Goode and Konikow (1990).

In applying an altered form of the model of Naff et al. (1989), the assumption of stationarity in the flow field at the Borden aquifer also has to be made. Again, using the gradient time series from the 1989 watertable data and predicting plume transverse second moments, the results obtained using this approach provided a poor fit to Freyberg's (1986) observed transverse moment data for the plumes at the Borden site.

It is important to compare the results of the Harmonic moment model to Rehfeldt's asymptotic approach. If the moment model is correct, it should produce a function that at later times plots near the straight line produced by the dispersivity value computed using Rehfeldt's model (see Figure 2.27). The dissimilarity between the two approaches indicates that the deterministic-harmonic approach does not capture the essence of the lateral mixing process under time-varying conditions. Therefore, a gap still exists between early and asymptotic time behaviour. Based on the work in this paper it does appear that a more general stochastic framework for plume evolution and dispersion in a heterogeneous media with an unsteady mean flow field is required.

Finally this work does suggest that flow transients are important contributors to the horizontal transverse dispersion process. Rehfeldt's model suggests that the observed dispersion process in an observed plume can be modelled by an enhanced horizontal dispersivity when flow field transients are present. It is important to note that the observed gradient variations in time are actually quite small at the Borden site and yet they account for almost all of the horizontal spreading. It is very common in contaminant transport modelling efforts to assume steady groundwater velocity. The implications here are that such models may not be universally applicable and that not only must variations in hydraulic conductivity be taken into account but also time variations of the hydraulic heads. This has further implications in site and risk assessment if perhaps years of prior monitoring at designated sites are required before commissioning.

References

Brigham, E. O., The Fast Fourier Transform, Prentice-Hall, 1974.

Dagan, G., Time-dependent macrodispersion for solute transport in anisotropic heterogeneous aquifers, Water Resour. Res., 24(9), 1491-1500, 1988.

Draper, N. R. and Smith, H., Applied Regression Analysis, 2nd ed., John Wiley, New York, 1981.

Freyberg, D. L., A natural gradient experiment on solute transport in a sand aquifer, 2, Spatial moments and the advection and dispersion of non-reactive tracers, Water Resour. Res., 22(3), 2031-2046, 1986.

Gelhar, L. W. and Axness, C. L., Three-dimensional stochastic analysis of macro-dispersion in aquifers, Water Resour. Res., 19(1), 161-170, 1983.

Goode, D. J. and Konikow, L. F., Apparent dispersion in transient groundwater flow, Water Resour. Res., 26(10), 2339-2351, 1990.

Hippel, K., Geophysical Model Discrimination Using the Akaike Information Criterion, IEEE Trans. Autom. Control, AC-26(2), 358-378, 1981.

Hoesksema, R. J. and Kitanidis, P. K., Analysis of the Spatial Structure of Properties of Selected Aquifers, WRR, 21(4), 563-572, 1985.

Journel, A. G. and Huijbregts C. J., Mining Geostatistics, New York, Academic Press, 1978.

Kanasewich, E. R., Time Sequence Analysis in Geophysics, The University of Alberta Press, 1981.

Kinzelbach, W. and Ackerer, P., Modelisation de la propagation d'un contaminant dans un champ d'ecoulement transitoire, Hydrogeologie, 2, 197-205, 1986.

Kleinbuam, D. G., Kupper, L. L. and Muller, K. E., Applied Regression Analysis and Other Multivariate Methods, PWS-Kent Publishing Company, 1987.

Lawson, C. L. and Hanson, R. J., Solving Least Squares Problems, Prentice-Hall, Englewood Cliffs, New Jersey, 1974.

Loaiciga, H. A., Shumway, R. H. and Yeh, W. W. -G., Linear spatial interpolation, Analysis with an application to San Joanquin Valley, Stochastic Hydrol. Hydraul., 2, p. 113-136, 1988.

MacFarlane, D. S., Cherry, J. A., Gilham, R. W. and Sudicky, E. A., Migration of contaminants at a landfill, A case study, 1, Groundwater flow and plume delineation, J. Hydrol., p. 63, 1-29, 1983.

Naff, R. L., J. T. -C. Yeh, and M. W. Kemblowski, A note on the recent natural gradient experiment at the Borden site, Water Resour. Res., 24(12), p. 2099-2104, 1988.

Naff, R. L., Yeh, J. T. -C. and Kemblowski, M. W., Reply, Water Resour. Res., 25(12), p. 2523-2525, 1989.

Neuman, S. P. and Jacobson, E. A., Analysis of non-intrinsic spatial variability by residual Kriging with applications to regional groundwater levels, Math. Geol., 16(5), p. 499-521, 1984.

Rajaram, H. and Gelhar, L. W., Three-dimensional spatial moments analysis of the Borden Tracer Test, Water Resour. Res., 27(6), p. 1239-1251, 1991.

Rehfeldt, K. R., Prediction of macro-dispersivity in heterogeneous aquifers, Ph. D.

dissertation, MIT, 1988.

Robinson, E. A., Multichannel Time Series Analysis with Digital Computer Programs, Holden Day, San Francisco, 1967.

Shafer, J. M. and Varljen, M. D., Approximation of confidence limits on sample semivariograms from single realizations of spatially correlated random fields, Water Resour. Res., 26(8), p. 1787-1802, 1990.

Smith, W. A., Elementary Numerical Analysis, Prentice-Hall, 1986.

Stedinger, J. R. and Tasker, G. D., Regional hydrologic analysis, 1., Ordinary, weighted and generalized least squares compared, Water Resour. Res., 21(9), p. 1421-1432, 1985.

Sudicky, E. A., A natural gradient experiment on solute transport in a sand aquifer, Spatial variability of hydraulic conductivity and its role in the dispersion process, Water Resour. Res., 22(13), p. 2069-2082, 1986.

Sykes, J. F., Pahwa, S. B., Lantz, R. B. and Ward, S. D., Numerical simulation of flow and contaminant migration at an extensively monitored landfill, Water Resour. Res., 18(6), p. 1687-1704, 1982.

Woodbury, A. D., Bayesian updating revisited, Math. Geol., 21(3), 287-308, 1989.

Woodbury, A. D. and Sudicky, E. A., The geostatistical characteristics of the Borden aquifer, Water Resour. Res., 27(4), p. 533-546, 1991.

Zhang, Y. -K. and Neuman, S. P., A quasi-linear theory of non-Fickian and Fickian subsurface dispersion, 2, Application to anisotropic media and the Borden site, Water Resour. Res., 26(5), p. 903-913, 1990.

Chapter 3

The 1978 Borden Tracer Experiment; Analysis of the Spatial Moments

3.1 Introduction

During the last two decades a few natural gradient tracer experiments have been conducted at various field sites. The most discussed of these experiments has been the Stanford-Waterloo tracer experiment which was conducted at the Borden aquifer (see Mackay et al., 1986). This experiment involved detailed three-dimensional monitoring of solutes injected into the aquifer under natural flow conditions. In addition, Sudicky (1986), and Woodbury and Sudicky (1991) based on the analysis of core samples provided a detailed characterization of the geostatistical properties of the hydraulic conductivity field of the aquifer. Other similar experiments were the 1978 tracer experiment at the Borden aquifer (see Sudicky et al., 1978) and the Cape Cod experiment (see LeBlanc et al., 1991). The results obtained from these experiments have confirmed (1.) the earlier results that dispersivity is influenced by the distance travelled (see Sauty, 1980) and increases with time (see Dieulin, 1980); and (2.) the dependence of the asymptotic longitudinal macrodispersivity on aquifer heterogeneity suggested by Gelhar and Axness (1983) (see Sudicky, 1986). In addition, these field experiments have indicated the presence of horizontal transverse dispersion processes within the aquifers which are not accounted for in the stochastic theories of Gelhar and Axness (1983) and Dagan (1982, 1984, 1987 and 1988). A number of researchers have suggested that the observed horizontal transverse dispersion may be due to the presence of flow transients at the sites (see Sykes et al.; 1982 and Sudicky, 1986). Expressions for the components of the asymptotic macrodispersivity due to unsteady flow have been developed by Rehfeldt (1988). These expressions have been field validated by the work of Garabedian et al. (1991) for the Cape Cod experiment and by Farrell et al. (1992) for the Stanford-Waterloo experiment.

Spatial moment analyses have been the primary tool for analyzing the evolution of solute plumes being transported in the subsurface. Traditionally such analyses have been limited to the examination of second and lower order moments, and so provide information on the amount of mass in the plume, the velocity of the centre of mass of the plume, and the macrodispersivity of the porous medium [see Freyberg (1986), Barry et al. (1988), Garabedian et al. (1988) and Rajaram and Gelhar (1991)]. In addition to these low order moments, higher order moments can also be determined to help in the characterization of subsurface plumes. In particular, the third and the fourth moments allow the skew and the kurtosis (respectively) of the concentration distribution in the plume to be examined. Gelhar et al. (1979) and Naff (1990) have examined the evolution of these higher moments for solute concentration distributions in stratified aquifers using theoretical approaches. Some differences exist between these two works with regard to the behavior of the skew. Naff (1990) indicates that the skew of the concentration distribution in the plume is not pronounced; the observed deviation from a normal distribution is the result of the platykurtic nature of the plume at early time. However, the work of Gelhar et al. (1979) shows that at early time the skew is significant; the concentration distribution within the plume being positively skewed. In regards to the higher moments very little work has been done at any of these tracer sites with respect to examining their behavior even though large data bases exist.

In this work a reanalysis of the 1978 tracer experiment data for the Borden site is performed using moment analysis techniques. In addition to the second and lower order moments and associated parameters (i.e. mass in solution, velocity of centre of mass and macrodispersivity) an analysis of the higher moments is also performed in order to examine the evolution of the skew and the kurtosis of the concentration distribution within the plume at early time. The results will be compared with the dispersivity and velocity estimates of Sudicky et al. (1983) for the plume as well as with the theoretical moments results of Gelhar et al. (1979) and Naff (1990). In addition, an examination and partial explanation of the contradiction between the theories of Gelhar et al. (1979) and Naff (1990) will be attempted.

3.2 Theory

3.2.1 Spatial Moments

Freyberg (1986) (see also Aris, 1956) defined the ijk^{th} moment of a concentration distribution in space, M_{ijk} as

$$M_{ijk}(t)=\int_{-\infty}^{\infty}\int_{-\infty}^{\infty}\int_{-\infty}^{\infty} nC(x,y,z,t)x^i y^j z^k \, dx \, dy \, dz \tag{3.1}$$

where C(x,y,z,t) is the mass concentration of solute in solution (above background), x, y and z are the spatial coordinates and n is the porosity of the porous medium. Equation (3.1) is defined for all space; however, it is clear that the integrand will be zero at points where the plume concentration is zero. Therefore, the spatial moment gives an integrated measure of the concentration field over the extent of a plume. To determine the plume properties such as the velocity, dispersivity, skew and kurtosis the zeroth to the fourth moments are required.

The zeroth moment is obtained when i+j+k=0 in (3.1) [see Freyberg, 1986], and provides a measure of the mass of solute present in solution. For a conservative tracer the total mass of solute in solution should remain constant. Hence the zeroth moment will give an indication of how well a plume has been sampled as it moves through the porous medium. For example, if the mass estimate obtained from the zeroth moment estimate is small when compared to the injected mass then it suggests that the plume is poorly sampled at a particular instant.

The first moment is obtained when i+j+k=1 in (3.1) [see Freyberg, 1986]. Normalizing the first moment with respect to the zeroth moment gives the location of the centre of mass of the plume (x_c,y_c,z_c).

$$x_c=\frac{M_{100}}{M_{000}} \qquad y_c=\frac{M_{010}}{M_{000}} \qquad z_c=\frac{M_{001}}{M_{000}} \tag{3.2}$$

Differentiation of the position of the centre of mass of the plume with respect to time gives the velocity, U of the centre of mass of the plume.

$$U = \left[\frac{\partial x_c}{\partial t}, \frac{\partial y_c}{\partial t}, \frac{\partial z_c}{\partial t} \right]^T \tag{3.3}$$

For the case i+j+k≥2 the moments about the centre of mass may be determined using (3.4) [see Naff[1], equation (5), 1990].

$$M_{ijk}(t) = \int_{-\infty}^{\infty}\int_{-\infty}^{\infty}\int_{-\infty}^{\infty} (x-x_c)^i (y-y_c)^j (z-z_c)^k \; nC(x,y,z,t) \; dx \; dy \; dz \tag{3.4}$$

The higher moments computed using (3.4) are important for characterizing the solute spread about the centre of mass of the plume and therefore provides an easy way for computing the dispersivity, skew and the kurtosis.

The second central plume moment is obtained when (3.4) is evaluated with i+j+k=2 [see Freyberg,1986]. Normalizing the second moments with respect to the plume mass produces the terms of the spatial covariance tensor.

$$\sigma^2 = \begin{bmatrix} \sigma^2_{xx} & \sigma^2_{xy} & \sigma^2_{xz} \\ \sigma^2_{yx} & \sigma^2_{yy} & \sigma^2_{yz} \\ \sigma^2_{zx} & \sigma^2_{zy} & \sigma^2_{zz} \end{bmatrix} \tag{3.5a}$$

$$\sigma^2_{xx} = \frac{M_{200}}{M_{000}} \qquad \sigma^2_{yy} = \frac{M_{020}}{M_{000}} \qquad \sigma^2_{zz} = \frac{M_{002}}{M_{000}} \tag{3.5b}$$

$$\sigma^2_{xy} = \sigma^2_{yx} = \frac{M_{110}}{M_{000}} \qquad \sigma^2_{xz} = \sigma^2_{zx} = \frac{M_{101}}{M_{000}} \qquad \sigma^2_{yz} = \sigma^2_{zy} = \frac{M_{011}}{M_{000}} \tag{3.5c}$$

The hydrodynamic dispersion tensor, **D** can be obtained from the spatial covariance tensor using the following equation developed by Einstein (1905).

$$D_{ij}=\frac{1}{2}\frac{d}{dt}\sigma_{ij}^{2}(t) \tag{3.6}$$

Here D_{ij} represents the ij^{th} term of the hydrodynamic dispersion tensor. This expression applies only when the solute displacement field converges to the Gaussian distribution (see Loaiciga, 1988). Bear (1972, p. 764) relates the hydrodynamic dispersion tensor to the pore water velocity by

$$D=D_d I+A|V| \tag{3.7}$$

Here D_d is the molecular diffusion coefficient of the solute in the porous medium; **I** is the identity matrix; **A** is the macrodispersivity tensor and $|V|$ is the magnitude of the velocity vector. The term D_d is usually assumed to be small compared to the second term at field scale. As a result the terms of the macrodispersivity tensor, **A** can be defined as

$$A_{ij}=\frac{1}{2|V|}\frac{d}{dt}\sigma_{ij}^{2}(t) \tag{3.8}$$

Loaiciga (1988) pointed out that if a plume does not approximate a Gaussian distribution then using (3.8) will result in an inappropriate macrodispersivity estimate. In light of this argument Freyberg's definition will be adopted (see Freyberg, 1986 and 1988) and the term "apparent macrodispersivity" used to define values computed by (3.5) in this work.

The third moment about the plume centre of mass is obtained when i+j+k=3 in (3.4). Normalizing the third moment with respect to the plume mass and the cube of the standard deviation of the plume concentration gives the skew, σ^3, in the plume concentration distribution. Note that the skew is actually a diad of order three. In this chapter the principal skew components along the horizontal axes of the reference coordinate system will be examined. These are given as [see Naff[1], 1990, equation (7)]:

$$\sigma^3_{xxx}=\frac{\overline{M}_{300}}{M_{000}\ \sigma_{xx}^{(\frac{3}{2})}} \tag{3.9a}$$

$$\sigma^3_{yyy}=\frac{\overline{M}_{030}}{M_{000}\ \sigma_{yy}^{(\frac{3}{2})}} \tag{3.9b}$$

The fourth moment about the plume centre of mass is obtained when i+j+k=4 in (3.4). Normalizing the fourth moment with respect to the plume mass and the square of the variance gives the kurtosis, σ^4, of the plume concentration distribution [see (3.10a) and (3.10b); compare to Naff[1], 1990, (7)]

$$\sigma^4_{xxxx}=\frac{\overline{M}_{400}}{M_{000}\ \sigma^2_{xx}} \tag{3.10a}$$

$$\sigma^4_{yyyy}=\frac{\overline{M}_{040}}{M_{000}\ \sigma^2_{yy}} \tag{3.10b}$$

As pointed out earlier the aim of this work is to determine the above moments and related parameters for the 1978 tracer experiment plume. In the following section a description of the 1978 tracer experiment will be presented as well as a discussion of the methods used in the evaluation of the spatial integrals.

3.3 The Field Data

The field site for the experiment is shown in Figure 3.1. Sudicky et al. (1983) describe the aquifer as being made up of glaciofluvial sand deposits, which range in thickness from 7.0m to 27.0m. The hydraulic conductivity of the aquifer is reported to be between 4.8×10^{-5} ms^{-1} and 7.6×10^{-5} ms^{-1} and the porosity of the deposit is estimated to be 0.38. Also shown in Figure 3.1 is the chloride component of the leachate plume emanating from the landfill. Sudicky et al. (1983) report that this chloride plume is approximately 2.5m below the zone of the tracer experiment. The background chloride concentration in the area of the tracer experiment is approximately $2.0 mgl^{-1}$ (see Sudicky et al., 1983) and as a result it is assumed to be negligible. Figure 3.2 shows a plan view of the geometry of the injection wells and the multilevel samplers. The horizontal spacing of the samplers ranged from 0.5m to 2.0m while the vertical spacing of the samplers ranged from 0.15m to 0.18m. A more detailed description of the experiment and the procedures used can be found in Sudicky et al. (1983). Chloride ions in solution were injected into the aquifer and allowed to migrate under the natural flow conditions present at the site. The chloride ion concentration distribution of the resulting plume was sampled after 1, 3, 5, 8, 12, 15, 21, 29, and 121 days following the start of the experiment. Figure 3.3 shows the vertical concentration distribution for the sampled part of the plume after one day. It is interesting to note that the forward extent of the plume appears to be staggered, with the plume front intersecting only some of the samplers along row A. The plume displays significant small scale spatial variability in the vertical plane, with concentration variations on the order of 300 mg/l being observed between adjacent

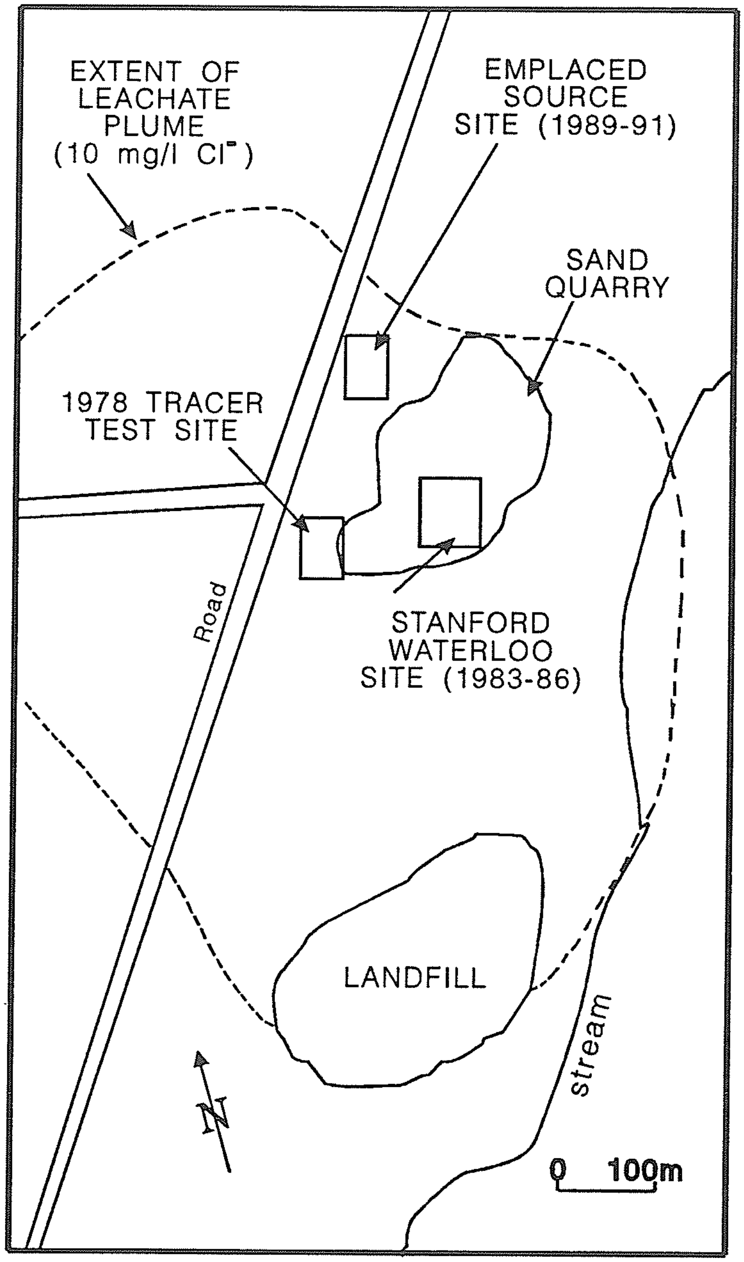

Figure 3.1 Map of the Borden Tracer-test site.

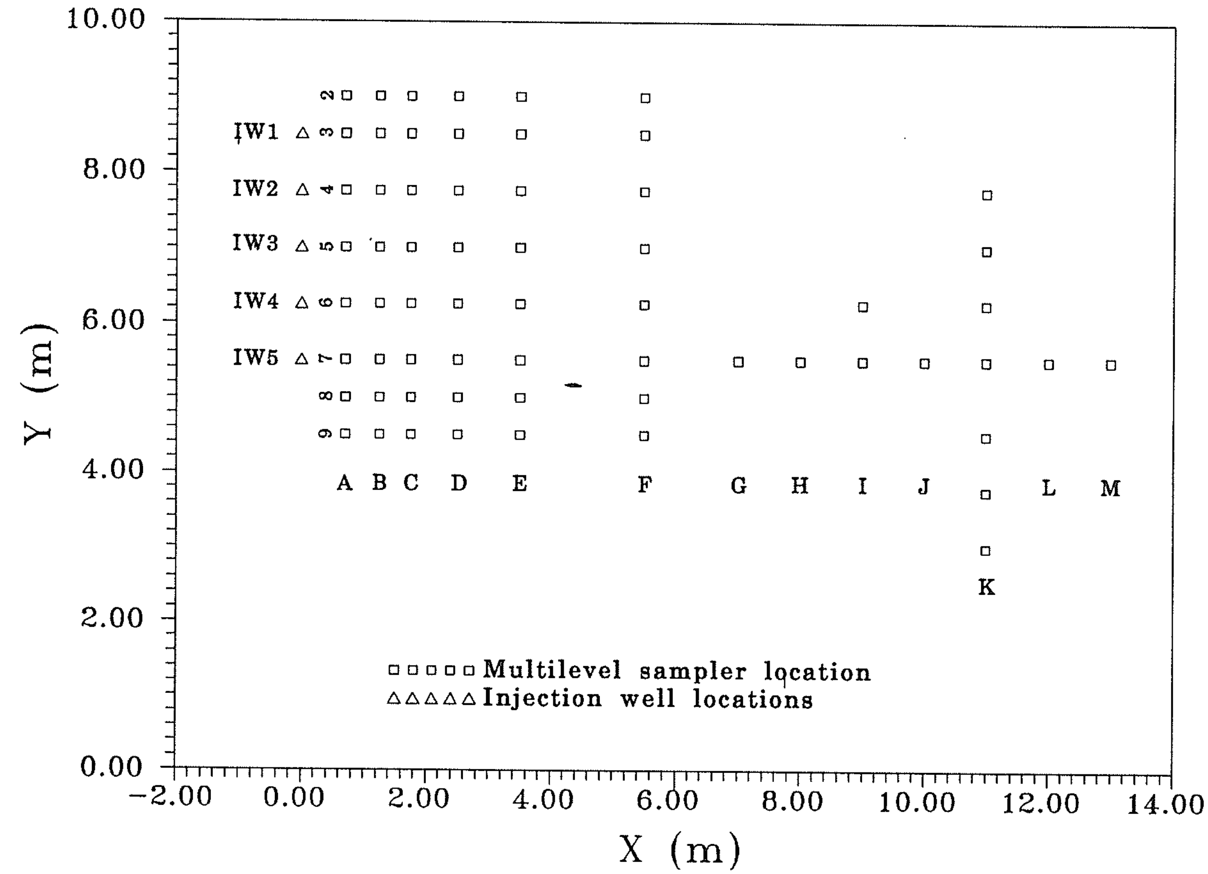

Figure 3.2 Plan view of the injection wells and multilevel sampler array.

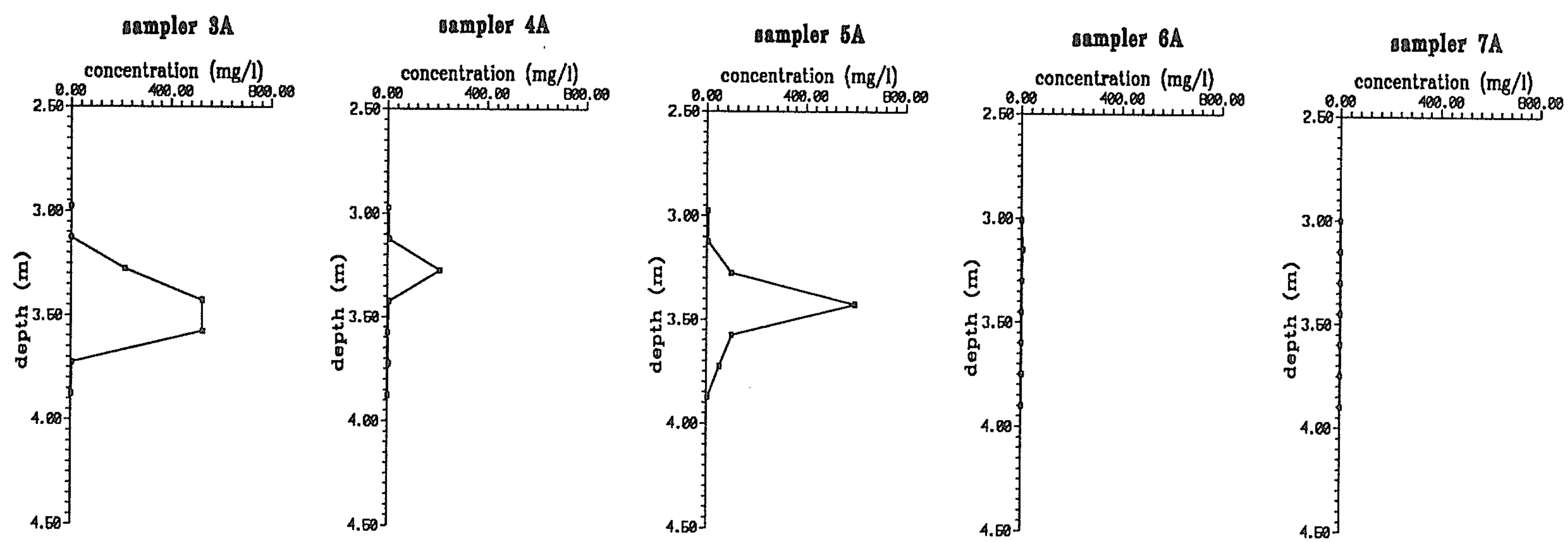

Figure 3.3 Vertical concentration profile after one day (along line A).

sampler ports. However, the vertical distribution profile does appear quite similar in shape along row A suggesting some possible large scale structuring in the aquifer. Sudicky et al. (1983) attributed this to presence of high conductivity lenses in the aquifer. In addition, it can be seen from Figure 3.3 that the multilevel samplers truncate the plume in various places. Rajaram and Gelhar (1991) have shown that if the truncated part of a plume is ignored the computed moment estimates will be underestimated. To account for the truncated mass several researchers have devised various extrapolation schemes to delimit the boundaries of the plume. These various extrapolation schemes will be discussed in the following sections.

Samples of the time evolution of the plume along lines 3, 5 and 7 are shown in Figures 3.4, 3.5 and 3.6. These figures show that with the passage of time the plume appears not to approximate a Gaussian type concentration distribution in the vertical direction. Further, examination of the vertical concentration profile of the plume at the sampling times presented show that the forward extent of the plume along line 7 appears to be retarded relative to those along line 3. This feature has also been described by Sudicky et al. (1983) who concluded that the plume evolved in a region with two different groundwater velocities. They also conclude that the plume should actually be considered as two separate plumes, with line 5 being the boundary between the two (see Sudicky et al.,1983 Figure 4.c).

3.4 Methodology

As a result of the complex concentration distribution present within the plume,

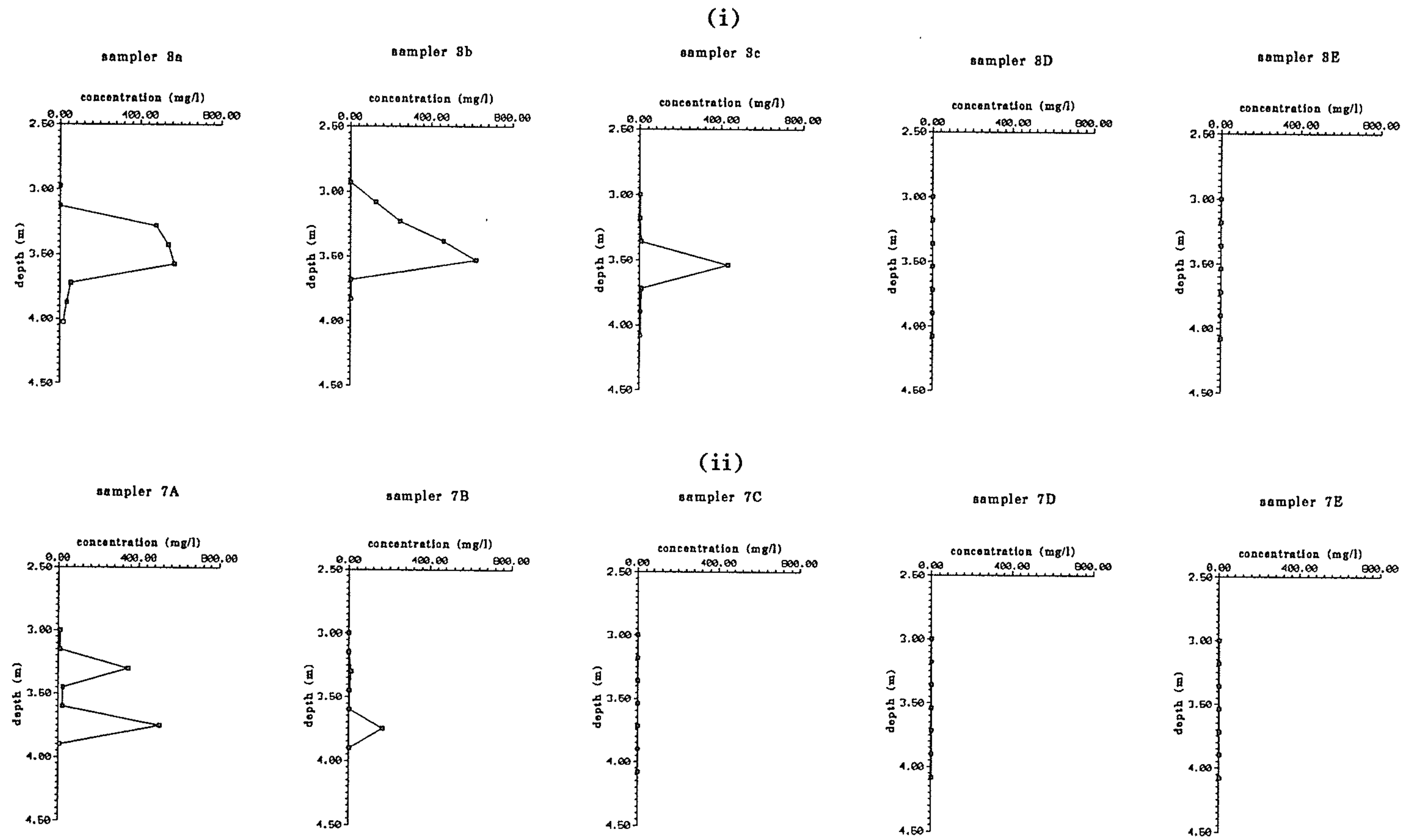

Figure 3.4 Vertical concentration profiles after 5 days along (i) line 3; (ii) line 7.

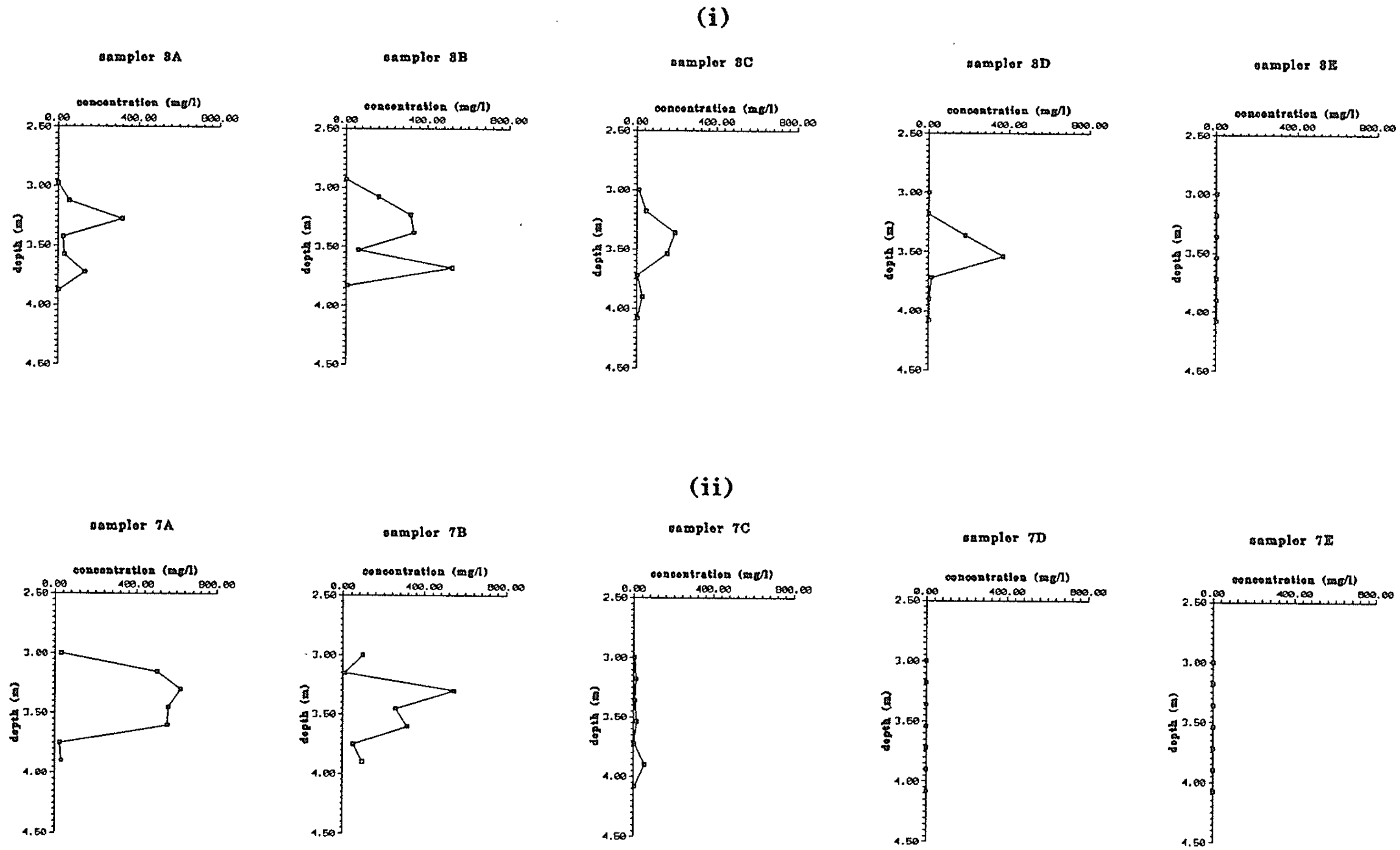

Figure 3.5 Vertical concentration profiles after 12 days along (i) line 3; (ii) line 7.

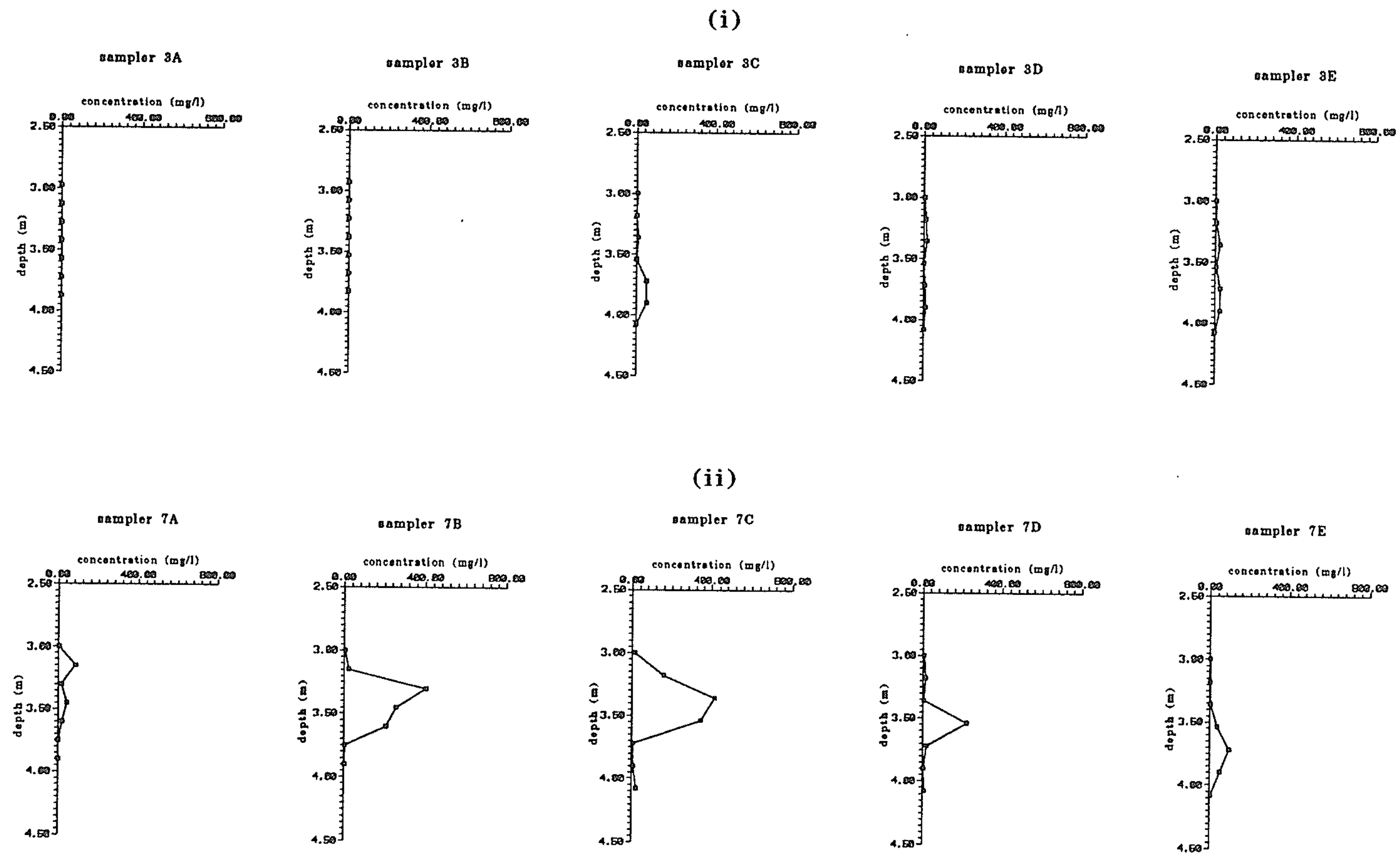

Figure 3.6 Vertical concentration profiles after 29 days along (i) line 3; (ii) line 7.

the spatial integrations are performed numerically to take advantage of the known discrete concentration data (see Freyberg, 1986). The layout of the sampling equipment given by Sudicky et al. (1983) for the experiment shows the spatial resolution of the data to be much greater in the vertical direction (0.15m to 0.18m) than in the horizontal plane (0.5m to 2.0m). Vertically, the sampler ports are evenly spaced whereas in the horizontal plane the data possess variable spacing. The difference in the data structure in the horizontal plane and the vertical plane requires different integration schemes to be employed in each plane. Freyberg (1986), Barry et al. (1988) and Rajaram and Gelhar (1991) have all used a similar approach in the analysis of the Stanford-Waterloo tracer experiment data which possessed a similar data structure.

In the following section an indepth description of the integration procedures used in both the vertical and the horizontal planes is presented.

3.4.1 Vertical Integration of the Plume

To perform the vertical integration of the concentration plume the upper and lower limits of the plume in the vertical plane must be determined. The determination of these limits is an easy task when the plume lies within the limits of a multilevel sampler bundle. However, in some instances the upper and lower limits of a plume may extend beyond the extent of a multi-level sampler bundle (i.e. the upper or lower sample port in the bundle records a non-zero concentration). In such cases, the vertical extent of the plume must be estimated using an appropriate extrapolation scheme. In this analysis two linear extrapolation schemes are used to estimate the vertical extent of the plume. The first scheme is described by Rajaram and Gelhar (1991) (see also Garabedian et al., 1991) and assumes that the limits of the plume extend to a distance equal to one vertical sampler interval from the upper or lower sampler port. The second approach (Freyberg, 1986) assumes that the limits of the plume extend to a distance equal to two vertical sampler port spacings from the upper or lower sampler port. The vertical integration of the plume is given by

$$C_z(x,y,t) = \int_{b_1}^{b_2} C(x,y,z,t)\ dz \tag{3.11}$$

where $C_z(x,y,t)$ represents the vertically integrated concentration; b_1 and b_2 are the depths to the upper and the lower limit of the plume respectively. Since the data in the vertical plane are evenly spaced the integration defined by (3.11) is performed easily using trapezoidal quadrature. The vertically integrated concentration is then substituted into (3.1) and (3.4) to yield

$$M_{ijk}(t) = \int_{-\infty}^{\infty}\int_{-\infty}^{\infty} x^i y^j\ nC_z(x,y,t)\ dx\ dy \tag{3.12a}$$

$$\overline{M}_{ijk}(t) = \int_{-\infty}^{\infty}\int_{-\infty}^{\infty} (x-x_c)^i (y-y_c)^j\ nC_z(x,y,t)\ dx\ dy \tag{3.12b}$$

3.4.2 Horizontal Integration of the Plume

To perform the integrations described by (3.12a) and (3.12b), the limits of the integration in the horizontal plane must be determined. In cases where the vertically integrated concentration has reached zero within the sampled domain the limits of integration are easily determined. However, in some cases the sampler array may truncate the plume (i.e. samplers on the border of the sampler array record non-zero concentrations). In such cases the lateral extent of the plume must also be inferred by the use of an extrapolation scheme. Again, the extrapolation schemes described by Freyberg (1986) and Rajaram and Gelhar (1991) and outlined above are employed. However, for this case the average sampler spacing in the horizontal plane must be determined and used. Later, by examining the amount of mass recovered the effectiveness of the two extrapolation schemes can be accessed.

Several approaches are available to perform the integration in the horizontal plane [see Freyberg (1986), Barry et al. (1988) and Garabedian et al. (1991)]. Barry and Sposito (1990) discussed the results obtained using these various approaches for the Stanford-Waterloo tracer experiment. They conclude that the various schemes all produce similar results. The relative equality in results is borne out by the similar apparent asymptotic macrodispersivity computed by these groups. The asymptotic macrodispersivities for the Stanford-Waterloo experiment obtained by the various researchers using different numerical schemes are within a factor of two of each other. For example, Freyberg's estimate of the apparent asymptotic horizontal transverse macrodispersivity was 0.039m (see Freyberg, 1986) while Rajaram and Gelhar's was 0.050m (see Rajaram and Gelhar, 1991). Woodbury and Sudicky (1992) have suggested that the differences between the various approaches is considered small particularly when the uncertainty in the input parameters is considered. In addition, Farrell et al. (1992)

(see also chapter 2) have constructed confidence limits for the apparent macrodispersivities due to unsteady flow at the site. The reader is reminded that the observed transverse spread is believed to be due to flow transients (see Sykes et al., 1982; Sudicky, 1986 and Farrell et al., 1992). Farrell et al. (1992) (see also chapter 2) have shown that both Freyberg's estimate and Rajaram and Gelhar's estimate lie within the computed 95% confidence intervals suggesting that both estimates are statistically equivalent.

The integration in the horizontal plane is performed by first interpolating the computed vertically integrated concentrations onto a regular grid. To accomplish this the inverse square distance (see Barry et al., 1988) and the kriging interpolation schemes are used. The kriging approach used is based on a linear variogram (see Journel and Huijbregts, 1978) and the method can be shown to be an exact interpolator at the control points. However, Barry et al. (1988) have pointed out the following advantages of the inverse square distance interpolation scheme:

1. The method also performs an exact interpolation;
2. The interpolated value is always bounded between the minimum and maximum values of the observed data;
3. The method results in a physically plausible two dimensional plume representation.

The spatial moments are computed by approximating the areal integrations by a nine node, local fourth order areal quadrature on the regular grid of estimated $C_z(x,y,t)$ values (see Abramowitz and Stegun 1970, equation 25.4.62; see also Freyberg, 1986). The use of two different interpolation schemes permits the sensitivity of the moment estimates to these schemes to be later examined.

In the following the results of the analysis will be divided in two major sections. An analysis for the entire plume will be presented in the first section while in the second section an analysis for the part of the plume in the lower hydraulic conductivity zone will be provided.

3.5 Results

3.5.1 The Vertically Integrated Plume

The vertical concentration profile at each multilevel sampler is extrapolated using the previously outlined schemes and then vertically integrated [see (3.11)]. The integration is performed numerically using trapezoidal quadrature. To facilitate contouring and numerical integration in the horizontal plane the vertically integrated data is then interpolated onto a regular grid. The interpolation is performed using both methods previously discussed.

Based on the analysis performed, it is found that the kriging interpolation scheme produces physically unrealistic (negative) concentration values in some cases. The inverse square distance method did not generate such values. In addition, it is found that the spatial concentration patterns produced using the kriging interpolation scheme display considerable smoothing (see Figure 3.7). This degree of smoothing displayed seems unrealistic in view of the complex nature of the hydraulic conductivity field present in aquifers. In comparison, the spatial patterns generated by the inverse square distance

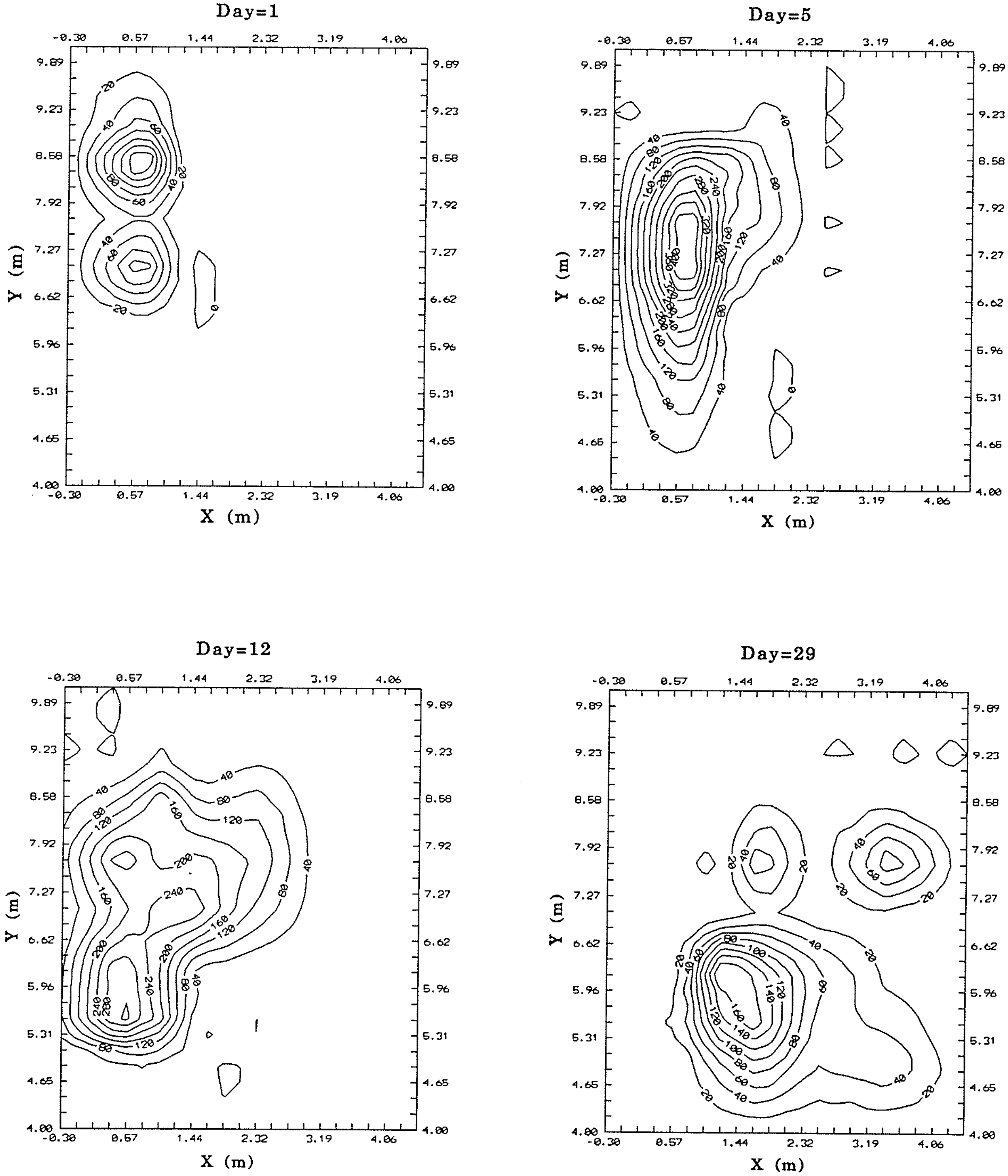

Figure 3.7 Vertically integrated plume using Freyberg extrapolation scheme and kriging interpolation scheme.

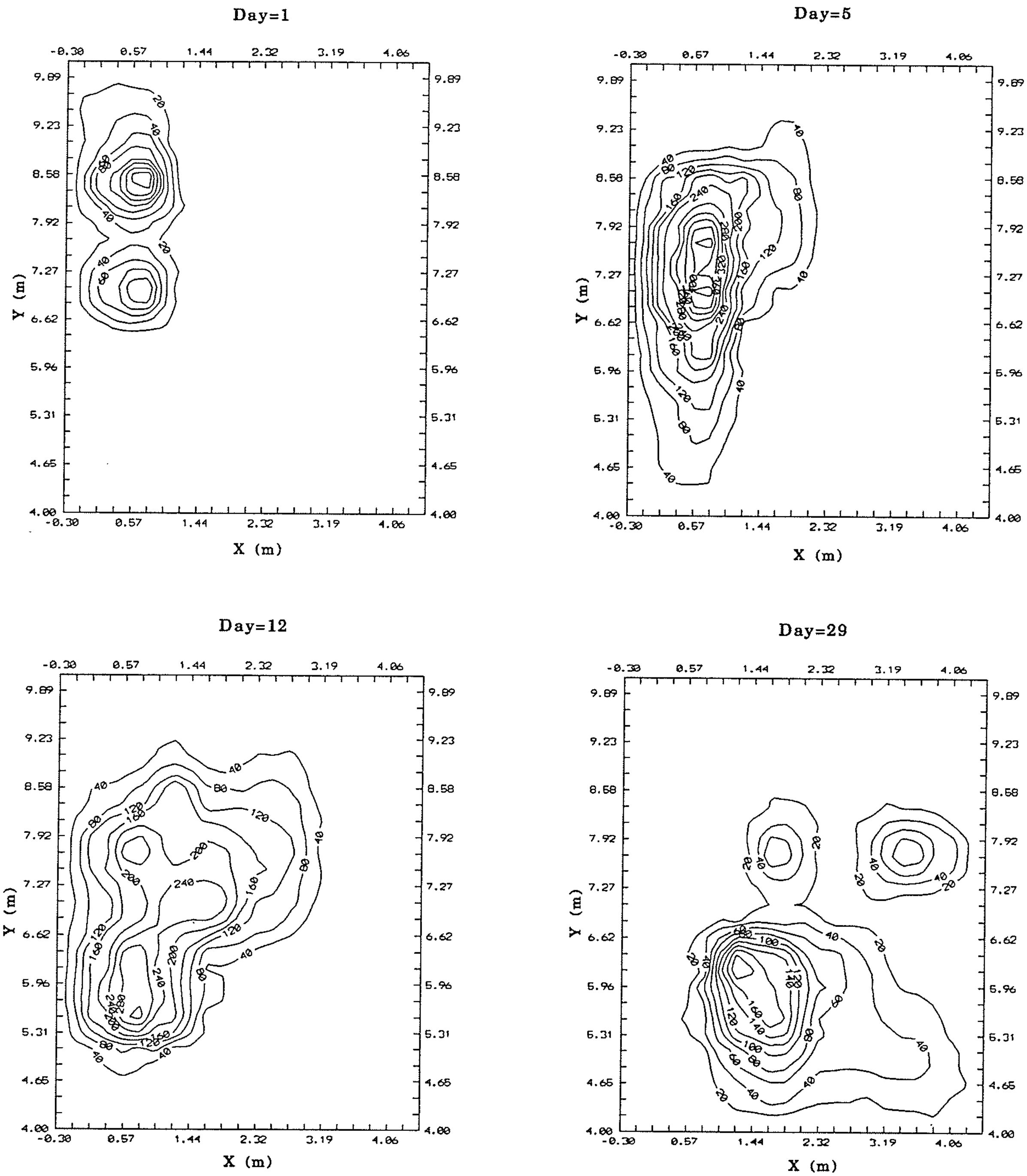

Figure 3.8 Vertically integrated plume using Freyberg extrapolation scheme and inverse square distance interpolation scheme.

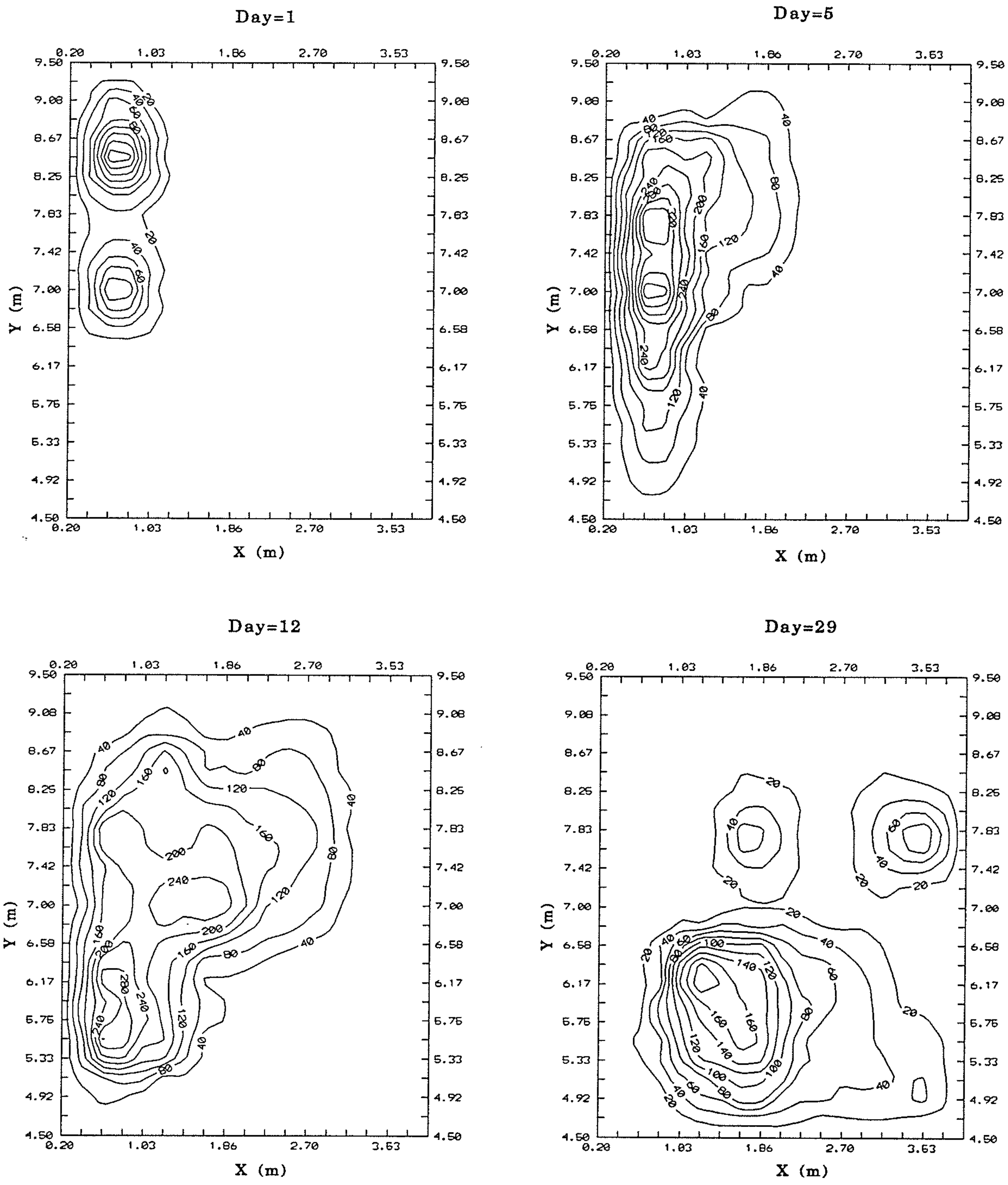

Figure 3.9 Vertically integrated plume using Rajaram and Gelhar extrapolation scheme and inverse square distance interpolation scheme.

approach produce much less smoothing, and qualitatively at least, appear much more realistic (see Figures 3.8 and 3.9). As a result the inverse square distance approach is the interpolation method of choice.

The contour maps of the vertically integrated concentration shown in Figures 3.7, 3.8 and 3.9 also show that the plume becomes increasingly distorted with time, with the northern section of the plume migrating at a much faster rate than the southern section. Sudicky et al. (1983) have attributed this behaviour to the plume migrating in two separate zones with different average hydraulic conductivities. The change in the shape of the plume indicates that the boundary between the two zones appears to be quite abrupt and runs parallel to the x-axis of the field coordinate system, with the northern zone having the higher hydraulic conductivity. Based on these figures it appears that the line separating the two hydraulic conductivity zones is about y=6.5m in the field coordinate system.

3.5.2 Full Plume Analysis

3.5.2.1 Recovered Mass Estimates

The recovered mass estimates obtained for the entire plume using the different interpolation schemes [but identical extrapolation schemes Freyberg (1986) scheme used] are shown in Tables 3.1 and 3.2. Comparison of these two tables shows that the recovered mass estimates are quite similar, with the maximum variation between the estimates being 7.0g on day twelve. This suggests that the recovered mass estimates are quite insensitive to the interpolation scheme used. When the different extrapolation

Table 3.1

Estimates of Mass in Solution, Location of Centre of Mass, and Spatial Covariance for 1978 Tracer Plume

Time (days)	M_{000} (g)	M_{100} (g m)	M_{010} (g m)	M_{200} (g m^2)	M_{020} (g m^2)	% Mass Recovered	x_c (m)	y_c (m)	σ_{xx} (m^2)	σ_{yy} (m^2)
1	78.355	42.747	82.182	31.483	146.047	19.770	0.546	1.048	0.104	0.764
3	188.180	114.955	131.181	96.146	249.507	47.481	0.611	0.697	0.138	0.840
5	432.914	336.363	122.553	378.886	501.737	109.232	0.777	0.283	0.272	1.079
8	576.053	549.482	69.958	785.214	804.717	145.548	0.954	0.121	0.453	1.382
12	550.661	581.560	23.520	945.112	619.887	138.941	1.056	0.043	0.601	1.123
15	516.793	821.313	-41.601	1810.45	621.348	130.396	1.589	-0.080	0.978	1.196
21	402.641	701.033	-189.688	1560.43	654.896	101.593	1.471	-0.471	0.844	1.405
29	234.238	510.919	-206.039	1319.22	453.384	59.102	2.181	-0.880	0.874	1.162

- Assumes the concentration goes to background at a distance equal to two sampler spacings.
- Interpolation performed using Kriging method.

Table 3.2

Estimates of Mass in Solution, Location of Centre of Mass, and Spatial Covariance for 1978 Tracer Plume

Time (days)	M_{000} (g)	M_{100} (g m)	M_{010} (g m)	M_{200} (g m^2)	M_{020} (g m^2)	% Mass Recovered	x_c (m)	y_c (m)	σ_{xx} (m^2)	σ_{yy} (m^2)
1	80.274	43.073	87.411	31.816	158.221	20.254	0.537	1.089	0.108	0.785
3	188.392	114.160	135.464	95.950	258.433	47.534	0.606	0.719	0.142	0.855
5	432.693	337.033	120.659	383.328	516.273	109.175	0.779	0.278	0.279	1.115
8	574.945	573.694	69.492	870.427	820.816	145.068	0.998	0.121	0.518	1.413
12	557.012	697.298	20.628	1216.88	682.669	140.544	1.252	0.037	0.618	1.134
15	513.179	814.692	-41.958	1787.07	619.895	129.484	1.588	-0.082	0.962	1.201
21	400.998	697.979	-188.888	1551.17	654.052	101.179	1.741	-0.471	0.839	1.409
29	234.109	511.808	-209.967	1326.38	459.545	59.070	2.186	-0.897	0.886	1.159

- Assumes the concentration goes to background at a distance equal to two sampler spacings.
- Interpolation performed using Inverse Square Distance method.

Table 3.3

Estimates of Mass in Solution, Location of Centre of Mass, and Spatial Covariance for 1978 Tracer Plume

Time (days)	M_{000} (g)	M_{100} (g m)	M_{010} (g m)	M_{200} (g m^2)	M_{020} (g m^2)	% Mass Recovered	x_c (m)	y_c (m)	σ_{xx} (m^2)	σ_{yy} (m^2)
1	48.322	34.853	45.305	27.444	73.317	12.192	0.721	0.930	0.048	0.638
3	122.946	96.134	82.943	84.681	144.312	31.021	0.782	0.675	0.077	0.719
5	301.619	294.220	109.252	348.985	322.156	76.104	0.975	0.362	0.206	0.936
8	413.953	477.073	94.501	700.964	524.016	104.447	1.152	0.228	0.365	1.214
12	451.650	645.659	48.007	1147.46	453.296	114.035	1.429	0.106	0.497	0.992
15	420.296	706.053	-7.800	1485.50	454.744	105.973	1.680	-0.019	0.712	1.082
21	331.168	585.485	-141.651	1239.90	471.958	83.559	1.768	-0.428	0.618	1.242
29	192.630	394.089	-152.212	928.843	302.592	48.604	2.046	-0.790	0.636	0.946

-Assumes the concentration goes to background at a distance equal to one sampler spacings.
-Interpolation performed using Inverse Square Distance method.

schemes are used with identical interpolation schemes (inverse square distance method used) it is found that significantly different recovered mass estimates are obtained (see Tables 3.2 and 3.3). The Freyberg (1986) extrapolation scheme is found to produce recovered mass estimates which significantly exceed those obtained using the Rajaram and Gelhar (1991) extrapolation scheme. For example, the recovered mass estimate on day twelve using Freyberg's extrapolation scheme is 557.0g (see Table 3.2) compared to 451.7g (see Table 3.3) obtained using the Rajaram and Gelhar (1991) scheme for the same time - an increase of 123.3%. Therefore it is apparent that the recovered mass estimates are sensitive to the extrapolation scheme used. Since the recovered mass estimates produced by the Rajaram and Gelhar (1991) extrapolation scheme are in better agreement with the injected mass (396.3g) it will be used as the extrapolation method of choice in this paper.

Tables 3.1, 3.2, and 3.3 also show that the recovered mass estimates have considerable variability, with the recovered mass estimates at early times being considerably smaller than the estimated injected mass (396.3g). This variability in the recovered mass estimate is directly related to the number of ports which sample the plume. At early and late times the plume is sampled by only a few of the ports in the array and this results in the low mass estimates. At more intermediate times (particularly days 8, 12 and 15) the mass estimates are more consistent indicating that the plume is being well sampled.

3.5.2.2 Motion of the Centre of Mass and Plume Velocity Estimates

The location of the centre of mass of the plume is obtained from the zeroth and first moment estimates using (3.2). The results of the centre of mass analysis for the entire plume using the Rajaram and Gelhar extrapolation scheme and the inverse square distance interpolation scheme are shown in the eighth and ninth columns of Table 3.3. The motion of the centre of mass for the entire plume both as a function of space is shown in Figure (3.10). The figure shows that the motion of the centre of mass for the entire plume appears to be displaced from the origin of the local coordinate system at early time (the local coordinate system is designed so that the origin lies at (0,7.0) of the field coordinate system) even though considerable care was taken to ensure that the local coordinate system was located at the centre of the injection well array. This observed behaviour is probably a result of the poor sampling of the plume at early times (see also Sudicky et al. 1983, Figure 4a and 4b). The mean velocity of the centre of mass of the plume estimated from ordinary least squares fits to the data is 8.70×10^{-7} ms^{-1}. This velocity estimate is biased because of the poor sampling of the plume and as a result should be considered crude. As pointed out, at early and late times mass estimates for the entire plume are low due to incomplete sampling of the plume. If recovered mass estimates below 70% and above 130% are ignored (see Figure 3.11), the estimate of the mean velocity of the plume centre of mass is 9.69×10^{7} ms^{-1}.

3.5.3.3 Second Moment, Spatial Covariance and Macrodispersivity Estimates

The second moment estimates and the terms of the spatial covariance tensor

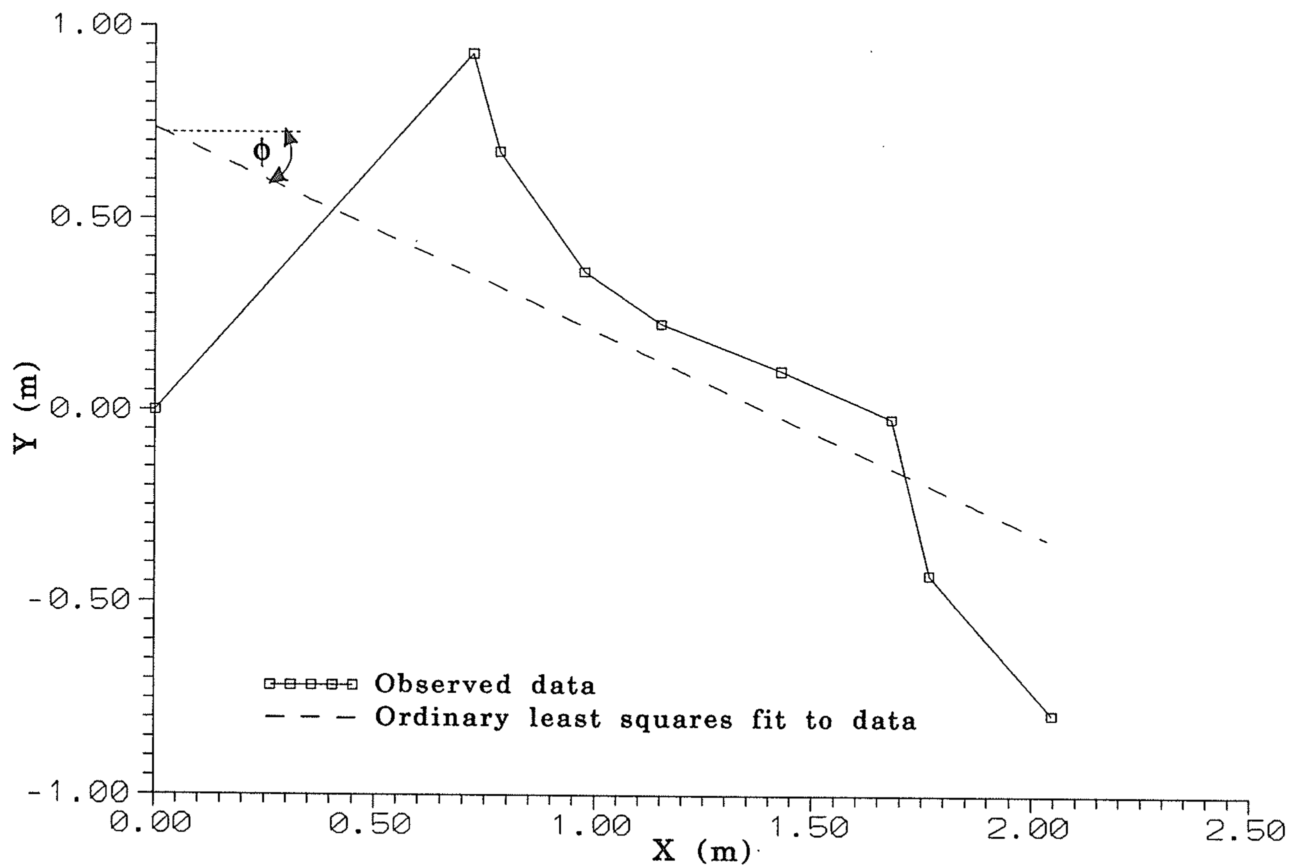

Figure 3.10 Motion of the centre of mass of the entire plume (all of the data used).

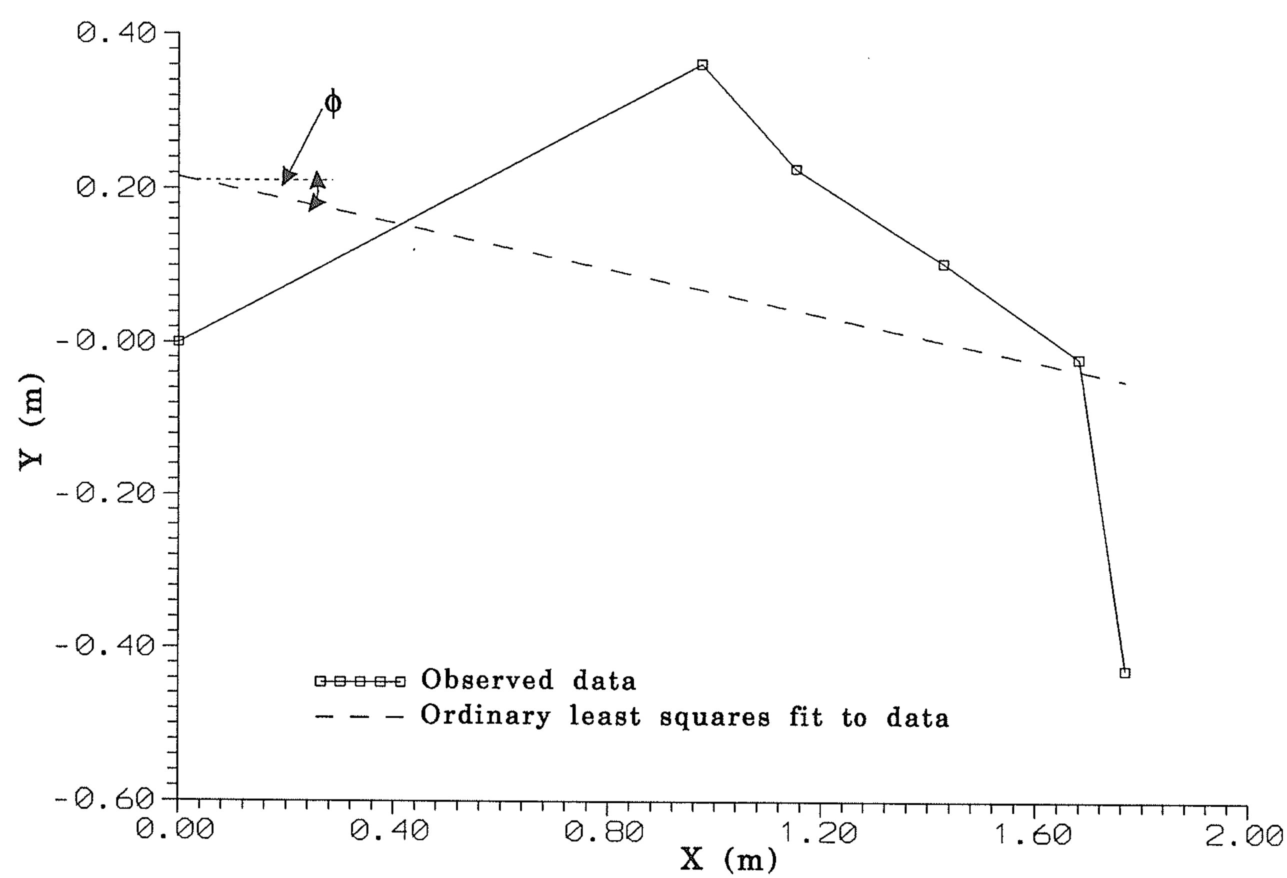

Figure 3.11 Motion of the centre of mass of the entire plume (reduced data set used).

[computed using (3.5b) and (3.5c)] in the field coordinate system for the entire plume computed using the Rajaram and Gelhar extrapolation scheme and the inverse square distance interpolation scheme are presented in Table 3.3.

The terms of the macrodispersivity tensor are usually defined with respect to the longitudinal and transverse directions where the longitudinal direction refers to the direction of the mean horizontal trajectory of the centre of mass of the plume (see Freyberg, 1986). To facilitate this definition the components of the spatial covariance tensor must be given in a coordinate system oriented in this way, where the x′ coordinate axis parallels the linear horizontal trajectory of the plume and the y′ coordinate axis is perpendicular to the trajectory (see Figure 3.12). Therefore, a rotation of the terms of the spatial covariance tensor defined in the field coordinate system is required. This rotation is given by the following matrix

$$R=\begin{bmatrix} \cos\phi & -\sin\phi \\ \sin\phi & \cos\phi \end{bmatrix} \tag{3.13}$$

and the spatial covariance terms in the rotated coordinate system are given by

$$\begin{bmatrix} \acute{\sigma}_{xx} & \acute{\sigma}_{xy} \\ \acute{\sigma}_{yx} & \acute{\sigma}_{yy} \end{bmatrix} = R^{T} \begin{bmatrix} \sigma_{xx} & \sigma_{xy} \\ \sigma_{yx} & \sigma_{yy} \end{bmatrix} R \tag{3.14}$$

where ϕ is the angle between the x-axis of the field coordinate system and the mean flow direction of the plume and the primed terms represent the terms of the spatial covariance tensor in the rotated coordinate system. Note that the angle ϕ is defined as positive when measured in the counter-clockwise direction.

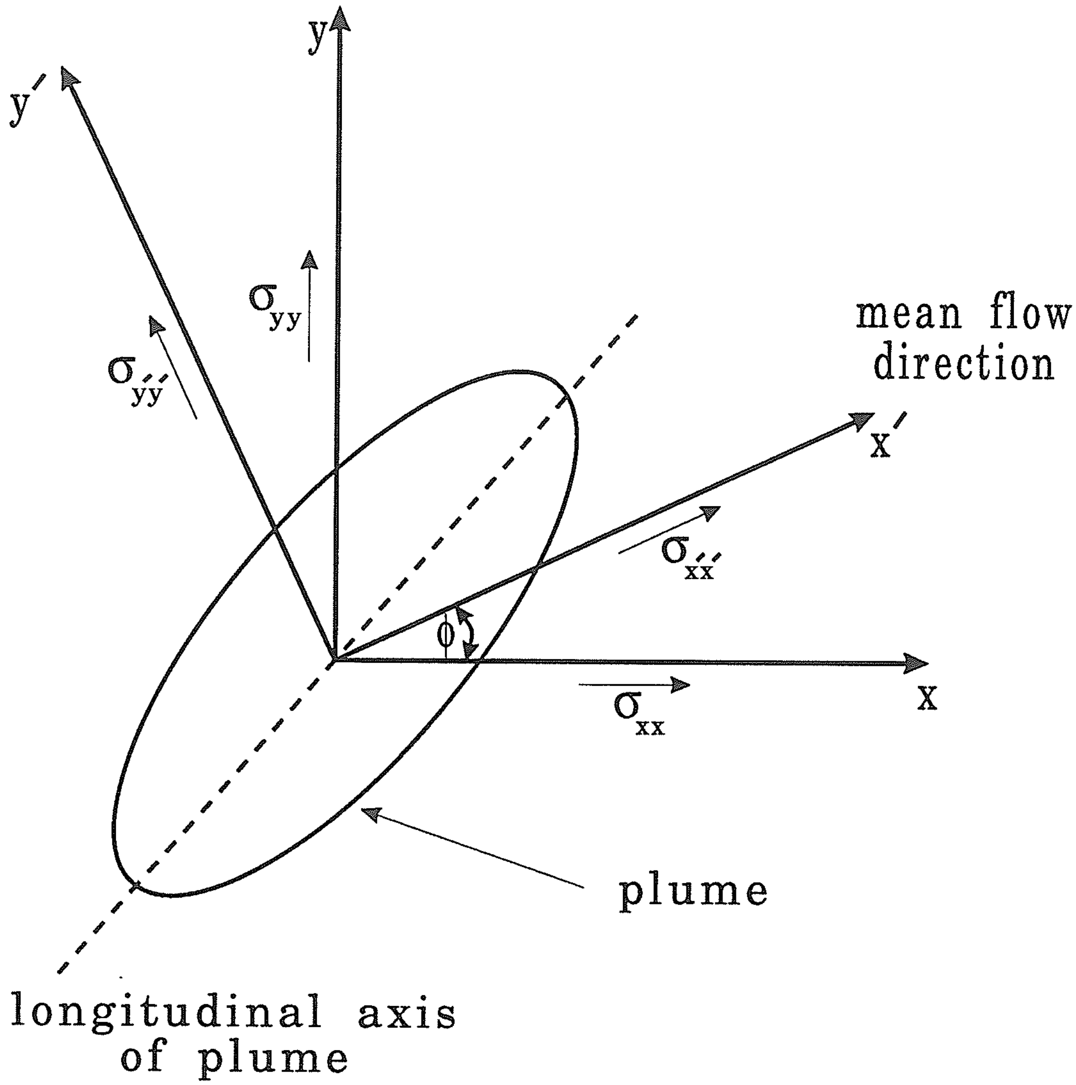

Figure 3.12 Scheme diagram showing the plume orientation with respect to the field coordinate system and the rotated coordinate system.

As described earlier, the entire plume is migrating in a medium which has two distinct average hydraulic conductivities. Since the design of the sampler array does not take this into consideration the entire plume is poorly sampled at early and late times. The component of the plume in the higher hydraulic conductivity zone is well sampled at early times but poorly sampled at later times, while the component of the plume in the lower hydraulic conductivity zone is poorly sampled at early times but well sampled at later times. This poor sampling of the entire plume results in the computed centre of mass of the plume having a complex trajectory (see Figures 3.10 and 3.11). As a result, it is difficult to determine whether computed rotation angles based on Figures 3.10 and 3.11 are meaningful. It is also difficult to determine whether the macrodispersivity parameter is meaningful when the concentration distribution of the plume is non-Gaussian (recall the plume appears to split into two). As a result, analyses of the second and higher moments for the entire plume are not performed. Instead, attention is focussed on the component of the plume in the lower hydraulic conductivity zone.

3.5.3 Plume in Lower Hydraulic Conductivity Zone

Contour maps of the vertically integrated plume in the lower hydraulic conductivity zone are shown in Figure 3.13. The figure shows that the plume migrates in a direction which is almost parallel to the X-axis of the field coordinate system. This suggests that the terms of the spatial covariance tensor will require very little, if any, rotation to align them to the mean displacement direction of the plume. The figure also shows that the plume in this zone attains an approximate Gaussian concentration

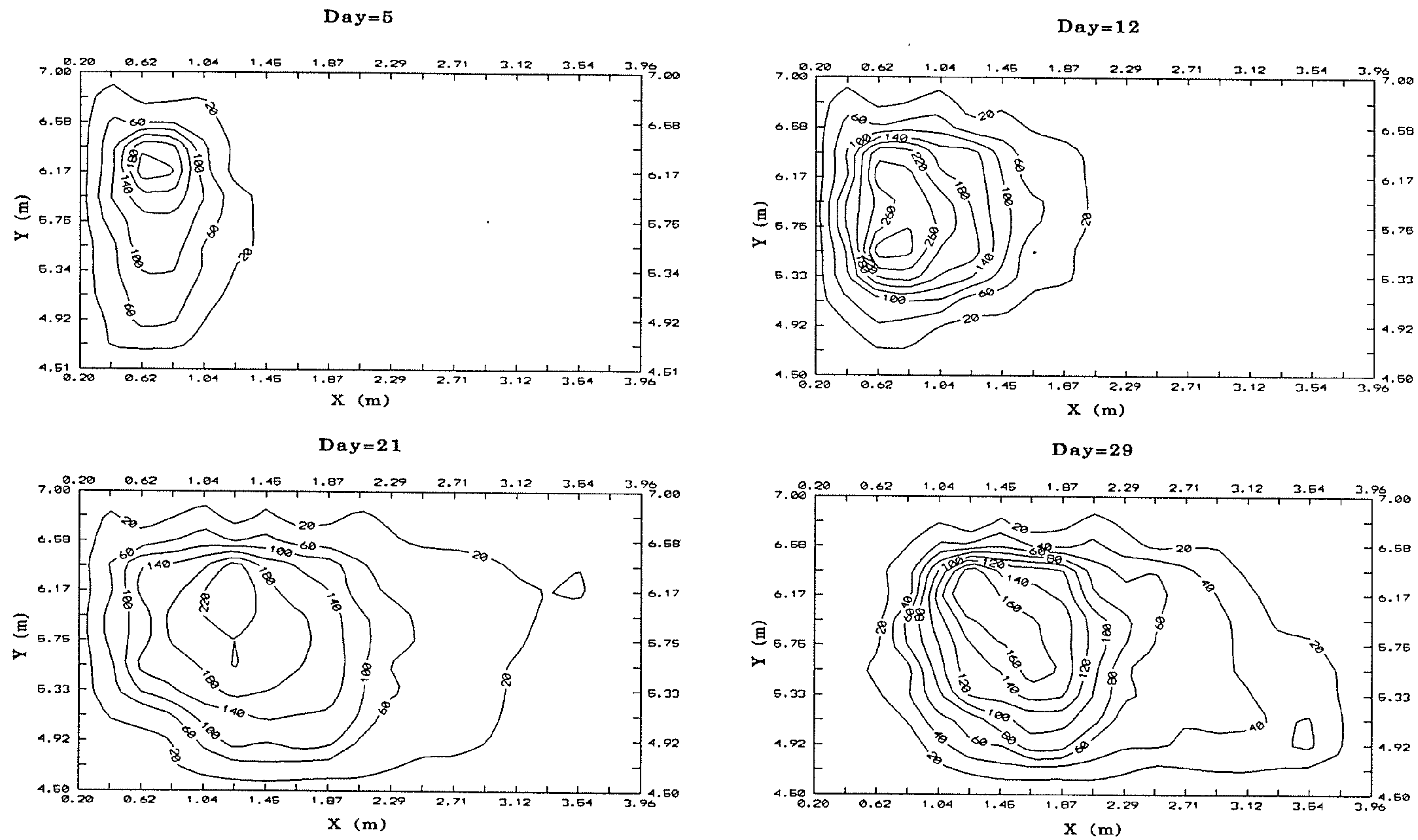

Figure 3.13 Vertically integrated plume in the lower hydraulic conductivity zone.

distribution.

3.5.3.1 Recovered Mass Estimates

In order to determine the percentage mass recovered in the lower hydraulic conductivity zone, the mass of the injected chloride into this zone must first be estimated. An assumption is made here that there was negligible movement of tracer mass across the interface separating the two hydraulic conductivity zones. Such an assumption is justified if the plume mass moves parallel to the interface so that the transfer of mass across the interface can occur only as a result of transverse dispersion and diffusion. The mass of chloride injected into the lower hydraulic conductivity zone (159.0g) is taken as the sum of the mass injected at wells IW4 and IW5. The zeroth moments for the plume in the lower hydraulic conductivity zone are computed using the approach outlined previously and are shown in the second column of Table 3.4. Using a value of 159.0g for the injected mass in the lower hydraulic conductivity zone the highest recovered mass estimate is 139% greater than the injected mass (see Table 3.4). This occurs on sample day 121 when the plume was poorly sampled and as a result is questionable. Overall, the results suggest that the assumption of negligible interaction between the two zones is reasonable.

3.5.3.2 Motion of Centre of Mass and Plume Velocity Estimates

The centre of mass of the plume in the lower hydraulic conductivity zone is computed. Figure 3.14 shows the motion of the centre of mass as a function of space. Here, the origin of the local coordinate system is located at (0, 5.875) of the field

Table 3.4

Estimates of Mass in Solution, Location of Centre of Mass, and Spatial Covariance for 1978 Tracer Plume

(plume in low velocity zone)

Time (days)	M_{000} (g)	M_{100} (g m)	M_{010} (g m)	M_{200} (g m^2)	M_{020} (g m^2)	% Mass Recovered	x_c (m)	y_c (m)	σ_{xx} (m^2)	σ_{yy} (m^2)
1	----	----	----	----	----	----	----	----	----	----
3	5.925	4.238	0.309	3.310	1.269	3.726	0.715	0.052	0.047	0.211
5	57.024	42.280	-0.733	34.812	14.279	35.856	0.741	-0.013	0.061	0.250
8	117.435	98.419	-8.977	94.165	25.918	73.842	0.838	-0.076	0.099	0.215
12	126.467	119.990	-3.325	133.971	24.579	79.521	0.949	-0.026	0.159	0.194
15	143.591	152.041	-10.976	189.039	32.462	90.288	1.056	-0.076	0.198	0.220
21	187.666	284.134	-21.729	515.905	50.446	118.002	1.514	-0.116	0.456	0.255
29	139.982	264.609	-21.439	575.046	40.986	88.019	1.890	-0.153	0.536	0.269
121	222.200	2242.25	-82.164	23242.6	201.177	139.717	10.091	-0.370	2.771	0.769

- Assumes the concentration goes to background at a distance equal to one sampler spacings.
- Interpolation performed using Inverse Square Distance method.

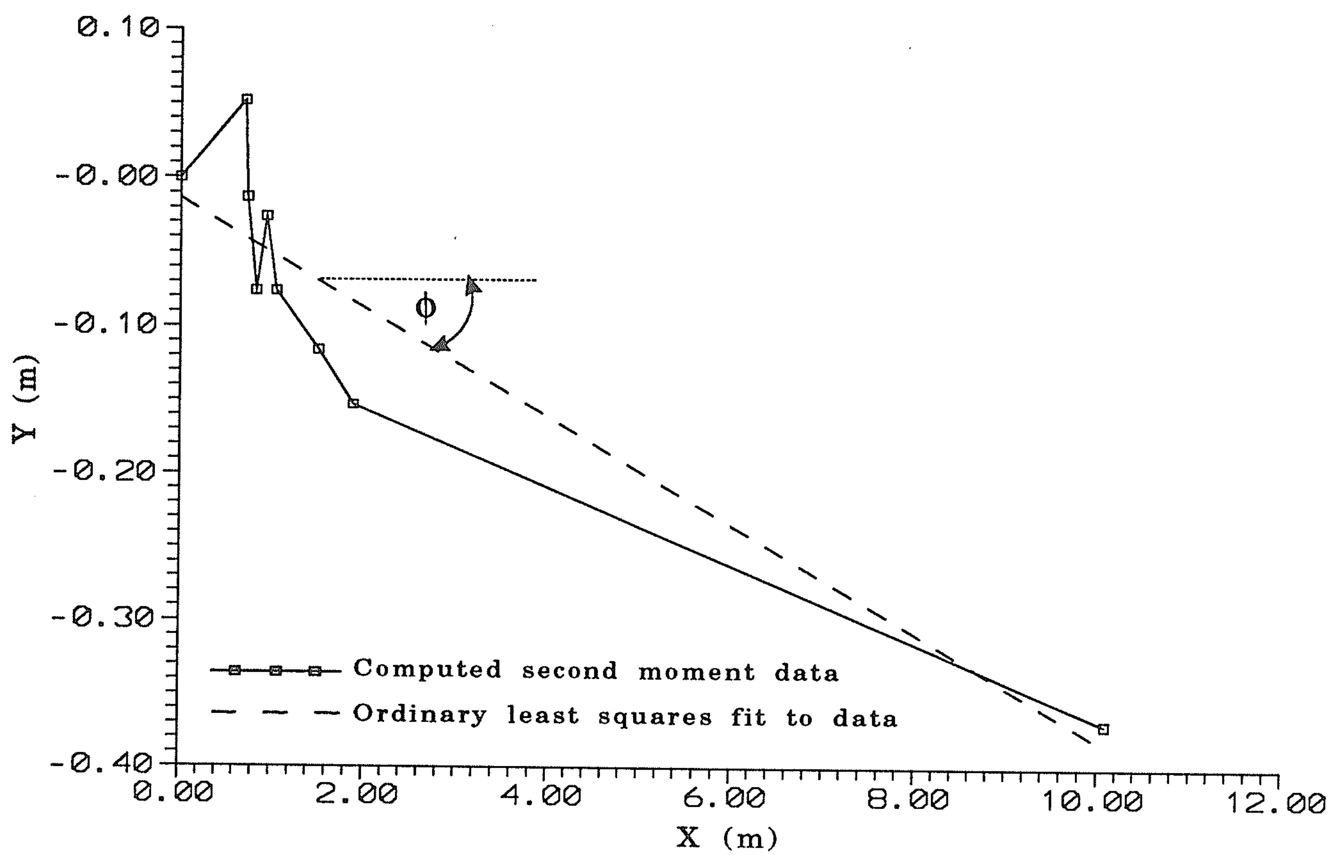

Figure 3.14 Motion of the centre of mass of the plume in the lower hydraulic conductivity zone (all the data used).

coordinate system. The centre of mass of this plume has a linear motion. The mean velocity of the centre of mass of this plume estimated from a first order ordinary least squares fit to the data is 9.38×10^{-7} ms^{-1} (see Table 3.5). If recovered mass estimates below 70% and above 130% are ignored the estimate of the mean velocity of the centre of mass of the plume is 7.31×10^{-7} ms^{-1} (see Figure 3.15 and Table 3.5). These velocity estimates are found to be in good agreement with the velocity estimate of 8.2×10^{-7} ms^{-1} obtained by Sudicky et al. (1983) for this zone.

Table 3.5

Estimated plume velocity for the 1978 tracer experiment

(plume in low hydraulic conductivity zone)

	Full Data	**Reduced Data**
V_x (m/s)	9.49×10^{-7}	7.29×10^{-7}
V_y (m/s)	-3.47×10^{-8}	-5.79×10^{-8}
$\|V\|$ (m/s)	9.50×10^{-7}	7.31×10^{-7}

Note: Reduced data refers to the data set containing recovered mass estimates between 70% and 130% of the injected mass.

3.5.3.3 Second moments, Spatial Covariance and Macrodispersivity Estimates

The second order moments and the spatial covariance tensor in the field coordinate system are computed. The rotation angle though which the terms of the spatial

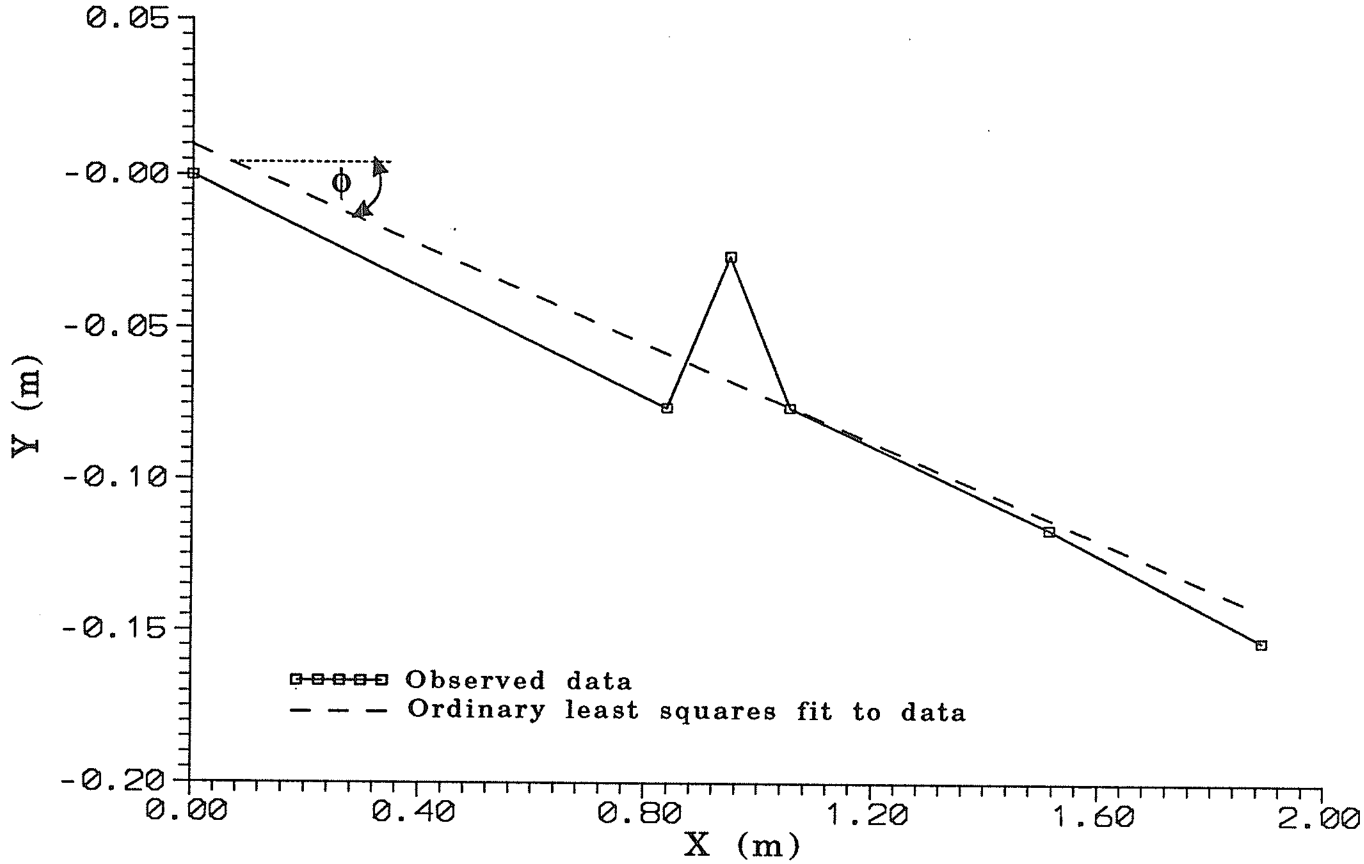

Figure 3.15 Motion of the centre of mass of the plume in the lower hydraulic conductivity zone (reduced data set).

covariance must be rotated, is computed by fitting a first order ordinary least squares line to the centre of mass data (see Figures 3.14 and 3.15). The angle of rotation for this plume is found to be -2.078° when all the data is used and -4.574° when only the data which represents 70% to 130% of the injected mass are used. These values are reasonable in view of the fact that the motion of the plume in the lower hydraulic conductivity is approximately linear and the entire plume is, in general, well sampled in this zone. Equations (3.13) and (3.14) are used to rotate the terms of the covariance tensor. The rotated covariance values are listed in Table 3.6. It is found that the rotation changes the values very little and as a result it appears that in this case the rotation not necessary.

Table 3.6a

Second Moments for Field and Rotated Coordinate Systems

(plume in low velocity medium)

Day	σ_{xx}	σ_{xy}	σ_{yy}	$\acute{\sigma}_{xx}$	$\acute{\sigma}_{xy}$	$\acute{\sigma}_{yy}$
3	0.047	-0.003	0.211	0.047	-0.008	0.211
5	0.061	-0.010	0.250	0.062	-0.017	0.249
8	0.099	-0.012	0.215	0.100	-0.016	0.214
12	0.159	0.074	0.194	0.154	0.073	0.199
15	0.198	-0.026	0.220	0.200	-0.027	0.218
21	0.456	-0.024	0.255	0.457	-0.017	0.254
29	0.536	-0.063	0.269	0.540	-0.053	0.264
121	2.771	0.043	0.769	2.765	0.115	0.775

Angle of rotation=-2.078 (measures anti-clockwise from the X-axis)
Note: $\sigma_{xy}=\sigma_{yx}$ and $\acute{\sigma}_{xy}=\acute{\sigma}_{yx}$.

Table 3.6b

Second Moments for Field and Rotated Coordinate Systems

(plume in low velocity medium)

Day	σ_{xx}	σ_{xy}	σ_{yy}	$\acute{\sigma}_{xx}$	$\acute{\sigma}_{xy}$	$\acute{\sigma}_{yy}$
3	0.047	-0.003	0.211	0.049	-0.016	0.209
5	0.061	-0.010	0.250	0.064	-0.025	0.247
8	0.099	-0.012	0.215	0.102	-0.021	0.212
12	0.159	0.074	0.194	0.147	0.070	0.206
15	0.198	-0.026	0.220	0.202	-0.027	0.216
21	0.456	-0.024	0.255	0.458	-0.008	0.252
29	0.536	-0.063	0.269	0.544	-0.041	0.260
121	2.771	0.043	0.769	2.765	0.117	0.775

Angle of rotation=-4.574 (measures anti-clockwise from the X axis).
Note: $\sigma_{xy}=\sigma_{yx}$ and $\acute{\sigma}_{xy}=\acute{\sigma}_{yx}$.

Stochastic theories of dispersion (see Dagan, 1982, 1984, 1987 and 1988) and field studies such as the Stanford-Waterloo experiment have shown that macrodispersivity initially increases with time before reaching asymptotic values (Freyberg, 1986). Table 3.7 shows the macrodispersivity computed as a function of time using a pseudo sequential calibration approach [see (15a) and (15b); see also Freyberg, 1986].

$$A_{x'x'}(t)=\frac{1}{2|U|}\frac{\sigma_{x'x'}(t)-\sigma_{x'x'}(3)}{t-3} \tag{3.15a}$$

$$A_{y'y'}(t)=\frac{1}{2|U|}\frac{\sigma_{y'y'}(t)-\sigma_{y'y'}(3)}{t-3} \tag{3.15b}$$

Table 3.7

Time Dependent Dispersivity Estimates for

the 1978 Tracer Experiment

(plume in low hydraulic conductivity zone)

Period (Day)	**Longitudinal Dispersivity (A_L) (m)**	**Transverse Dispersivity (A_T) (m)**
5	0.059	0.150
8	0.084	0.005
12	0.086	-0.003
15	0.101	-0.005
21	0.180	0.019
29	0.151	0.016
121	0.181	0.044

Note: Values computed using data in Table 3.6b

The results show some that the macrodispersivity appears to fluctuate with time with the macrodispersivity appearing to be negative at some times in the transverse direction. This fluctuation indicates that the plume is being strongly influenced by the heterogeneity in the medium. However, the general trend in the data indicates that the macrodispersivity in both the longitudinal and transverse directions increases with time. Due to the short length of the time series and the poor sampling of the plume particularly at later times it is impossible to determine the asymptotic limits for the dispersivity in the longitudinal and transverse directions using this approach. Approximate estimates for the components of the apparent asymptotic macrodispersivity in the longitudinal and transverse directions are computed by performing first order ordinary least squares fits to the spatial covariance data in the longitudinal and transverse directions (see Figures 3.16 to 3.19). This allows the slope of the spatial covariance as a function of time to be estimated. The longitudinal and transverse terms of the apparent asymptotic macrodispersivity are then calculated according to (3.8). These estimates of the apparent asymptotic macrodispersivity for the plume in the lower hydraulic conductivity zone are shown in Table 3.8. It must be pointed out that although the terms of the covariance tensor increase with time it is difficult to determine (due to the short length of the data) whether asymptotic limits have been reached.

Table 3.8

Dispersion and Dispersivity Estimates for the 1978 Tracer Experiment

(plume in lower hydraulic conductivity zone)

	Longitudinal Dispersivity (m)	**Longitudinal Dispersion (m^2/s)**	**Transverse Dispersivity (m)**	**Transverse Dispersion (m^2/s)**
Full plume	0.143	1.36×10^{-7}	0.029	2.78×10^{-8}
Reduced data	0.160	1.17×10^{-7}	0.027	1.94×10^{-8}

The results show that the apparent asymptotic horizontal transverse macrodispersivity is found to be between 0.027m and 0.029m. These values are almost

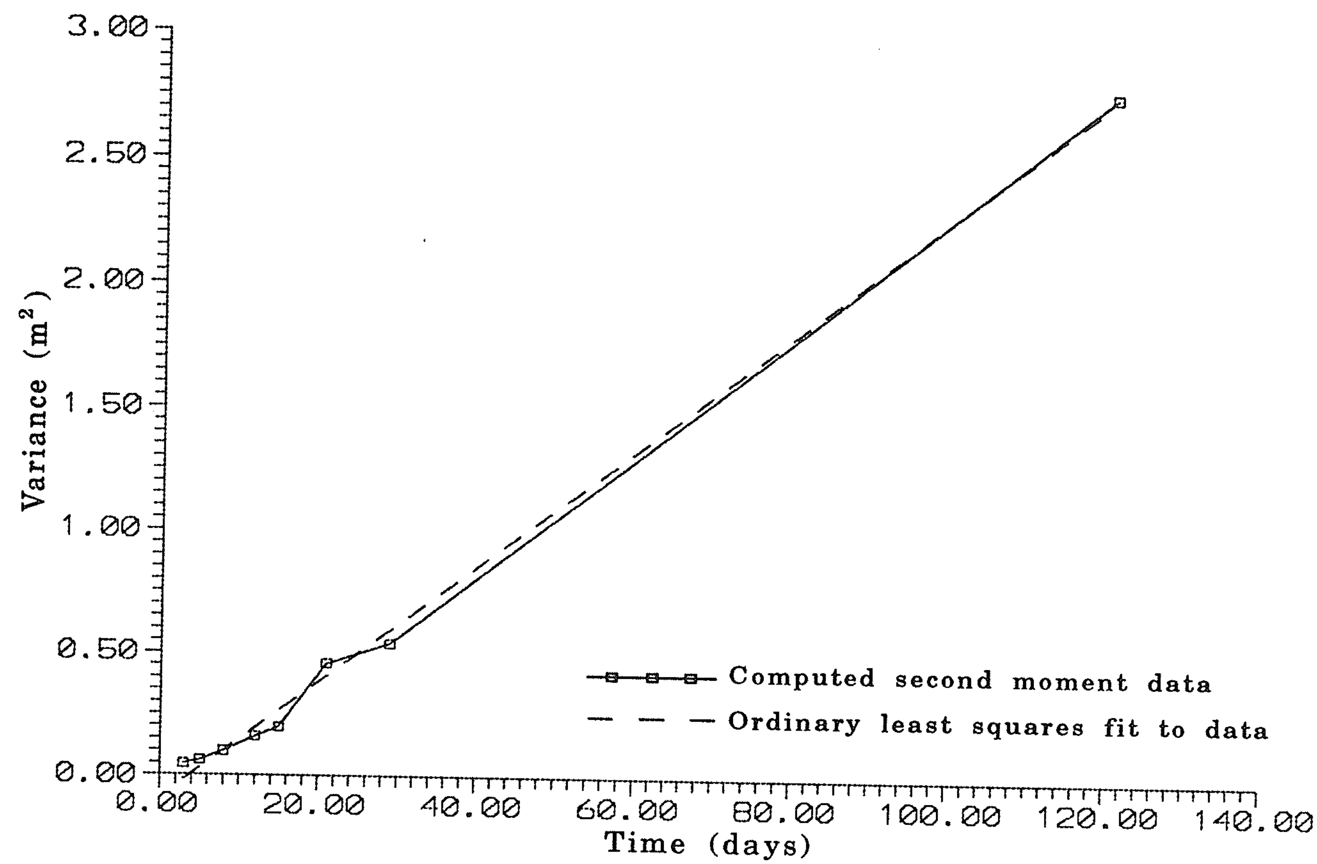

Figure 3.16 Variance in the longitudinal direction for the plume in the lower hydraulic conductivity zone (all the data used).

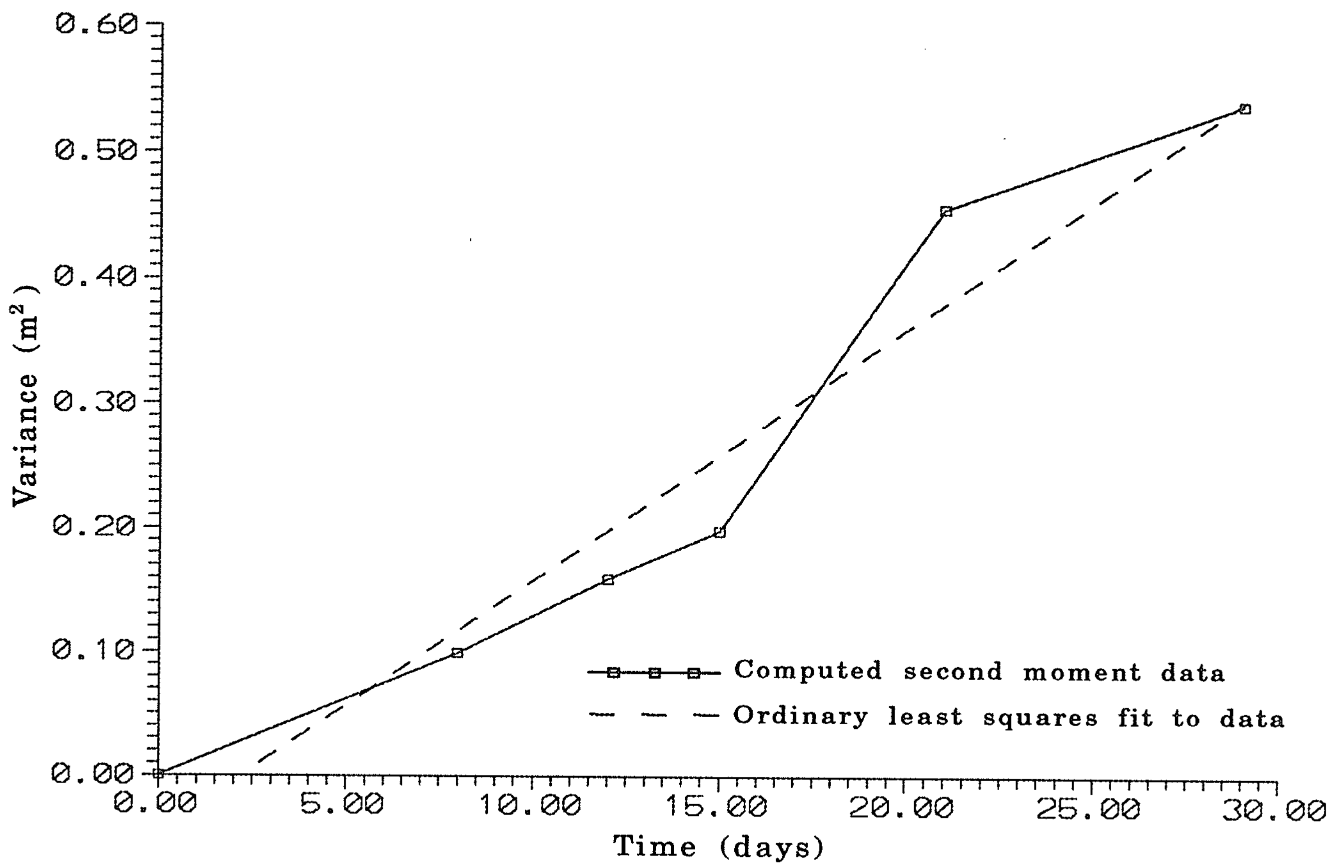

Figure 3.17 Variance in the longitudinal direction for the plume in the lower hydraulic conductivity zone (reduced data set used).

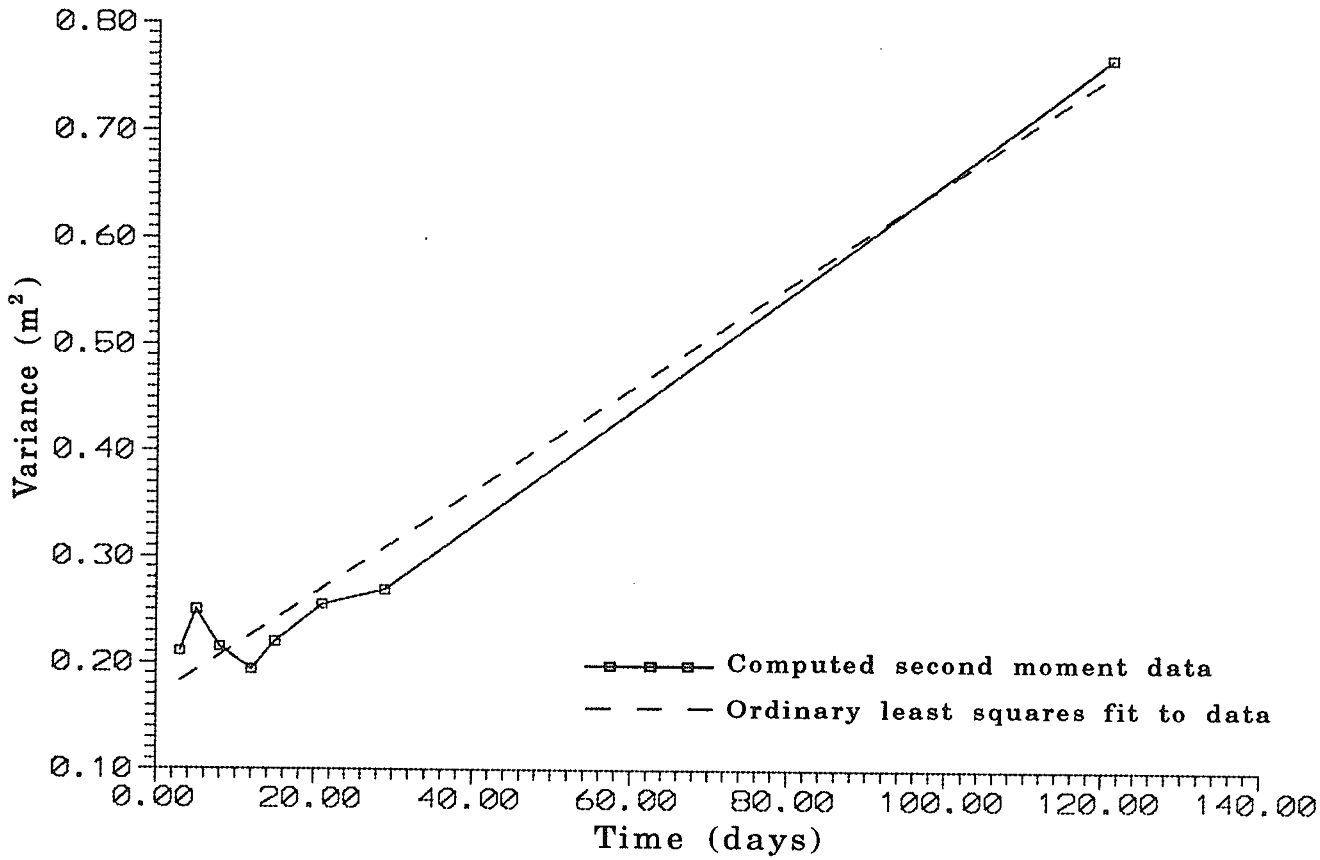

Figure 3.18 Variance in the transverse horizontal direction for the plume in the lower hydraulic conductivity zone (all the data used).

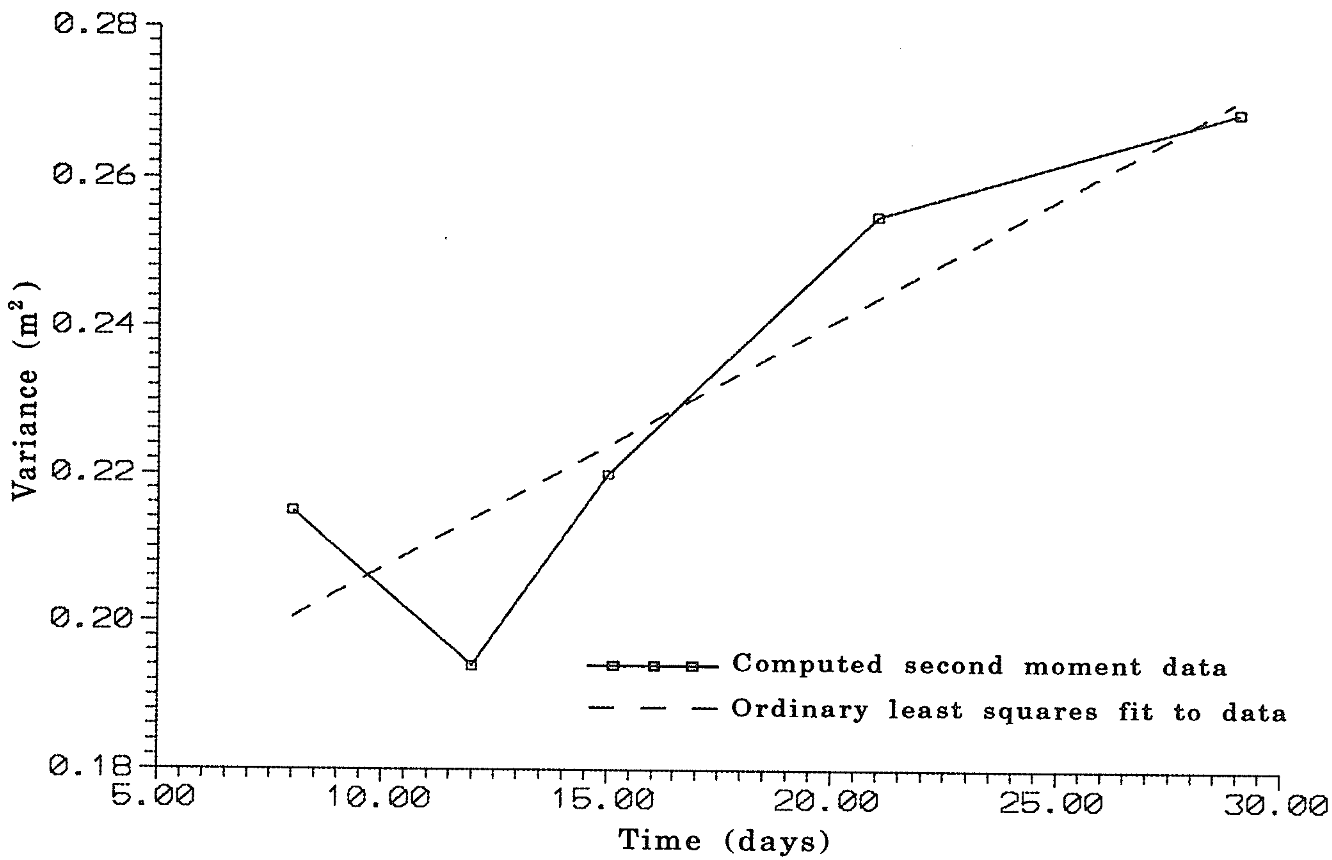

Figure 3.19 Variance in the transverse horizontal direction for the plume in the lower hydraulic conductivity zone (reduced data set used).

identical to the value of 0.030m found by Sudicky et al. (see Table III, 1983). Sudicky et al. (1983) determined the dispersivity parameters by comparing the concentration profiles produced by the Carslaw and Jaeger (1959) 3D analytic model to observed longitudinal concentration profiles. The dispersivity parameters used in the model are continuously updated until a good fit is obtained between the observed concentration profile and the computed profile. These values also compare well to the apparent asymptotic horizontal transverse macrodispersivity value of 0.039m determined by Freyberg (1986) for the Stanford-Waterloo tracer experiment at the Borden site and are also found to agree with the value of 0.030m determined by Farrell et al. (1992) (see chapter 2) based on the unsteady stochastic transport theory of Rehfeldt (1988). This latter approach is based on consideration of the hydraulic gradient fluctuations at the site.

The computed value for the apparent asymptotic longitudinal macrodispersivity for the site is found to be between 0.143m and 0.160m (see Table 3.8). These values are higher than the possible asymptotic longitudinal macrodispersivity value of 0.08m found by Sudicky et al. (see Table III, 1983). Gelhar et al. (1992) report that a moment analysis performed by them on the 1978 tracer data has produced a longitudinal macrodispersivity which is 2-4 times that given by Sudicky et al. (1983). This value is consistent with the estimates determined in this work. In addition, Gelhar et al. (1992) point out that in the near source region where dispersivities are increasing with displacement the approach used by Sudicky et al. (1983) will tend to underestimate the magnitude of the dispersivity since such an analysis only examines localized spread (i.e. spread along a transect of the plume) and not the spread over the entire plume. The apparent asymptotic longitudinal macrodispersivity values calculated in this work are also lower than the apparent asymptotic longitudinal macrodispersivity value of 0.36m reported by Freyberg (1986) for the Stanford-Waterloo tracer experiment. This difference may be attributed to the difference in the scale of the two experiments. It may be argued that since the Stanford-Waterloo experiment was conducted over a much longer time period than the 1978 tracer experiment (3 years for the former compared to 4 months for the latter) it was able to fully interact with the heterogeneity present in the aquifer. The solute associated with the 1978 experiment may not have fully interacted with the heterogeneity in the aquifer and as a result the observed longitudinal dispersivity would be less than the asymptotic value.

3.5.3.3 Third Moment and Skew Estimates

The third moment estimates for the plume in the lower hydraulic conductivity zone have been computed using the inverse square distance interpolation scheme and the extrapolation scheme described by Rajaram and Gelhar (1991). The third moments and the computed skew in the plume concentration distribution for both the longitudinal and the transverse direction at the various sample times are shown in Table 3.9.

A plot of the skew results (see Figure 3.20) shows that in the longitudinal direction the skew fluctuates and is greater than zero at early times. However, at the 121 day sample time the skew is found to be negative. An examination of the longitudinal concentration profile for the plume given by Sudicky et al. (Figure 3.10, 1983) also shows positive skew at early time. As pointed out earlier, Gelhar et al. (1979) have

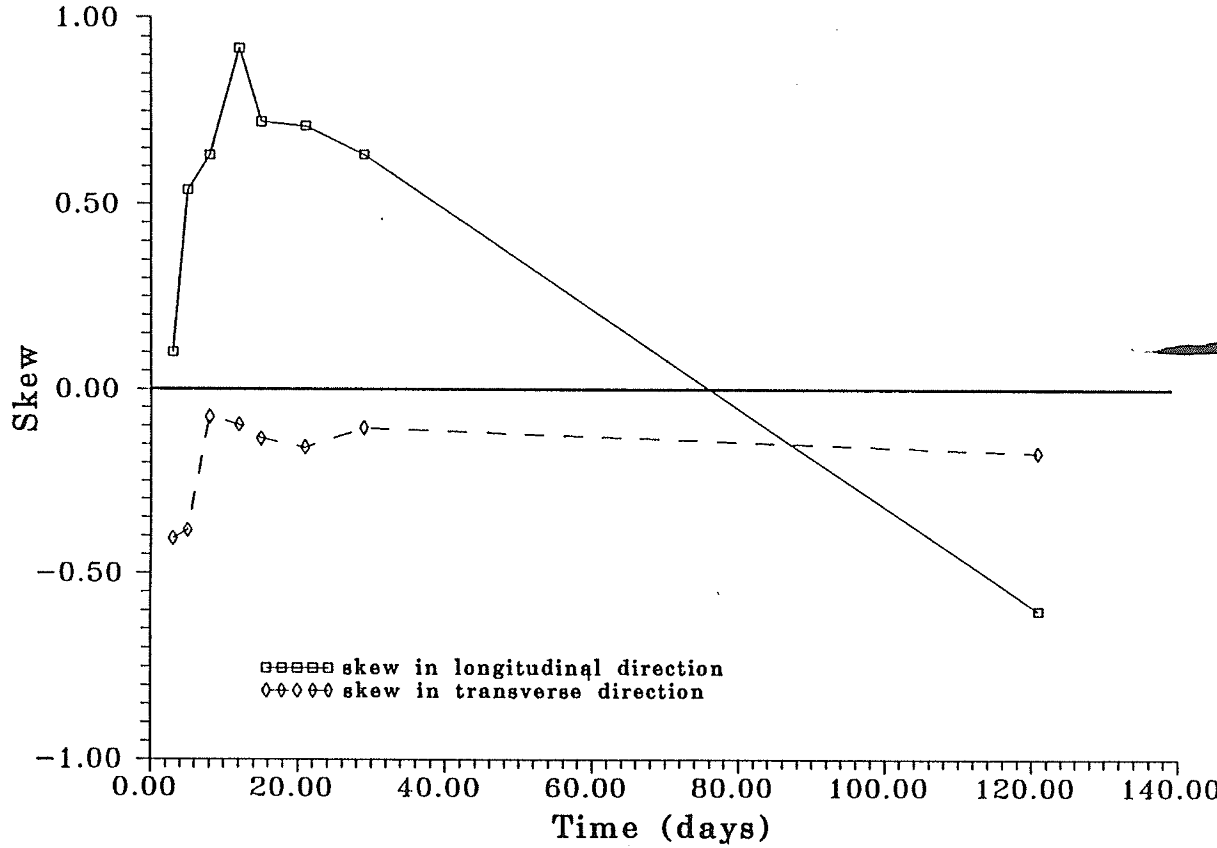

Figure 3.20 Longitudinal and transverse skew in the plume concentration vs time.

derived expression for the skew of the concentration distribution of a plume in perfectly

Table 3.9

Computed Skew for the Plume in the

Low Velocity Zone

Time (days)	**Skew**	
	Longitudinal direction	**Transverse direction**
3	0.101	-0.407
5	0.537	-0.385
8	0.631	-0.076
12	0.919	-0.097
15	0.722	-0.134
21	0.710	-0.158
29	0.633	-0.106
121	-0.602	-0.173

stratified aquifer in which the flow is unidirectional and parallel to the stratification. Their approach treats the variability of hydrologic phenomena as a stochastic process and assumes that the variations in the hydraulic conductivity and the concentration are statistically homogeneous. In addition, the approach explicitly accounts for the local dispersivity. Their theoretical results show that at early times the skew in the concentration distribution is positive but quickly tends to zero at later times. This supports the early time finding obtained in this work but contradicts the late time finding. However, the late time results (i.e. in particular our 121 day result) obtained in this work may be considered questionable due to the poor sampling of the plume at this time. Naff (1990) also examine spreading in a heterogeneous aquifer. In his analysis the variability of hydrologic processes are considered as stochastic processes; however the variations in the hydraulic conductivity and the concentration are not restricted to being statistically homogeneous. From his work Naff (1990) defines a term called the skew factor, B_s which has the following properties:

1. $\sigma^3 \propto B_s$
2. $B_s < 0$ for $t < \infty$;
3. $B_s = 0$ for $t = \infty$ (normal distribution)

(see Figure 3.21; note that τ in the figure represents dimensionless time).

The skew factor is supposed to reflect the behavior of the skew of a concentration distribution at all time. However, since the theory (Naff, 1990) neglects local dispersivity, the skew factor may not adequately represent the skew in the concentration distribution at early time when such effects are important. Comparison of the theoretical behavior of the skew factor to the observed skew in the concentration distribution in the longitudinal direction shows poor agreement at early time. Since Naff's (see Naff, 1990) approach ignores the effects of local dispersion at early times it can be argued that the results show the importance of the local dispersivity in the evolution of the plume at early time. The computed skew in the concentration distribution in the transverse direction is negative at all time. However, the skew is quite small and may be considered negligible; hence the concentration distribution in this direction can be considered to be normal.

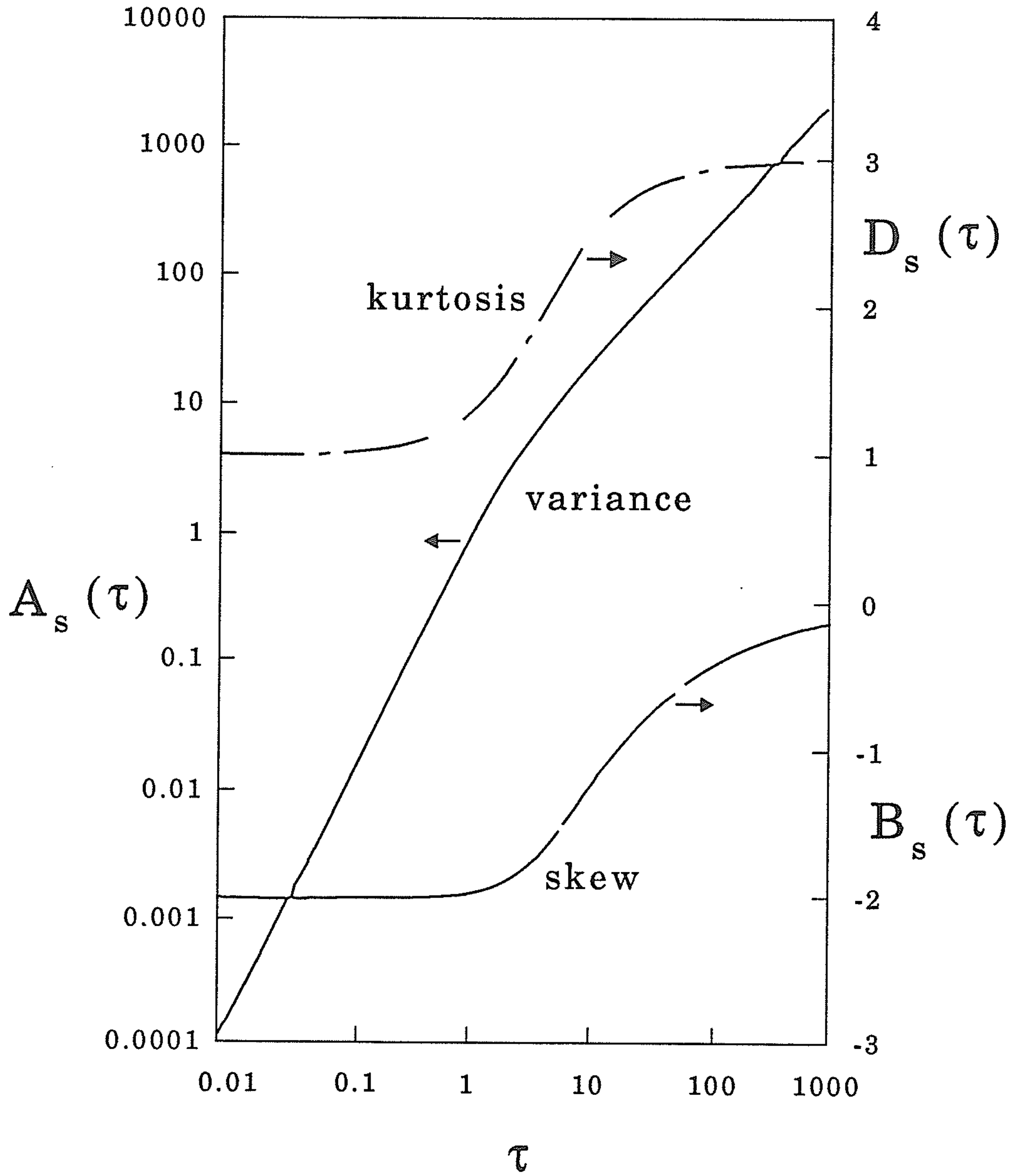

Figure 3.21 Plot of normalized variance, skewness, and kurtosis for large stratification as functions of dimensionless time (after Naff, 1990).

3.5.3.4 Fourth Moment and Kurtosis Estimates

The kurtosis is a property which is used to describe whether a symmetric distribution is sharper or flatter than a normal distribution. The computed kurtosis values in the longitudinal direction and the transverse direction at each sample time are shown in Table 3.10.

<u>Table 3.10</u>

Computed Kurtosis for the Plume in the

Low Velocity Zone

Time (days)	Kurtosis	
	Longitudinal direction	Transverse direction
3	2.442	2.638
5	3.587	2.388
8	3.237	2.444
12	4.395	2.453
15	3.541	2.412
21	3.376	2.237
29	2.822	2.154
121	2.589	2.612

As with the skew, the kurtosis in the longitudinal direction shows considerable fluctuation at early time (see Figure 3.22). For example after 3 days, the kurtosis value is found to be 2.442, indicating that the plume is flatter than the normal distribution (i.e. platykurtic). However, after 5 days the kurtosis value has changed to 3.587, indicating

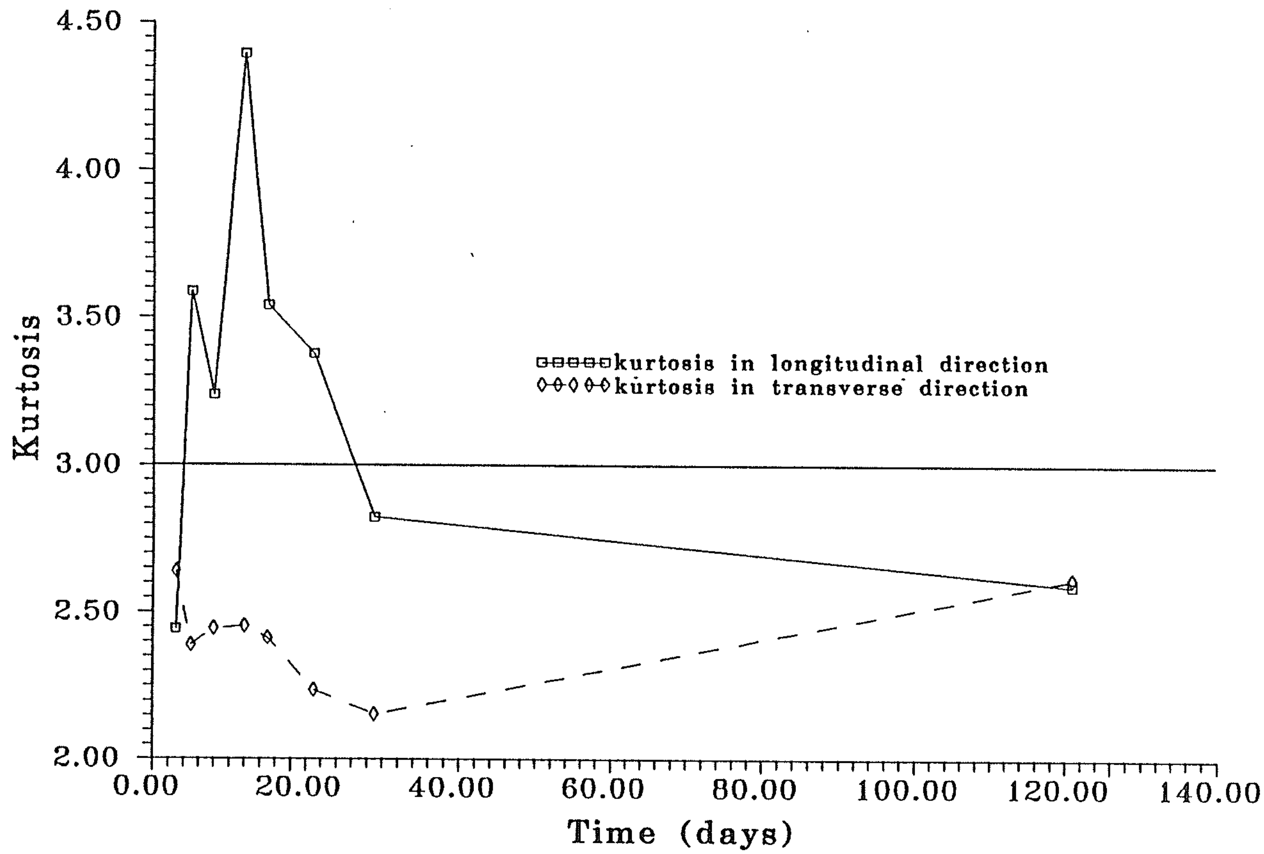

Figure 3.22 Longitudinal and transverse kurtosis in the plume concentration vs time.

that the concentration distribution is sharper than the normal distribution. Gelhar et al. (1979) point out that the kurtosis at later times should be $\leqslant 3$ and that this "non-normal" kurtosis should persist quite far down stream. This is somewhat consistent with the findings in this work for the concentration distribution between 29 and 121 days (see Table 3.10) and the longitudinal profile given by Sudicky et al. (Figure 3.11, 1983). Naff (1990) describes a parameter called the kurtosis factor, D_s which reflects the behavior of the kurtosis. The kurtosis factor has the following properties:

1. $\sigma^4 \propto D_s$
2. $D_s < 3$ for $t < \infty$;
3. $D_s = 3$ for $t = \infty$ (normal distribution)

(see also Figure 21).

At early times the kurtosis factor may not provide an accurate representation of the kurtosis since the theory neglects local dispersivity effects. Comparison of the kurtosis factor and the observed kurtosis in the longitudinal direction shows little agreement, with the computed kurtosis indicating that the concentration profile is sharper than the normal distribution. The computed kurtosis is reflected by the observed concentration profiles given by Sudicky et al. (Figure 3.10, 1983) which indicate that the observed concentration profiles are sharper than the normal distribution. At 121 days the longitudinal concentration profile Sudicky et al. (1983) are quite flat indicating that the kurtosis factor is well below 3. This is consistent with our finding and the results reported by Gelhar et al. (1979). In the transverse direction the computed kurtosis in the concentration distribution (see Figure 3.16) is observed to show better agreement with the kurtosis factor.

3.6 Discussion and Conclusions

The most significant result obtained from the analysis is the remarkable agreement between the estimate for the asymptotic horizontal transverse macrodispersivity computed in this work and that of Freyberg (1986) for the Stanford-Waterloo tracer experiment. This result strongly suggests that the transverse dispersivity at both sites is due to the same mechanism: transients in the flow field at the site. This result also suggests that the flow field at the Borden aquifer is stationary in both space and time (see Farrell et al., 1992). However, further waterlevel measurements need to be carried out over a long period of time to confirm this. Since transverse spreading in the subsurface appears to strongly influenced by the transient nature of the flow field then these results mean that for an accurate prediction of the fate of subsurface solutes an accurate knowledge of the groundwater flow field and how it changes with time. Such knowledge becomes critical when the solutes involved are highly toxic. In such cases if the effect of the flow transients are ignored and the transverse dispersivity is assumed to solely influenced by the heterogeneity in the hydraulic conductivity field then the transverse dispersivity will be underestimated. As a result the predicted spread of the solute in the transverse direction will underestimate the actual spread. An underestimation of the transverse spread may have a detrimental effect on any proposed remediation measures.

The findings of this work show that both the skew and the kurtosis are important indicators of the deviation of the concentration distribution from the normal distribution.

This result supports the earlier findings of Gelhar et al. (1979). The contradiction between the theoretical results of Naff (1990) and the observed skew and kurtosis of the solute plume emphasizes the importance of the local dispersivity in influencing the spread of solutes in the groundwater system at early time. Naff's theory (see Naff, 1990) suggests that at early time plumes tend to be negatively skewed. As a result, steep concentration gradients are predicted to develop at the front of plumes. However, from our analysis we have found that this is not the case. Instead, it has been found in this work that at early times the plume tends to be positively skewed so that shallow concentration gradients exist at the front of the plume. This result is also supported by the theoretical work of Gelhar et al. (1979). Naff (personal communication) points out that the first order analysis presented in his earlier analysis (Naff, 1990) does not produce good parameter estimates and in fact second order estimates are required. The use of second order estimates results in positive skews in the concentration distribution at very early time followed by negative skews at intermediate time. These results may suggest that at early times the local dispersivity is an important mechanism for moving mass ahead of the advective front of the plume. Naff (personal communication) suggests that advective forces may be responsible for the observed positive skew at early time; however, as pointed out by Naff (personal communication) the transport process at such time is quite complex. In addition the work does confirm that significant departures from Fickian transport do occur at early time.

Finally, it must be pointed out that care must be taken in accepting all of the results of this work due to the amount of extrapolation used in determining the plume boundaries at each sample time and the coarse sampling used at early times. Since these results do compare well with the results of others (e.g. Sudicky et al., 1983 and Gelhar et al., 1985) it appears that they are quite representative of the processes at the site. However, for the higher moment estimates the approach used here should be repeated on a better sampled data set (e.g. the Stanford-Waterloo tracer experiment data set) in order to validate these findings.

References

Abramowitz, M., and I. A. Stegun (Eds), Handbook of Mathematical Functions, App. Math. Ser. 55, National Bureau of Standards, Washington, D. C., 1970.

Barry, D. A., J. Coves, and G. Sposito, On the Dagan model of solute transport in groundwater: Applications to the Borden site, Water Resour. Res., 24(10), p. 1805-1817, 1988.

Barry, D. A., and G. Sposito, Three-dimensional statistical moment analysis of the Stanford/Waterloo Borden tracer data, Water Resour. Res., 26(8), p. 1735-1747, 1990.

Bear, J., Dynamics of Fluids in Porous Media, American Elsiever, New York, N. Y., p. 764, 1972.

Carslaw, H. S., and Jaeger, J. C., Conduction of Heat in Solids, Clarendon Press, Oxford, p. 510, 1959.

Dagan, G., Stochastic modelling of groundwater flow by unconditional and conditional probabilities, 2, The solute transport, Water Resour. Res., 18(4), p. 835-848, 1982.

Dagan, G., Solute transport in heterogeneous porous formations, J. Fluid Mech., 145, p. 151-177, 1984.

Dagan, G., Theory of solute transport in groundwater, Ann. Rev. Fluid. Mech., 19, p. 183-215.

Dagan, G., Time-dependent macrodispersion for solute transport in anisotropic heterogeneous aquifers, Water Resour. Res., 24(9), p. 1491-1500, 1988.

Dieulin, A., Propogation de pollution dans un aquifère alluvial: l'effet de parcours. D. Ing. Thesis, University of Sciences and Medicine of Grenoble, Grenoble, 1980.

Einstein, A., On the movement of suspended particles in stationary fluids deduced from molecular-kinetic theory of heat (in German), Ann. Phys., 17, p. 539-560, 1905.

Farrell, D. A., A. D. Woodbury, E. A. Sudicky, M. Rivett, A geostatistical analysis of fluctuating waterlevels at the Borden tracer-test site, Submitted to Water Resour. Res., 01/05/1992.

Freyberg, D. L., A natural gradient experiment on solute transport in a sand aquifer; 2. Spatial moments and the advection and dispersion of nonreactive tracers, Water Resour. Res., 22(13), p. 2031-2046, 1986.

Freyberg, D. L., Reply, Water Resour. Res., 24(7), p. 1223, 1988.

Garabedian, S. P., D. R. LeBlanc, L. W. Gelhar, and M. A. Celia, Large scale natural gradient tracer test in sand and gravel, Cape Cod, Massachusettes: 2. Analysis of spatial moments for a non-reactive tracer, Water Resour. Res., 27(5), p. 911-924, 1991.

Gelhar, L. W., and C. L. Axness, Three-dimensional stochastic analysis of macrodispersion in aquifers, Water Resour. Res., 19(1), p. 161-180, 1983.

Gelhar, L. W., A. L. Gutjahr, and R. L. Naff, Stochastic analysis of macrodispersion in a stratified aquifer, Water Resour. Res., 15(6), p. 1387-1397, 1979.

Guven, O., and F. J. Molz, Deterministic and stochastic analyses of dispersion in unbounded stratified porous medium, Water Resour. Res., 22(1), p. 1565-1574, 1986.

LeBlanc, D. R., S. P., Garabedian, K. M. Hess, L. W. Gelhar, R. D. Quadri, K. G. Stollenwerk, and W. W. Wood, Large-scale natural gradient tracer test in sand and gravel, Cape Cod, Massachusetts, 1, Experimental design and observed tracer movement, Water Resour. Res., 27(5), p. 895-910, 1991.

Loaiciga, H. A., Comment on "A natural gradient experiment on solute transport in a sand aquifer 2. Spatial moments and the advection and dispersion of nonreactive tracers" by D. L. Freyberg, Water Resour. Res., 24(7), p. 1221-1222, 1988.

Naff, R. L., On the nature of the dispersive flux in saturated heterogeneous porous media, Water Resour. Res., 26(5), p. 1013-1026, 1990.

Naff[1], R. L., Temporal and spatial moments for solute transport in hetrogeneous porous media: The imperfectly stratified aquifer, Proceedings of the International Conference and Workshop held in Ottawa, Canada, Oct. 1-4, 1990, Vol. 2, p. 419-441.

Rajaram, H., and L. W. Gelhar, Three-dimensional spatial moments analysis of the Borden tracer test, Water Resour. Res., 27(6), p. 1239-1251, 1991.

Rehfeldt, K. R., Prediction of macro-dispersivity in heterogeneous aquifers, Ph. D. dissertation, MIT, 1988.

Sauty, J. P., An analysis of hydrodispersive transfer in aquifers, Water Resour. Res., 16, p. 145-158, 1980.

Sudicky, E. A., A natural gradient experiment on solute transport in a sand aquifer: Spatial variability of hydraulic conductivity and its role in the dispersion process, Water Resour. Res., 22(13), p. 2069-2082, 1986.

Sudicky, E. A., J. A. Cherry, and E. O. Frind, Migration of contaminants in groundwater at a landfill: A case study; 4. A natural gradient dispersion test, Journal of Hydrology, 63, p. 81-108, 1983.

Sykes, J. F., S. B. Pahwa, R. B. Lantz, S. D. Ward, Numerical simulation of flow and contaminant migration at an extensively monitored landfill, Water Resour. Res., 18(6), p. 1687-1704, 1982.

Woodbury, A. D., and E. A. Sudicky, The geostatistical characteristics of the Borden aquifer, Water Resour. Res., 27(4), p. 533-546, 1991.

Woodbury, A. D., and E. A. Sudicky, The inversion of the Borden tracer experiment data: Investigation of three-dimensional stochastic moment models, Water Resour. Res., 28(9), p. 2387-2398, 1992.

Chapter 4

Discussion and Conclusions

4.1 Introduction

This chapter provides a summary of the results discussed in the previous two chapters with the goal of putting the results into perspective. In particular, the assumption of spatial and temporal stationarity in the flow field will be discussed as well as the implications of non-Fickian behavior at early time. This chapter is concluded with a discussion of future areas of research related to this work.

4.2 Discussion of Stationarity Assumption

The transverse horizontal asymptotic macrodispersivity estimates computed for the 1978 Borden tracer experiment (this work) and the Stanford-Waterloo tracer experiment (see Freyberg, 1986, and Rajaram and Gelhar, 1991) are shown to be quite similar even though the experiments were conducted at different times and in different parts of the Borden aquifer. If Sudicky's contention is correct (that the observed transverse horizontal dispersion at the Borden site is probably due the presence of known flow transients at the site) then the observed similarity in the transverse horizontal asymptotic macrodispersivity for the two experiments suggests that the flow field at the Borden site is stationary with respect to space and time. In Chapter 3, several arguments are put forward to justify the assumption of stationarity in the Borden flow field. It is shown that the range in the flow angle deviation, the range in the gradient magnitude and the mean gradient magnitude computed from the 1989-91 watertable data are in agreement with the values given by MacFarlane et al. (1982) and Sudicky (1986) in different parts of the aquifer at different times. The geostatistical parameters (i.e. the variances and the integral scales) derived from the 1989 Borden watertable data, when used in Rehfeldt's unsteady theory, produces transverse and longitudinal asymptotic macrodispersivity estimates. These are shown to be in good agreement with the apparent transverse horizontal asymptotic macrodispersivity estimates of Freyberg (1986), and Rajaram and Gelhar (1991) for the Stanford-Waterloo tracer data. Further, the estimate of the transverse horizontal asymptotic macrodispersivity computed using Rehfeldt's unsteady theory is also shown to be in good agreement with the apparent transverse horizontal asymptotic macrodispersivity computed from the 1978 Borden tracer data (see Chapter 2). The agreement between the results of the theoretical model and the results computed from the field data strengthen the argument for stationarity (both temporal and spatial) in the Borden flow field. However, it must be pointed out that additional waterlevel data for the site is required to confirm whether the flow field at the site is actually stationary (see Chapter 3).

4.3 Early Time Plume Behavior

This work also examines the early time behavior of an evolving solute plume at the Borden aquifer. For this plume, it is found that the macrodispersivity increases with time and displacement [see Sauty (1980), Dieulin (1980), Sudicky et al. (1983)]. Based on an examination of the second, third and fourth order moments it is found that at early time the evolving solute plume does not conform to classical Fickian behavior as is commonly assumed in practice. Instead, the concentration profile of the evolving solute plume is found to be both positively skewed and platykurtic. Comparison of these findings with the theoretical results of Gelhar et al. (1979) and Naff (1990) show that the observed behavior of the skew and the kurtosis (obtained in this work) agree with the former and disagree with the latter (with respect to the nature of the skew). The tendency of the concentration distribution in solute plumes to be positively skewed at early time is also supported by the work of Tompson (1988). Recall that the work of Gelhar et al. (1979) was based on the assumption that an aquifer was perfectly stratified. Therefore, it does appear that the Borden aquifer can be viewed as being a near perfectly stratified aquifer from a hydrogeological perspective.

4.4 Practical Implications

The results obtained from this work have significant practical implications with respect to modelling groundwater contamination. In particular, this work shows that small fluctuations in the hydraulic gradient over time can account for nearly all of the transverse dispersion observed at a site. Previously, it was pointed out that it is common practice to model contaminant transport using a spatially varying hydraulic conductivity and a steady groundwater velocity. It is apparent from this work that such an approach will underestimate the transverse spread in areas where a transient flow field is present. This suggests that in areas where toxic materials (for example, radioactive waste and

PCB's) will be stored, a detailed knowledge of the flow field at the site should be known prior to commissioning. This protects the area in the event that modelling of contaminant transport is required to facilitate remediation measures. Failure to consider the enhanced spread due to flow transients may result in an expensive but ineffective remediation program. Depending on the nature of the nature of the contaminant, this failure may be catastrophic.

The non-Fickian behavior of a plume at early time strongly suggests that the standard approach of modelling contaminant transport using a Fickian approach (i.e. constant macrodispersivity values) may in some cases be inappropriate. Such an approach will lead to an underestimation of the solute spread and an overestimation of the solute concentration at the centre of the plume at early time. However, as pointed out by Naff (1990), if the travel distance of the centre of mass of the plume is greater than twenty integral scales of hydraulic conductivity, then the use of the Fickian approach is reasonable.

4.5 Further Research

The results of this work indicate that there are some areas of contaminant transport modelling which need to be further studied. In particular, the effects of transient flow fields on the dispersion process at early time requires further examination in light of the failure of Naff's (see Naff, 1989) model to adequately predict the transverse spread at the Borden site at pre-asymptotic times. In fact, one possible approach may be to recast Naff's deterministic approach into a stochastic form with the harmonic frequencies and associated amplitudes being considered to have mean values and variances. Such an approach will generate an ensemble behavior which may improve the ability of the model to predict transverse spread.

As pointed in Chapter 3, the tracer plume associated with the 1978 Borden tracer experiment was not very well sampled at very early and very late times. In particular, it was found that in several instances the sampler array truncated the solute plume and as a result, a considerable amount of extrapolation involving the use of various assumptions had to be performed in order to perform the numerical integrations. The used of extrapolation methods was shown to have an influence on the various moments computed in this work and as a result influenced the various parameter estimates (centre of mass location, velocity, macrodispersivity, skew and kurtosis). In addition, watertable data collected from a different site at a different were incorporated in the analysis using various assumptions. As a result, there will be some question as to the accuracy of the result presented in this work.

To verify whether the results produced from this and other similar work employing similar assumptions are valid, a tracer experiment along the lines of the Stanford-Waterloo and the Cape Cod experiments should be carried out. In addition to a carefully designed sampler array which captures the essential features of the early time behavior of the solute plume and a good knowledge of the geostatistical properties of the hydraulic conductivity, field emphasis should also be placed on monitoring the hydraulic head at the site in three-dimensions. Such an experiment, though costly, would produce a reliable database of information. This database, could be used to test both current and future transport theories with minimal assumptions with respect to aquifer properties being required.

It should be recalled that the approaches employed by Gelhar et al. (1979) and Tompson (1988) in the study of the early time dispersion process consider the effects of local dispersivity whereas the Naff's approach does not. This raises the question of the importance of the local dispersivity in the early time evolution of solute plumes. This is an area which should be further examined if the total phenomena of solute transport in groundwater are to be well understood.

References

Dieulin, A., Propagation de pollution dans un aquifére alluvial: l'effet de parcours. D. Ing. Thesis, University of Sciences and Medicine of Grenoble, Grenoble, 1980.

Freyberg, D. L., A natural gradient experiment on solute transport in a sand aquifer; 2. Spatial moments and the advection and dispersion of nonreactive tracers, Water Resour. Res., 22(13), p. 2031-2046, 1986.

Gelhar, L. W., A. L. Gutjahr, and R. L. Naff, Stochastic analysis of macrodispersion in a stratified aquifer, Water Resour. Res., 15(6), p. 1387-1397, 1979.

MacFarlane, D. S., J. A. Cherry, R. W. Gilham, and E. A. Sudicky, Migration of contaminants at a landfill, A case study, 1, Groundwater flow and plume delineation, J. Hydrol., 63, p. 1-29, 1983.

Naff, R. L., On the nature of the dispersive flux in saturated heterogeneous porous media, Water Resour. Res., 26(5), p. 1013-1026, 1990.

Naff, R. L., J. T. -C. Yeh, and M. W. Kemblowski, Reply, Water Resour. Res., 25(12), p. 2523-2525, 1989.

Rajaram, H., and L. W. Gelhar, Three-dimensional spatial moments analysis of the Borden tracer test, Water Resour. Res., 27(6), p. 1239-1251, 1991.

Rehfeldt, K. R., Prediction of macrodispersivity in heterogeneous aquifers, Ph. D. dissertation, MIT, 1988.

Sauty, J. P., An analysis of hydrodispersive transfer in aquifers, Water Resour. Res., 16, p. 145-158, 1980.

Sudicky, E. A., A natural gradient on solute transport in a sand aquifer, Spatial variability of hydraulic conductivity and its role in the dispersion process, Water Resour. Res., 22(13), p. 2069-2082, 1986.

Sudicky, E. A., J. A. Cherry, and E. O. Frind, Migration of contaminants in groundwater at a landfill: A case study; 4. A natural gradient dispersion test, Journal of Hydrology, 63, p. 81-108, 1983.

Tompson, A. F. B., On a new functional form for the dispersive flux in porous media, Water Resour. Res., 24(11), p. 1939-1947, 1988.

Appendix 1

Derivation of the Expression for the Unsteady Component of the Macrodispersivity

In this appendix a summary of the derivation given by Rehfeldt (1988) for the component of the macrodispersivity due to unsteady flow is given.

Governing Equations

The Transport Equation

The equation describing the transport of an ideal conservative solute in saturated porous media is given by

$$n\frac{\partial c}{\partial t}=\frac{\partial}{\partial x_i}\left[E_{ij}\frac{\partial c}{\partial x_j}-cq_i\right] \tag{A1}$$

where n is the porosity; c is the dimensionless solute concentration; E_{ij} is the local bulk dispersion coefficient tensor and q_i is the component of the specific discharge vector. For the conservation of mass this formulation requires that

$$\frac{\partial q_i}{\partial x_i}=0 \tag{A2}$$

and that the local coefficient of bulk dispersion be constant. If the concentration and specific discharge are assumed to be random variables composed of a mean and a small perturbation then we may write

$$q_i = \bar{q}_i(x_i,t) + q_i'(x_i,t) \tag{A3}$$

$$c = \bar{c}(x_i,t) + c'(x_i,t) \tag{A4}$$

Here the mean quantities are indicated with an overbar and the primed quantities are zero mean perturbation. Substitution of (A3) and (A4) into (A1) and subsequent manipulation leads to the following mean and perturbed forms for the transport equation.

$$n\frac{\partial \bar{c}}{\partial t} + \frac{\partial}{\partial x_i}(\bar{q}_i\bar{c} + \overline{q_i'c'}) = \frac{\partial}{\partial x_i}\left[E_{ij}\frac{\partial c}{\partial x_j}\right] \tag{A5}$$

where $q_i'c'$ represents the macroscopic dispersive flux which if it is Fickian in nature, can be represented as

$$\overline{q_i'c'} = -qA_{ij}\frac{\partial \bar{c}}{\partial x_j} \qquad i=1,2,3 \tag{A6}$$

and

$$n\frac{\partial c'}{\partial t} + \frac{\partial}{\partial x_i}(\bar{q}_i\, c') + \frac{\partial}{\partial x_i}(q_i'\, \bar{c}) = \frac{\partial}{\partial x_i}\left[E_{ij}\frac{\partial c'}{\partial x_j}\right] \tag{A7}$$

Note that if the coordinate axes are aligned with the mean flow direction, such that $\bar{q}_1 = q$ and $\bar{q}_2 = \bar{q}_3 = 0$ then the local bulk dispersion tensor can be written as

$$E_{ij} = \begin{bmatrix} \alpha_L q & 0 & 0 \\ 0 & \alpha_T q & 0 \\ 0 & 0 & \alpha_T q \end{bmatrix} \tag{A8}$$

Taking into consideration the conservation of mass (2) and substituting (A8) into (A7) leads to the following expression for the perturbed form of the transport equation.

$$n\frac{\partial c'}{\partial t} + q\frac{\partial c'}{\partial x_1} + q_i'\frac{\partial \bar{c}}{\partial x_i} = q\left[\alpha_L \frac{\partial^2 c'}{\partial x_1^2} + \alpha_T\left(\frac{\partial^2 c'}{\partial x_2^2} + \frac{\partial^2 c'}{\partial x_3^2}\right)\right] \tag{A9}$$

One approach to solving this equation is through the use of spectral methods.

Spectral Solution

Assuming statistical homogeneity in space and time the solution of (A9) can be developed using Fourier-Stieltjes representations for the perturbed quantities (Lumley and Panofsky, 1964). Therefore let the perturbed quantities c′ and q′ be expressed as

$$c' = \int_{-\infty}^{\infty} e^{(ikx+i\omega t)}\, dZ_c(k,\omega) \tag{A10a}$$

$$q_i' = \int_{-\infty}^{\infty} e^{(ikx+i\omega t)}\, dZ_{q_i}(k,\omega) \tag{A10b}$$

Substituting (A10) into (A9) and recalling the uniqueness of the spectral representation gives

$$\{ni\omega+\left[ik_1+\alpha_L k_1{}^2+\alpha_T(k_2^2+k_3^2)\right]q\}dZ_c=-\frac{\partial\bar{c}}{\partial x_i}dZ_{q_i} \tag{A11}$$

where $\partial\bar{c}/\partial x_i$ is assumed constant at the local scale over which (A7) applies. Multiplying (A11) by the complex conjugate $dZ_{q_i}^*$ and taking the expected value leads to

$$\{ni\omega+\left[ik_1+\alpha_L k_1^2+\alpha_T(k_2^2+k_3^2)\right]q\}\ S_{cq_i}(k,\omega)=-\frac{\partial\bar{c}}{\partial x_j}S_{q_iq_j}(k,\omega) \tag{A12}$$

where $S_{q_iq_j}(k,\omega)$ represents the specific discharge spectrum and $S_{cq_i}(k,\omega)$ represents the macroscopic dispersive flux. Equations (A6) and (A12) may then be combined to give the following form for the macrodispersivity

$$A_{ij}=\int_{-\infty}^{\infty}\frac{S_{q_iq_j}(k,\omega)\quad dk\ d\omega}{ni\omega q+\left[ik_1+\alpha_L k_1^2+\alpha_T(k_2^2+k_3^2)\right]q^2} \tag{A13}$$

Before this equation can be used to determine the macrodispersivity an appropriate form for the specific discharge spectrum has to be determined.

Determination of the Specific Discharge Spectrum

The transient form of the groundwater equation can be written in terms of the natural logarithm of hydraulic conductivity, K as

$$\frac{\partial^2\phi}{\partial x_i\partial x_j}+\frac{\partial \ln K}{\partial x_i}\frac{\partial\phi}{\partial x_i}=\frac{S_s}{K}\frac{\partial\phi}{\partial t} \tag{A14}$$

where ϕ is the hydraulic head and S_s is the specific storage coefficient. Since this expression implies a change in storage. It is therefore apparent that this expression is inconsistent with the conservation of mass assumption made earlier [see (A2)]. It will later be shown that this change in storage term does not contribute to the additional dispersive flux.

If the hydraulic conductivity is considered a random variable with zero mean perturbation then we can write

$$\ln K = F + f, \qquad E[f] = 0 \tag{A15}$$

$$K = e^F e^f = K_g e^f, \qquad \ln K_g = F = E[\ln K] \tag{A16}$$

Using the above expressions and retaining only first order terms the flow equation may be rewritten as

$$\frac{\partial^2 \phi}{\partial x_i \partial x_j} + \frac{\partial \ln K}{\partial x_i}\frac{\partial \phi}{\partial x_i} = \frac{S_s}{K_g}(1-f)\frac{\partial \phi}{\partial t} \tag{A17}$$

This equation applies to unsteady flow in three-dimensions where the temporal forcing is supplied by the boundary conditions. Using spectral methods does not allow boundary conditions to be modelled explicitly and as a result unsteadiness must be brought into this formulation through the mean hydraulic gradient and the mean hydraulic head. The hydraulic head, ϕ is assumed to be composed of a slowly varying mean in space and time and a perturbation about that mean.

$$\phi(x,t) = \bar{H}(x,t) + H'(x,t) + h(x,t) \tag{A18}$$

Here $\bar{H}(x,t)$ is the slowly varying ensemble mean, $H'(x,t)$ is a temporal perturbation about the mean hydraulic head and $h(x,t)$ is the local perturbation in space and time.

Gelhar and Axness (1983) have shown that field scale dispersion under steady flow conditions results from the randomness in the specific discharge vector (A19). This randomness is caused by the variations in the hydraulic conductivity field.

$$q_i=-K\frac{\partial\phi}{\partial x_i} \tag{A19}$$

From the expression for the specific discharge it is apparent that changes in ϕ that are random in time but uniform in space do not change q_i, therefore the rising and falling of H' does not strongly influence dispersion at the field scale. Hence for the temporal variability of ϕ to have an effect on q_i and hence dispersion the spatial gradient of ϕ must also be variable in time.

If it is assumed that the hydraulic gradient can be decomposed into a slowly varying mean and a perturbation hence we may write

$$-\frac{\partial \bar{H}}{\partial x_i}=\mathcal{J}_i; \qquad -\frac{\partial H'}{\partial x_i}=J_i' \tag{A20}$$

Note that J_1' is assumed to be random in time, but at the local scale, constant in space.

Substitution of (A18) and (A20) into the flow equation (A17) and subsequent manipulation leads to the following perturbed form for the flow equation

$$\frac{\partial^2 h}{\partial x_i \partial x_j}-\mathcal{J}_i\frac{\partial f}{\partial x_i}=\frac{S_s}{K_g}\left[\frac{\partial H'}{\partial t}+\frac{\partial h}{\partial t}\right] \tag{A21}$$

Using equations (A15) and (A16) the Darcy equation may be written in the form

$$q_i=-K_g(1+f)\frac{\partial\phi}{\partial x_i} \tag{A22}$$

with the perturbed form of this expression being

The perturbed quantities in (A21) and (A23) can be expressed in spectral form using

$$q_i' = -K_g \left[-J_i' + \frac{\partial h}{\partial x_i} - \mathcal{J} f \right] \tag{A23}$$

Fourier-Stieltjes integrals as

$$h = \int_{-\infty}^{\infty} e^{(ikx+i\omega t)}\, dZ_h(k,\omega) \tag{A24a}$$

$$f = \int_{-\infty}^{\infty} e^{(ikx+i\omega t)}\, dZ_f(k,\omega) \tag{A24b}$$

$$J_i' = \int_{-\infty}^{\infty} e^{(ikx+i\omega t)}\, dZ_{J_i}(k,\omega) \tag{A24c}$$

$$q_i' = \int_{-\infty}^{\infty} e^{(ikx+i\omega t)}\, dZ_{q_i}(k,\omega) \tag{A24d}$$

$$H' = \int_{-\infty}^{\infty} e^{(ikx+i\omega t)}\, dZ_H(k,\omega) \tag{A24e}$$

Note that f, H', and J_i' have been represented as space-time random processes even though f is time invariant and J_i' and H' are spatially uniform. This space-time representation is necessary to produce a consistent form for the entire equation. Since one can treat a constant as a random variable with a covariance of infinite correlation length and a spectrum with all the power concentrated at zero frequency then there is no inconsistency when using the above spectral forms. Substitution of (A24) into (A21) and (A23) and recalling the uniqueness of the spectral representation gives

$$-k^2 dZ_h - ik_i J_i dZ_f = \frac{S_s}{K_g}(i\omega dZ_H + i\omega dZ_h) \tag{A25}$$

for the flow equation (A21) and

$$dZ_{q_i} = K_g\left[dZ_{J_i} - ik_i dZ_h + J_i dZ_f\right] \tag{A26}$$

for the Darcy equation (A23). Combining (A25) and (A26) and rearranging gives

$$dZ_{q_i} = K_g\left[dZ_{J_i} - \frac{J_1 k_i k_1 dZ_f - \frac{S_s}{K_g} k_i \omega dZ_H}{k^2 + i\omega \frac{S_s}{K_g}} + J_i dZ_f\right] \tag{A27}$$

The specific discharge spectrum, $S_{q_iq_j}(k,\omega)$, is obtained by multiplying (A27) by its complex conjugate $dZ_{q_j}^*$ and using the properties of the spectral representation theorem

$$S_{q_iq_j}=K_g^2\left[S_{J_iJ_j}+\frac{\frac{S_s}{K_g}k_j\omega}{k^2-\frac{S_s}{K_g}i\omega}S_{J_iH}+\frac{\frac{S_s}{K_g}k_i\omega}{k^2+\frac{S_s}{K_g}i\omega}S_{J_jH}+\frac{\frac{S_s^2}{K_g^2}k_ik_j\omega^2}{k^4+\left(\frac{S_s}{K_g}\omega\right)^2}S_{HH}\right.$$

$$\left.+\left(\delta_{il}-\frac{k_ik_1}{k^2+\frac{S_s}{K_g}i\omega}\right)\left(\delta_{jm}-\frac{k_jk_m}{k^2-\frac{S_s}{K_g}i\omega}\right)\mathcal{J}_1\mathcal{J}_mS_{ff}\right] \tag{A28}$$

The expression for macrodispersivity can be greatly simplified by recognizing the form of the input spectra. The hydraulic conductivity is time invariant, hence, its spectrum is given by

$$S_{ff}(k,\omega)=S_{ff}(k)\delta(\omega) \tag{A29}$$

where $\delta(\omega)$ is the Dirac delta function. Likewise, the variables J_i' and H' were assumed to be spatially uniform. Their spectra, and presumably the cross spectra, will be of a form

$$S_{J_iJ_j}(k,\omega)=S_{J_iJ_j}(\omega)\delta(k) \tag{A30a}$$

$$S_{HH}(k,\omega)=S_{HH}(\omega)\delta(k) \tag{A30b}$$

$$S_{J_iH}(k,\omega)=S_{J_iH}(\omega)\delta(k) \tag{A30c}$$

Macrodispersivity

The macrodispersivities can thus be written

$$A_{ij}=\int_{-\infty}^{\infty}\frac{K_g^2 S_{J_iJ_j}(\omega,k)+K_g^2\left[\delta_{i1}-\frac{k_ik_1}{k^2}\right]\left[\delta_{jm}-\frac{k_jk_m}{k^2}\right]J_1J_mS_{ff}(\omega,k)}{ni\omega q+\left[ik_1+\alpha_L k_1^2+\alpha_T(k_2^2+k_3^2)\right]q^2}\,dk\,d\omega \tag{A31}$$

Using (A29) and (A30) equation (A31) decomposes into two components, one incorporating the effect of temporal variability and the other spatial variability. The term involving spatial variability (see Rehfeldt, 1988, equation 2-39) is identical to that given by Gelhar and Axness (1983, equation 62) for the steady flow case. The component of macrodispersivity due to unsteady flow is given by

$$A_{ij}^{(u)}=\int_{-\infty}^{\infty}\frac{K_g^2 S_{J_iJ_j}(\omega)}{ni\omega q}d\omega \tag{A32}$$

This expression reduces to (see Rehfeldt, 1988)

$$A_{ij}^{(u)}=\frac{K_g^2\pi}{nq}S_{J_iJ_j}(0) \tag{A33}$$

To be consistent with the results of Gelhar and Axness (1983) (A33) is rewritten in the following form

$$A_{ij}^{(u)}=\left[\frac{1}{\gamma^2}\right]\frac{q\pi}{nJ_1^2}S_{J_iJ_j}(0) \tag{A34}$$

where γ is the flow factor defined by Gelhar and Axness (1983) as

$$\gamma = \frac{q}{K_g J_1} \tag{A35}$$

Assuming the cross and autocovariance functions to be exponential in form, then

$$S_{J_iJ_j}(0) = \frac{1}{\pi} \sigma^2_{J_iJ_j} \lambda_{J_iJ_j} \tag{A36}$$

Thus the macrodispersivity due to transient flow can be written as

$$A_{ij}^{(u)} = \frac{1}{\gamma^2} \frac{q}{n} \frac{\sigma^2_{J_iJ_j}}{J_1^2} \lambda_{J_iJ_j} \tag{A37}$$

Correction

The following articles were referenced in Chapter 2 but were not included with the references at the end of that chapter:

Cressie, N., and D. Hawkins, Robust estimation of the variogram, Math. Geol., 12(2), p. 115-125, 1980.

Matheron, G., Principles of geostatistics, Econ. Geol., 58, 1246-1266, 1963.

NOTE

Copies of the data used to produce this thesis can be obtained on diskette from the following sources:

1. David Farrell
Department of Geological Engineering
University of Manitoba
Winnipeg, Manitoba
Canada.

E-mail: david@woodsun1.geoeng.umanitoba.ca
dfarrel@ccu.umanitoba.ca

2. Dr. A. D. Woodbury
Department of Geological Engineering
University of Manitoba
Winnipeg, Manitoba
Canada.

E-mail: allw@woodsun1.geoeng.umanitoba.ca

3. Department of Geological Engineering
University of Manitoba
Winnipeg, Manitoba
Canada.